THESIS FOR THE DEGREE OF DOCTOR OF PHILOSOPHY

A statistical approach to multi-input equivalent fatigue loads for the durability of automotive structures

Gwenaëlle Genet

CHALMERS | GÖTEBORG UNIVERSITY

Department of Mathematical Sciences
Division of Mathematical Statistics
CHALMERS UNIVERSITY OF TECHNOLOGY
AND GÖTEBORG UNIVERSITY

Göteborg, Sweden 2006

A statistical approach to multi-input equivalent fatigue loads for the durability of automotive structures
GWENAËLLE GENET
ISBN 91-7291-847-0

Doktorsavhandlingar vid Chalmers Tekniska Högskola
Ny serie nr 2529
ISSN 0346-718X

Department of Mathematical Sciences
Division of Mathematical Statistics
Chalmers University of Technology and Göteborg University
SE-412 96 Göteborg
Sweden
Telephone + 46 (0)31-772 1000
Göteborg, 2006

Abstract

In the automotive industry, due to temporal and financial constraints, we need to strongly reduce the duration of the design phase, but still ensure reliability and robustness. Structures in service are often exposed to complex variable amplitude loads. In order to characterize the severity of customers, to define specification for designing metallic structures by computation or for the validation on test rigs, simple forces are more useful. The equivalent fatigue approach, developed at PSA PEUGEOT CITROËN, is a method for transforming variable amplitude measured forces into simpler loads, equivalent in terms of damage. The transformation should be performed without information about the geometry of the structure undergoing the loads. The aim of this work is to extend the one-input equivalent fatigue method, to the multi-input forces.
A great part of the work is devoted to the condition of equivalence of damage between the measured forces and the equivalent ones, when information about the structures is limited. The structures are considered to be elastic and quasi-static. Models of life prediction like Basquin's criterion, for structures submitted to uniaxial fatigue at their critical points, and Morel's model for structures exposed to multiaxial fatigue, are used. Three types of multi-input equivalent fatigue loads are developed. The sinusoidal and the Gaussian multi-input equivalent fatigue loads are studied, as well as the Markov chain multi-input loads. For the Markov loads, a new theory needs to be developed in order to evaluate the rainflow content of linear combinations of multi-input Markov chain. Several applications of those three models are presented, and a set-up of experiments is proposed.

Keywords : Equivalent fatigue, uniaxial and multiaxial high cycle fatigue, multi-input variable amplitude loads, rainflow counting, Morel's model, Basquin's model, Gaussian process, Markov chain

Acknowledgements

I did my PhD thesis in the department of Mathematical Statistics, at Chalmers University of Technology. First of all, I would like to thank my supervisors Pär Johannesson and Jacques de Maré. Their continuous support, their encouragement and their patience were simply essential in the progression of this work.

I did the thesis in collaboration with PSA PEUGEOT CITROËN, in the MAST team (Mécanique Appliquée des Solides et des sTructures), directed first by Jean-Jacques Thomas and now by Laurent Rota. We have got the financial resources from PSA PEUGEOT CITROËN and ANRT (Association Nationale de la Recherche Technique). I am grateful to my two supervisors David Gualandris and Ida Raoult for their support and their valuable comments and advice during this work. I would also like to thank Mac Lan Nguyen-Tajan and Jean-Jacques Thomas, for welcoming me in the team and their constant interest and optimism regarding my work.

Many thanks go again to Pär Johannesson, Jacques de Maré, Ida Raoult and Mac Lan Nguyen-Tajan for reading carefully my manuscript.

Working in two different areas like mechanics and statistics has its obvious difficulties, mainly the use of different languages and approaches. The only way to overcome them is by having open mind and the desire to collaborate. Thank you for making this possible for me.

The LAMEFIP (LAboratoire Matériaux, Endommagement, Fiabilité et Ingénierie des Procédés), Thierry Palin Luc and Nicolas Sainthier, has carried out the experiments on the suspension triangle. I thank them for this and their helpful advice regarding the experiments. Special thanks go to Alain Blanc, engineer at PSA PEUGEOT CITROËN, for his help in the finite element softwares IDEAS and NASTRAN.

Professor Igor Rychlik, Chalmers and Lund University, has contributed to my work with valuable comments about the rainflow method.

Clara Escuer has successfully applied the bi-dimensional equivalent fatigue approach, during her three months trainee period at PSA PEUGEOT CITROËN.

I am grateful to Ann-Rozen Guichard, secretary of the MAST team, for her help concerning the administrative tasks.

I would like to thank my friends from France and Sweden, for their presence. Special thanks to São, you were so helpful.

My family has provided me with continuous encouragements, not only during these last years. Hopefully you were there.

Warm thanks to Vincent, for his unfailing and so precious support.

Gwenaëlle.

Göteborg, September 2006

Contents

Nomenclature

Forces	
$\boldsymbol{F}$	The multi-input measurements
$\boldsymbol{F^e}$	The multi-input equivalent fatigue loads (EFL)
F_i	The i-th component of the multi-input measurement
F_i^e	The i-th component of the multi-input EFL
$F^*(A_c, \boldsymbol{F})$	A linear combination of the components of $\boldsymbol{F}$
$F^{e*}(A_c, \boldsymbol{F^e})$	A linear combination of the components of $\boldsymbol{F^e}$
$F_{ri}^*(A_c, \boldsymbol{F})$	The i-th range (or min-max amplitude) of a rainflow reversal of $F^*(A_c, \boldsymbol{F})$
$F_{ri}^{e*}(A_c, \boldsymbol{F})$	The i-th range (or min-max amplitude) of a rainflow reversal of $F^{e*}(A_c, \boldsymbol{F})$
$\boldsymbol{\theta}$	The vector containing the parameters defining $\boldsymbol{F^e}$
N_0	The expected number of cycles of $\boldsymbol{F^e}$
T_0	The time period of the forces $\boldsymbol{F}$ and $\boldsymbol{F^e}$

Geometry	
A_c	The critical point on a structure
$\boldsymbol{\Sigma}(A_c, \boldsymbol{F})$	The stress tensor at the critical point A_c
$\sigma_{ij}(A_c, \boldsymbol{F})$	The component of the stress tensor $\boldsymbol{\Sigma}(A_c, \boldsymbol{F})$
$\boldsymbol{\Sigma}_d(A_c, \boldsymbol{F})$	The diagonalised stress tensor at the critical point A_c
$\sigma_{d,ij}(A_c, \boldsymbol{F})$	A component of the stress tensor $\boldsymbol{\Sigma}_d(A_c, \boldsymbol{F})$
(α, β)	The coefficients defining the components of a proportional stress tensor $\boldsymbol{\Sigma}(A_c, \boldsymbol{F})$

Morel's model

REV	The representative elementary volume
$\boldsymbol{\tau}$	The mesoscopic resolved shear stress acting in a grain of the REV
τ_y	The yield limit of a crystal
$\boldsymbol{n}$	The normal unit vector of a plane of the REV
(θ, ϕ)	The polar angles defining $\boldsymbol{n}$
$\boldsymbol{m}$	The unit vector defining a direction on the critical plane
ψ	The polar angle defining $\boldsymbol{m}$ on the plane
γ_p	The mesoscopic shear plastic strain acting along $\boldsymbol{m}$
Γ	The accumulated plastic mesostrain
P	The hydrostatic pressure
$\boldsymbol{N}$	The macroscopic normal stress acting on a plane of the REV
$\boldsymbol{C}$	The macroscopic shear stress acting on a plane of the REV
α_d, β_d	The coefficient of Dang Van's criterion
$\boldsymbol{\tau}$	The macroscopic resolved shear stress acting along $\boldsymbol{m}$
τ_a	The amplitude of constant amplitude macroscopic resolved shear stress
τ_{ri}	The Min-max (or range) of the i-th rainflow cycle of variable amplitude macroscopic resolved shear stress
τ_{lim}	The threshold in amplitude of non-damaging rainflow cycles of $\boldsymbol{\tau}$
$C(A_c)$	The multiplier in the relation linking the forces to the macroscopic resolved shear stress
$\mathbf{a}(A_c)$	The vector of n coefficients, linking the multi-input forces to the macroscopic resolved shear stress
$T(A_c, \boldsymbol{F})$	The threshold in range of non-damaging rainflow cycles of $F^*(A_c, \boldsymbol{F})$
q	A constant depending on the material

Basquin's criterion

B	The constant of Basquin's criterion
β	Basquin's exponent
$\mathbf{a}(A_c)$	The linear combination linking the components of the forces to the uniaxial stress tensor
$C_B(A_c)$	The multiplier in the relation linking the forces to the uniaxial stress tensor

Damage

$D(A_c, \boldsymbol{F})$	The damage induced by a sequence of forces $\boldsymbol{F}$ at the critical point A_c of a structure
$D^e(A_c, \boldsymbol{\theta})$	The expected damage induced by the EFL, defined by parameters contained in $\boldsymbol{\theta}$ at the critical point A_c of a structure

Sinusoidal EFL

ω	The angular frequency of the components of $\boldsymbol{F^e}$
A_i	The amplitude of the sinusoidal component F_i^e
ϕ_i	The phase shift of the sinusoidal component of F_i^e
A^*	The amplitude of the sinusoidal load $F^{e*}(A_c, \boldsymbol{F^e})$
ϕ^*	The phase shift of the sinusoidal load $F^{e*}(A_c, \boldsymbol{F^e})$

Gaussian EFL

$\mu(h)$	The intensity of rainflow cycles with amplitude h
$\mu^+(u)$	The intensity of upcrossings of a level u
$\mu^+_{T_0}(u)$	The expected number of upcrossings of a level u during the time period T_0
$\boldsymbol{X}$	The multi-input independent stationary Gaussian process
σ_{X_i}	The standard deviation of the i-th component of $\boldsymbol{X}$
$\sigma_{\dot{X}_i}$	The standard deviation of the derivative of the i-th component of $\boldsymbol{X}$
h	The random variable representing the amplitude of a rainflow cycle of a Gaussian process

Markov chain EFL

S	The finite state space
(u, v)	The levels of the maximum and the minimum of a rainflow cycle, respectively
$\mu^{osc}(u, v)$	The intensity of upcrossings of the interval $[u, v]$
$\mathbf{P}$	The transition matrix
p_{ij}	The transition probability to go from the state i to the state j
$\boldsymbol{\pi}$	The stationary distribution

Markov chain EFL with peaks

T_p	The life of a structure
N_p	The number of peaks during the time period T_p
(u_p, v_p)	The levels for which the number of downcrossings of the level u_p and upcrossings of the level v_p is N_p
S_p	The finite state space defining the peaks
S_{wp}	S/S_p
$\boldsymbol{\theta}_{mcp}$	The vector of parameters defining the Markov chain with peaks
$\boldsymbol{\theta}^p_{mcp}$	The vector of parameters defining the peaks of the Markov chains with peaks
$\boldsymbol{\theta}^{wp}_{mcp}$	$\boldsymbol{\theta}_{mcp}/\boldsymbol{\theta}^p_{mcp}$
$D_p(A_c, \boldsymbol{F^e})$	The damage induced by the peaks of the measurements $\boldsymbol{F}$
$D^e_p(A_c, \boldsymbol{F^e})$	The damage induced by the peaks of the Markov chain with peaks $\boldsymbol{F^e}$
$D_{wp}(A_c, \boldsymbol{F})$	$D(A_c, \boldsymbol{F^e}) - D_p(A_c, \boldsymbol{F^e})$
$D^e_{wp}(A_c, \boldsymbol{F^e})$	$D^e(A_c, \boldsymbol{F^e}) - D^e_p(A_c, \boldsymbol{F^e})$

Chapter 1

Introduction

In structures submitted to repeated variable loads, initiation and growth of cracks in the material are the most common causes of the deterioration of structures. When it happens after a long time, this failure mode is called fatigue. Under variable amplitude and repeated loads, some local cracks initiate on critical points of the structures. The fatigue phenomenon is the cause of different well-known accidents over the last hundred years. The complicated phenomenon has been discussed in many articles and books, in order to observe, explain and model it. All fields of engineering have been confronted to failures of structures incurring fatigue.

This is why proper fatigue design methods have been developed after observing, testing and analyzing structures or specimens incurring fatigue mechanisms. Nowadays, the fatigue behaviour of the mechanical components, exposed to well-known loads, can be estimated. The main problem that the designers have to solve now is the reliability of the structures in service. Structures in service are designed so that they do not reach failure during their design life when they are submitted to loads in service.

In this study, we will be particularly interested in fatigue caused by mechanical loads. The mechanical loads depend on the usage of the structure. In the automotive industry, loads on wheels depend on different factors. They are influenced by the types of roads (e.g. mountain roads or cross country), associated with the behaviour of the driver (depending on the "driving style"). The huge number of different customers implies variability in the loads. Another source of variability refers to the structure

itself, its geometry and the mechanical properties of the material. This last source is essentially due to the manufacturing process. The designers take into account these sources of variability for designing structures in service.

In order to design structures in service, forces representative of a population of customers are needed. They are called specifications. The designers adapt the geometry of the new structures so that the component will have high reliability when exposed to these specifications. This is performed by the computations of finite element models and the validation of the new structures on test rigs.

In order to be used easily, the specifications need to be simple. They are deduced from complex measurements of forces stored during the usage of the customers, or on test tracks. The equivalent fatigue approach can be a useful method for transforming complex loads, like measured forces, into simpler loads, equivalent in terms of damage. The equivalence of damage has to be fulfilled for any structures, in order to have specifications that do not depend on a particular component. The resulting forces are called the Equivalent Fatigue Loads (EFL). The EFL are not only used for calculations or test rigs. They also inform us about the severity of customers or markets.

The framework of the equivalent fatigue approach is the high cycle fatigue for metallic structures in the finite life domain. The equivalent fatigue approach has been developed for a one-input force. It allows us to evaluate a simple force, equivalent in terms of damage to a complex one-input force, see [9, 65]. Moreover, the one-input equivalent fatigue approach has been developed to structures undergoing uniaxial fatigue at their critical points, i.e. exposed to uniaxial stress field. The equivalence of damage between the one-input EFL and the measurement is verified on structures exposed to uniaxial fatigue. The one-input equivalent fatigue approach is now widely used at PSA PEUGEOT CITROËN.

However, structures in service can be submitted to multi-input forces, acting at the same time, with different amplitudes and phases. Moreover, structures can undergo uniaxial and multiaxial fatigue at their critical points, when exposed to uniaxial and multiaxial stress fields. The condition of equivalence of damage between the measurements and the EFL governs the equivalent fatigue approach. Thus, a tool for evaluating the damage of a structure undergoing multiaxial high cycle fatigue is needed. Consequently, it is necessary to extend the equivalent fatigue approach to structures submitted to multi-input forces and incurring multiaxial high cycle fatigue.

In most cases, the damage is based on local variables linked to the geometry and the material of a structure, e.g. stresses and strains. If a structure is not known, neither are these variables known. That is why it is necessary to express these variables from the forces, in order to evaluate the damage directly from the forces. However, the geometry and the material still interfere in the evaluation of the damage. Can we get rid of it in the characterization of the EFL?

The aim of this work is to extend the approach of equivalent fatigue to multi-input forces. We aim to predict the damage induced by the EFL from parameters defining them. We evaluate these parameters so that the condition of equivalence of damage is fulfilled. We also aim to extend the domain of application of the equivalent fatigue approach to the structures undergoing multiaxial fatigue.

In order to test the equivalence of damage between the measurements and the EFL, a proposition of experimental design is developed. Finally, a method to analyze the results is proposed. It is not within the scope of this thesis to discuss the results of the experiments.

1.1 Previous work

In the design process of the structures, it is essential to know the loads representative of their lives, see [62]. The variability in the forces, due to the wide panel of different customers and markets, is associated with the variability in the properties of the material and its geometry, due to the manufacturing process. The stress-strength method, presented in [13, 35, 64], is widely used in design methods, see [65]. From the stress-strength method, we can control the risk of failure of the structures. Associated with the equivalent fatigue approach, the stress strength method provides specifications and acceptance criteria for designing structures. The one-dimensional equivalent fatigue approach is exposed in [65, 9].

The prediction of the fatigue life for structures submitted to multidimensional stress fields is discussed in numerous research works and described in books and papers. In [22, 61], the multiaxial fatigue phenomena are explained in detail. In [25, 47], a state of art of the methods of multiaxial fatigue prediction is discussed. The most advanced and efficient prediction methods are mostly based on the micro-macro approach of the fatigue phenomenon, see [12, 47]. The evaluation of the damage is computed

from macroscopic stresses, using a model of the fatigue phenomenon at the scale of the grains of the metal. The damage is due to accumulated plastic deformation appearing on grains of the metal. Moreover, the application of multiaxial criteria in the frequency domain has been explored in [51, 52].

Most of the methods of life prediction from variable amplitude loads are based on the rainflow cycle counting method, see [20, 21]. The Palmgren-Miner rule of accumulation of the damage is the most frequently used because of its simplicity. Authors like [56, 57] evaluate the rainflow content from Gaussian processes. In [6, 66], the study of the damage for non-Gaussian processes was presented. From Markov chain random loads, the rainflow content has been predicted from states and a transition matrix, see [59]. The switching Markov chain is dealt with in [32]. These methods provide tools to evaluate the expected rainflow content of one-dimensional random processes. In the case of multi-input equivalent fatigue method, the expected damage needs to be evaluated from multi-input random processes.

The extension of the rainflow method to a multiaxial cycle counting method has been explored in [34]. In [18], a tool to define multiaxial rainflow cycles has been described as well. In order to deal with the multi-input equivalent fatigue approach, we need to evaluate the damage from multi-input forces. Moreover, the evaluation of the damage from multidimensional forces has been discussed in [7, 17], where a multiaxial fatigue prediction method has been used. An expression of the stresses from the forces can be found in [7, 17], but an expression of the damage from forces is not proposed.

A first proposition of equivalent fatigue approach for structures exposed to multiaxial fatigue has been described in [39]. A method to transform a variable amplitude multiaxial stress tensor, into a sinusoidal multiaxial stress tensor has been proposed. However, in the equivalent fatigue approach, the stress tensor is not known. The equivalence of damage between the forces has to be performed instead.

1.2 Overview of the thesis

An overview of the structure of the thesis is given in Fig. 1.1. It shows the different links between the chapters. The circled numbers refer to the

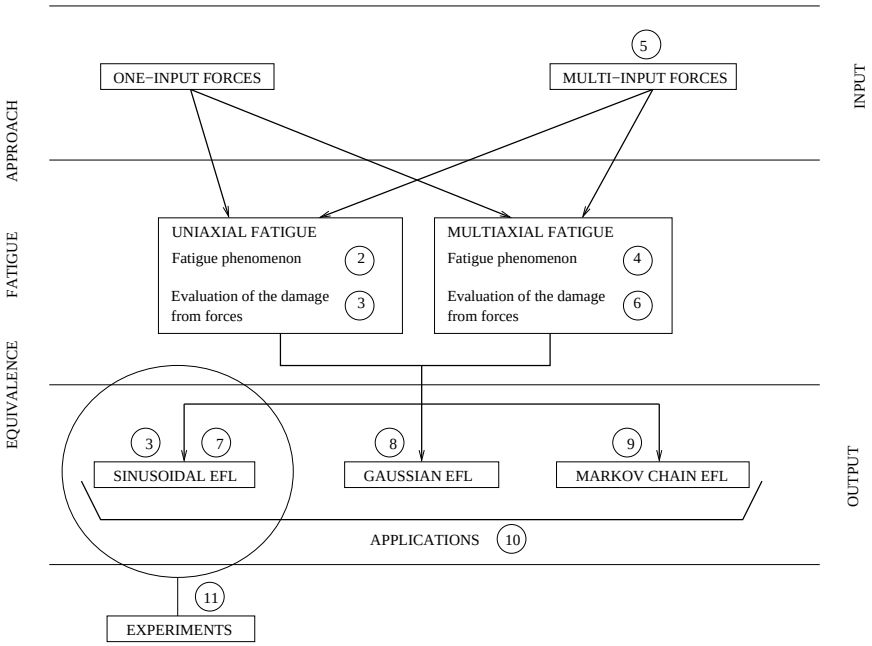

Figure 1.1: Overview of the thesis.

chapters. We aim to give a summary of the content of the chapters in the following.

Uniaxial fatigue phenomenon and uniaxial EFL

In Chapter 2, we briefly discuss the uniaxial fatigue phenomenon in high cycle fatigue. Basquin's life prediction method is presented. In order to predict life under variable stress, two methods of counting cycles are presented: the range counting method and the rainflow counting method. The latter is now widely used in fatigue analysis. In Chapter 3, the one-input equivalent fatigue approach for uniaxial stress fields, as it is used at PSA PEUGEOT CITROËN, is explained. After a brief presentation of the stress-strength method, the different steps of the process are detailed.

Multiaxial fatigue

In order to introduce the multiaxial fatigue phenomenon, several approaches and criteria for predicting life under multiaxial stress fields are explained in Chapter 4. The high cycle fatigue criteria for infinite life and finite life are differentiated. We focus on a criterion based on the micro-macro approach of the damage, Dang Van's criterion. Morel's model provides a method for the prediction of finite life. Both of them base the evaluation of the damage from macroscopic stresses, using a model of the fatigue phenomenon at the microscopic scale of the metal.

Evaluation of the damage

Part II deals with the proposition of multi-input equivalent fatigue approach. Chapter 5 deals with the motivations and needs for such a method. In this work, three different EFL are described. The motivations for the choice of such loads are given. The EFL is characterized by a set of parameters, determined by the condition of equivalence of damage between the measurements and the EFL. A synopsis exposing the different steps of the proposed method is presented at the end of Chapter 5.

In Chapter 6, the evaluation of the damage from multi-input forces is detailed. We will assume that the structures are elastic and quasi-static. This allows us to express the multi-input stress tensors from the multi-input forces. We have chosen to use Morel's model and Basquin's criterion, in order to evaluate the damage from the forces. For structures incurring multiaxial fatigue, we assume that the multiaxial stress tensor is proportional. Thus, the principal directions of the stress tensor are fixed. For uniaxial fatigue, the stronger assumption of unidirectional stress tensor is needed. We end up with two expressions of damage, depending on which criterion we use. The equivalence of damage can be deduced from these expressions of the damage from the multi-input forces.

However, the expression of the equivalence of damage does not only depend on the forces, but also on the geometry and on the material of the structures. Using Basquin's criterion, the equivalence of damage depends on a material constant, the Basquin's exponent. Using Morel's model, the equivalence of damage depends on a threshold under which a rainflow cycle of force does not induce damage, depending on the geometry, on the material and on the mean value of the loads. The concept of optimal structures is introduced, in order to evaluate this threshold.

The equivalence of damage is expressed for one-input and multi-input EFL. In the case of one-input EFL, the equivalence of damage leads to the equality between the damage induced by the EFL and the one induced by the measurements. In the case of multi-input EFL, the equality between the two types of damage is not possible to obtain. Our approach aims to minimize the difference between these two types.

Characterization of the EFL

We describe the construction of the EFL in two steps: the evaluation of the expected damage from the EFL and the characterization of the parameters defining the EFL and influencing the damage, by the condition of equivalence of damage. The development of the one-input and the multi-input EFL is detailed, using Basquin's and Morel's criteria.

The sinusoidal EFL is first described in Chapter 7. The multi-input equivalent fatigue loads with several blocks of sinusoids are also discussed. The sinusoidal EFL are characterized by amplitudes and phase shifts. Then, we have chosen to study two different probabilistic EFL. In Chapter 8, stationary narrow band Gaussian EFL are considered. The ability to determine the expected rainflow content of a narrow-band Gaussian process enables us to evaluate the expected damage induced by multi-input stationary narrow band Gaussian EFL. The multi-input Markov chain EFL are described in Chapter 9. The expected rainflow content of a multi-input Markov chain has been evaluated. We characterized the states and transition matrix of the EFL by the equivalence of damage. An extension of the Markov chain for Markov chain with peaks is proposed. The aim is to reproduce peaks occurring in the measurements, into the Markov chain EFL with peaks.

Some applications of three-input EFL are proposed in Chapter 10. Examples of three-input EFL are described. The multi-input EFL using Basquin's and Morel's criteria are compared. A threshold of non-damaging rainflow cycle are compared when using Basquin's and Morel's criteria. Finally, a method of data reduction of multi-input variable amplitude forces has been applied.

Numerical calculations

For the numerical calculations, MATLAB has been used, together with the WAFO toolbox, see [11][1].

Experiments

In Chapter 11, a proposition of validation experiments is detailed. The aim is to test the equivalence of damage between two input measurements and the bidimensional sinusoidal EFL. The evaluation of the EFL is made using Morel's model. The experimental set-up is described.

[1] The toolbox and the full documentation can be found at http://www.maths.lth.se/matstat/wafo

Part I

Background

Chapter 2

Fatigue phenomenon in uniaxial loading

Uniaxial fatigue aims to predict the durability of structures submitted to constant amplitude or variable amplitude uniaxial loading. The uniaxial stress tensors, at any location A of a structure, can be written as,

$$\mathbf{\Sigma}(A) = \sigma(A) \begin{pmatrix} 1 & 0 & 0 \\ 0 & 0 & 0 \\ 0 & 0 & 0 \end{pmatrix}.$$

The material and the geometry of the structures, as well as the loading influence the durability. Tests are carried out and models are built, in order to predict the life of the structures.

The following chapter presents only a part of the wide domain of uniaxial fatigue. The fatigue phenomenon in constant amplitude and variable amplitude loading is explored. Models of life prediction and accumulation of damage, as well as methods of counting cycles will be presented and illustrated. This chapter also aims to introduce the different tools used in the uniaxial equivalent fatigue approach.

2.1 Life prediction for constant amplitude loading

The different parameters characterizing the uniaxial constant amplitude stresses are presented in Fig. 2.1.

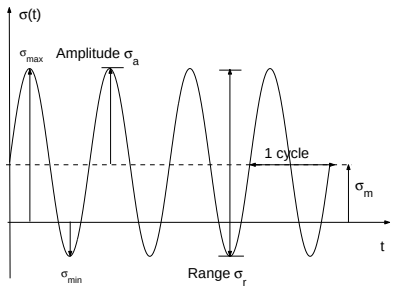

Figure 2.1: Characterization of constant amplitude loading.

The stress ratio R is often used to define the loading,

$$R = \frac{\sigma_{min}}{\sigma_{max}}.$$

The case of $R = -1$ is referred to as "fully reversed" condition of testing, and $R = 0$ as the "pulsating tension" condition.

2.1.1 S-N curve

After testing specimens at different amplitudes of loading, the S-N curve, also called the Wöhler curve, is derived. It represents the number of cycles or life to failure against the stress amplitude σ_a. Failure can be defined as fracture or crack initiation. Different stress ratios lead to different S-N curves. We often define the S-N curve for a loading at $R = -1$. In Fig. 2.2, a typical S-N curve is shown. We observe three different zones on the S-N curve (for more details, see [60]).

- The low cycle fatigue is related to the number of cycles from 10^2 to approximately 10^3 or 10^4. Stresses are close to the ultimate tensile strength σ_u. Some macroscopic plastic deformation appears.

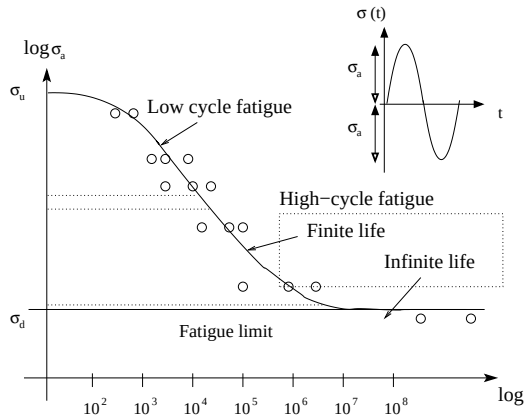

Figure 2.2: S-N curve.

- In the high cycle fatigue for finite life, the number of cycles goes from 10^4 to approximately $5\,10^5$ cycles.
- The last part is related to weak stresses and infinite fatigue life. The fatigue phenomenon can appear after a long run of loading with an amplitude close to the threshold σ_d, or may even never happen. The scatter is very high in this region. The threshold σ_d represented in Fig. 2.2 is called the fatigue limit. It is usually defined at around 10^6, 10^7 cycles. This last part is usually modeled by the asymptotic $\sigma_a = \sigma_d$.

2.1.2 Basquin's model

Basquin's relation provides an analytical expression of the S-N curve, for finite life (low or high cycle fatigue). It is the most commonly used model, see [5].

$$N = B\,\sigma_a^{-\beta}. \tag{2.1}$$

The parameters β and B are both constant, depending on the material and on the geometry, respectively. We usually represent the S-N curve in the log-log scale (see Fig. 2.2).

The simple Basquin's curve provides an estimation of life prediction, with little information on the material. The curve presented in Fig. 2.3 from [3]

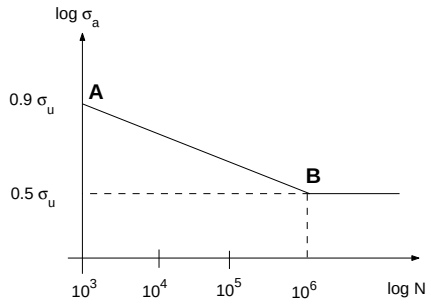

Figure 2.3: Approximation of S-N curve from the tensile strength σ_u.

is defined for a smooth specimen, with the tensile strength σ_u. Basquin's curve is deduced from the points $A : [\sigma_{a,A}, N_A]$ and $B : [\sigma_{a,B}, N_B]$, see Fig. 2.3.

$$\sigma_{a,A} = 0.9\,\sigma_u, \quad N_A = 10^3,$$

$$\sigma_{a,B} = 0.5\,\sigma_u, \quad N_B = 10^6.$$

In this case,

$$\beta = 11.75$$

From the approximation, the Basquin's coefficient can be derived. Some tests at different amplitudes of stresses are of course still essential to get the right S-N curve.

The S-N curve is a very convenient tool to predict life. However, parameters like the stress ratio, the temperature, the surface roughness or the corrosive environment substantially modifies the durability of the specimen. The influence of the stress ratio, or the mean value, is developed next.

2.1.3 Influence of the mean stress on the S-N curve

In general, positive mean stress is more damaging and negative mean stress is beneficial. The level of the S-N curve is slightly different for positive or negative mean stress. This influence is illustrated in Fig. 2.4. Different models take into account the impact of the tensile mean stress on the evaluation of life, and it particularly transferred the influence of it

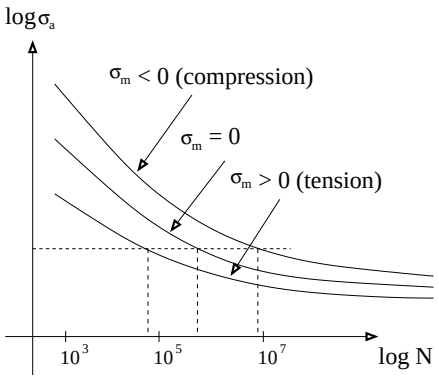

Figure 2.4: Impact of the mean stress on the S-N curve.

on the endurance limit σ_d (see [63]). One of them is the Gerber parabola, representing the tensile mean stress effect on σ_d,

$$\frac{\sigma_d}{(\sigma_d)_{\sigma_m=0}} + \left(\frac{\sigma_m}{\sigma_u}\right)^2 = 1, \quad \text{with} \quad |\sigma_m| \leq \sigma_u.$$

The Gerber parabola, illustrated in Fig. 2.5, can still be used for high values of N (see [22, 43, 60]).

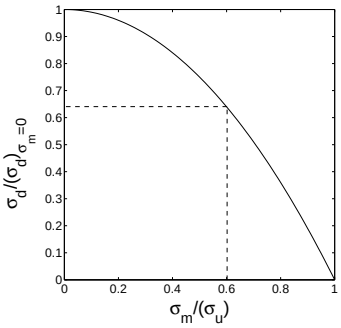

Figure 2.5: Gerber parabola.

Goodman's model is more appropriate in order to predict the positive ef-

fect of compressive mean stress,

$$\frac{\sigma_a}{\sigma_d} + \frac{\sigma_m}{\sigma_u} = 1 \quad \text{with} \quad |\sigma_m| \leq \sigma_u.$$

2.1.4 Cumulative damage and life prediction

Any cyclic stress over the fatigue limit produces permanent fatigue damage in the structure. The damage D_i induced by n_i cycles of amplitude σ_{ai} is related to N_i, the total number of cycles before failure at constant amplitude σ_{ai}. In order to estimate the partial damage induced by n_i cycles, Miner has suggested the following expression of D_i (see [38]),

$$D_i = \frac{n_i}{N_i}. \tag{2.2}$$

Let's consider k different blocks of sinusoids, with different stress levels σ_{ai} and number of cycles n_i. We will assume that the mean value of the different blocks is 0. The damage induced by each block is given by Eq. (2.2). The damage induced by the k blocks is called D. In [46], Palmgren suggested that,

$$D = \sum_{i=1}^{k} D_i \tag{2.3}$$

Together with Eq. (2.2), the Palmgren-Miner rule gives,

$$D = \sum_{i=1}^{k} \frac{n_i}{N_i}. \tag{2.4}$$

Failure is predicted if :

$$D = D_1 + D_2 + \ldots D_k \geq 1.$$

However, there are different cumulative fatigue damage and prediction theories, discussed e.g. in [22]. Indeed the sequential effect is neglected in the linear accumulation of damage, e.g. in the case of blocks of constant amplitude loading. This is the main drawback of it. Then, from Fig. 2.6,

$$D_{\text{Case1}} \neq D_{\text{Case2}}.$$

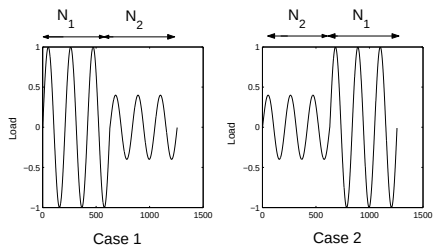

Figure 2.6: Sequential effects on blocks of constant amplitude loading.

In the case of random loading, cumulative damage rules including sequential effects are not more accurate than models neglecting them. That is why the Palmgren-Miner accumulation of damage is still used (see [63, 44]).

2.2 Variable amplitude loading and damage

Structures in service generally incur variable amplitude loading. Examples of possible loading in service are given in Fig. 2.7. In fatigue application, it is a well-known fact that only maxima and minima influence the life prediction, and not the points between them. In this context, we suppose that the frequency of loads has no impact on life prediction. Minima and maxima are called the turning points of the process. For variable amplitude loading, it is quite common to decompose the signal into basic cycles. Different methods of extracting cycles will be presented.

2.2.1 Range counting

The range counting method is a method of extracting cycles of a variable amplitude process. It counts the load ranges. A load range starts at a turning point, at a level u, and is completed by the successive turning point at a level v. Consequently, the range is the difference $v - u$. A positive range comes from a minimum to a maximum ($u < v$). A negative range comes from a maximum to a minimum($v < u$). The range counting method is illustrated in Fig. 2.8. Each range cycle can be characterized by its minimum, its maximum and its number of occurrences.

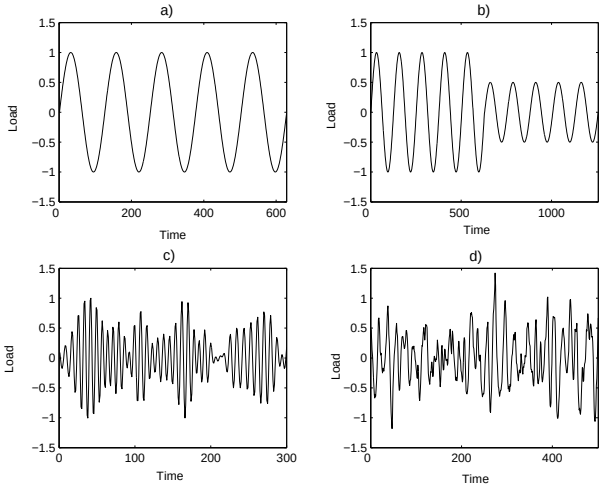

Figure 2.7: Samples of sinusoidal loading (graph a), sinusoidal loading by blocks (graph b), narrow band loading (graph c) and broad band loading (graph d).

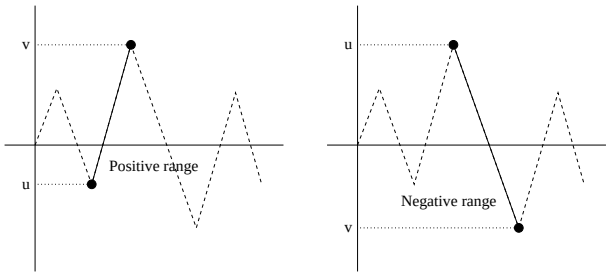

Figure 2.8: Range counting method: The ranges are the differences in heights between the maximum and minimum.

2.2.2 Rainflow counting

The rainflow counting method is performed to extract cycles from successive turning points. It has been proposed by Endo in 1967, [20, 21]. The rainflow cycle counting method is actually the most popular and effective way of extracting cycles (see [14, 63]) in the context of fatigue life prediction. Rainflow cycles and damage are assumed to be a function of hysteresis loops in the stress-strain plane, see Fig. 2.9.

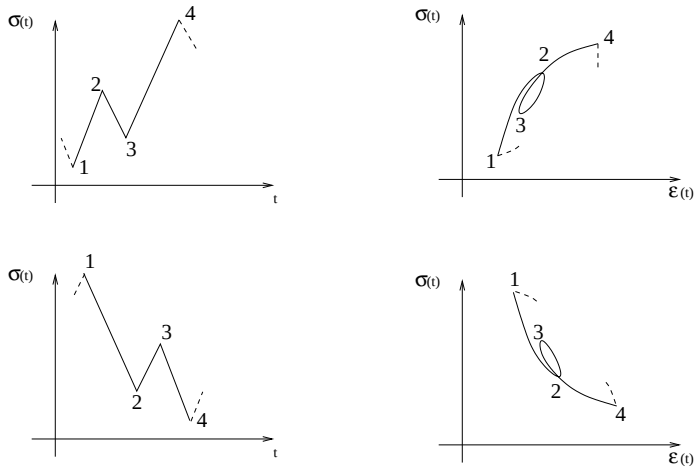

Figure 2.9: Hysteresis loops in the stress strain plane.

Here follows a definition of the rainflow cycle algorithm, given by Rychlik in [55]. Rainflow cycles are related to level crossings of the process. Upcrossings and downcrossings are illustrated in Fig. 2.10. The intensity of upcrossings and downcrossings of the level u is called $\mu^+(u)$, and $\mu^-(u)$, respectively. The intensity of level crossings of u is called $\mu(u)$,

$$\mu(u) = \mu^+(u) + \mu^-(u). \tag{2.5}$$

We will adopt the following definition of the rainflow counting cycles, from [55].

Definition 2.1. ***Rainflow cycle counting.*** *Let $X(t)$ be a function with $0 \leq t \leq T$, with finite number of local maxima and minima. Let's consider that a local maxima M_i appears at a time point t_i. Let $t_i^+ \in [t_i, T]$ be the time of the*

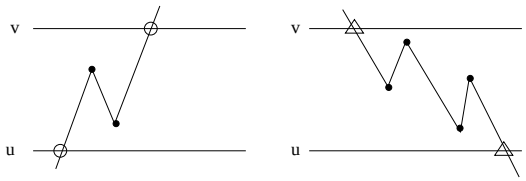

Figure 2.10: Markers ∘ are upcrossings and markers △, the downcrossings, among the turning points •.

first upcrossing of the level $X(t_i)$. If no such upcrossings appear in the time interval $[t_i, T]$, then $t_i^+ = T$. The time point $t_i^- \in [0, t_i]$ is defined as the last downcrossing of the level $X(t_i)$. If no such downcrossing appear in the time interval $[0, t_i]$, then $t_i^- = 0$. We define:

$$\begin{aligned} m_i^- &= \inf\{X(t) : t_i^- < t < t_i\} \\ m_i^+ &= \inf\{X(t) : t_i < t < t_i^+\}. \end{aligned}$$

The i:th rainflow cycle of the process $X(t)$ is defined by its minimum m_i^{rfc} and its maximum M_i^{rfc} such as:

$$\begin{aligned} M_i^{rfc} &= M_i \\ m_i^{rfc} &= \begin{cases} max(m_i^-, m_i^+) & \text{if } t_i^+ < T, \\ m_i^- & \text{if } t_i^+ = T. \end{cases} \end{aligned}$$

We call cycles $\{m_i^{rfc}, M_i^{rfc}\}$ standing cycles, when the minimum occurs before the maximum. For hanging cycles, the maximum occurs before the minimum. This refers to the hysteresis loop, in Fig. 2.9.

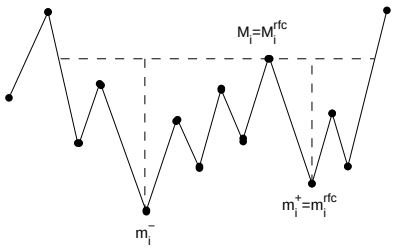

Figure 2.11: Definition of rainflow cycles.

Another common technique of rainflow counting is the method of the "four-points", recommended by the AFNOR, see [1]. It is based on the comparison of the three different amplitudes composed by four successive points of the process. The condition of extracting cycles is $Y \leq X$ and $Y \leq Z$ with $Y = |X(t_{i+1}) - X(t_{i+2})|$, $X = |X(t_i) - X(t_{i+1})|$ and $Z = |X(t_{i+2}) - X(t_{i+3})|$. These two techniques lead to the same rainflow cycles.

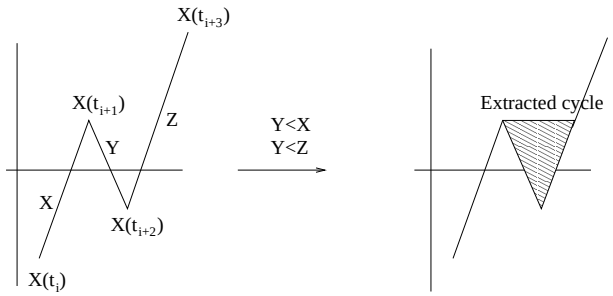

Figure 2.12: Illustration of extracting rainflow cycles [1].

The points that do not belong to any rainflow cycle representing close hysteresis loops are part of the residual. It contains the maximum and the minimum turning points over the sequence. A treatment of the residual is proposed in [1].

The rainflow cycles can be represented from the triplet $\{m_i, M_i, n_i\}$, or from $\{\sigma_{ai}, \sigma_{mi}, n_i\}$, such as,

$$\sigma_{ai} = (M_i - m_i)/2$$
$$\sigma_{mi} = (M_i + m_i)/2$$
n_i : number of occurrences.

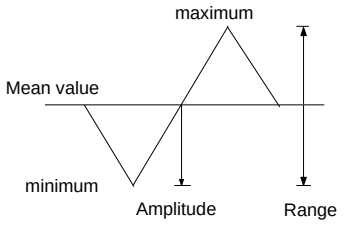

In Fig. 2.13, rainflow cycles are represented in a rainflow matrix.

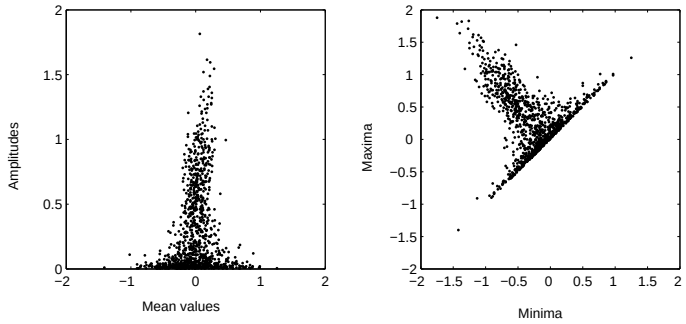

Figure 2.13: Two representations of the same rainflow cycles.

The discretization of the turning points is often carried out. The recommended number of classes is usually 64.

2.2.3 Damage accumulation

It has been seen that the rainflow cycle counting method used together with the Palmgren-Miner accumulation of damage gives an acceptable assessment of life (see [15]). It is used on every cycle $\{\sigma_{ai}, \sigma_{mi}, n_i\}$. Consequently, damage induced by the n_i number of rainflow cycles is defined by the ratio between n_i and N_i, the number of sequences deduced from the S-N curve, at the amplitude σ_{ai}:

$$D_i = \frac{n_i}{N_i}.$$

Then, the damage induced by the whole sequence, with k rainflow cycles extracted can be evaluated:

$$D = \sum_{i=1}^{k} D_i = \sum_{i=1}^{k} \frac{n_i}{N_i}.$$

However, the S-N curve is usually evaluated for zero mean stresses. It is recommended to convert non-zero mean stress cycles, into a fully reversed cycle, equivalent in terms of damage. If the mean stress diagrams are

available for the proper material, these data may be used. If not, models like Gerber parabola can be used, in order to transform cycles $\{\sigma_{ai}, \sigma_{mi}, n_i\}$ into $\{\sigma'_{ai}, 0, n_i\}$, equivalent in terms of fatigue.

From the point of view of fatigue, small rainflow cycles will create less damage than others, or even no damage at all. Rainflow filter can be proceeded in life prediction methods. However, the most important problem is to fix the threshold, under which an amplitude of rainflow cycle does not induce damage. Series of experiments have shown that neglecting cycles with amplitudes below the fatigue limit can lead to dangerous non-conservative results. An allowable filter of 50% of the fatigue limit seems to be more appropriate. For more details, see [16, 31].

Chapter 3

Uniaxial equivalent fatigue loading

In this chapter, the uniaxial equivalent fatigue approach is presented. However, in order to get an overview of the domain of application of this method, we will first recapitulate the main aims of the stress-strength method.

3.1 Stress-strength method

The stress-strength is a tool to control the risk of failure in the design process of new structures, taking into account the variability of the mechanical properties of the structures and the variability in the loads. In the stress-strength method, the mechanical properties are called strength, and the loads, stress.

In the automotive industry, in order to estimate the variability in the loads, measurements on test tracks or during customers'usage are stored and analyzed. For each customer, the measurements are transformed into an equivalent fatigue load. The equivalent load is usually a constant amplitude force, defined by an amplitude. The number of cycles is usually fixed, see [8, 65]. The amplitude of the equivalent load represents the severity of

the customer. Each customer has a different severity. A population of customers is represented by a distribution of severities.

Information about the distribution of the strength is actually gained by experience. Consequently, the variability induced by the manufacturing process is usually well known from the designers. The main tasks of the designers is to adapt the mean strength of the new component in order to respect the risk of failure, imposed by the manufacturer.

The value of the equivalent fatigue loading is the scalar measuring the severity of the customers. The analysis of the equivalent fatigue loading in a population allows us to determine the distribution of the severity. We do not have information about the structures the forces are applied to as it does not exist yet. Consequently, the evaluation of the EFL has to be performed independently of the structure.

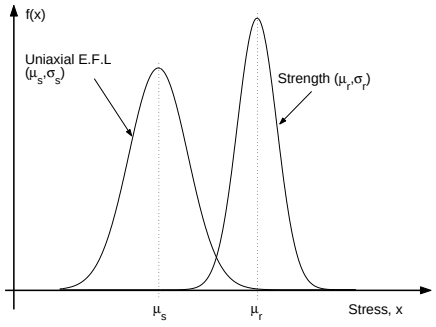

Figure 3.1: Probability distributions of stress and strength.

Stress distribution

Usually, the stress distribution can be modeled by a normal distribution, defined by the mean value μ_s and the standard deviation σ_s, see Fig. 3.1. The random variable defining the stress is called s. The distribution is estimated from the analysis of amplitudes of equivalent fatigue loads, deduced from customers'usage. The greater the amplitude of the EFL is, the more severe is the customer.

Strength distribution

In order to be homogeneous with the stress distribution, the strength is also defined as forces. We often assume that the distribution of the strength r is normal, and defined by the mean and the standard deviation μ_r and σ_r. The parameter $q = \sigma_r / \mu_r$ is known often from experience. This parameter q partly corresponds to the control of the process of manufacturing. The scatter is also intrinsic to the material. The parameter q is small for a well-controlled process of manufacturing.

The risk

Let's now consider the following random variable z as $z = r - s$, which is normally distributed with mean value μ_z and standard deviation σ_z. The distribution of z is defined by its standard deviation $\sigma_z = \sqrt{\sigma_s^2 + \sigma_r^2}$ and its mean value $\mu_z = \mu_r - \mu_s$. The risk R is deduced from the probability that z is negative. It is the probability to failure,

$$R = P(z < 0).$$

3.2 The uniaxial equivalent fatigue approach

The target is to evaluate the characteristics of the uniaxial EFL F^e. The uniaxial EFL is a sinusoidal force, with an amplitude called F_a^e and N_0 cycles. In practice, N_0 is settled at 10^6. The mean of the EFL is zero. The first step of this section is the evaluation of the damage from the force. We will then describe the characterization of F^e so that it fulfills the equivalence of damage with F. The uniaxial equivalent fatigue approach is governed by two assumptions.

Assumption 3.1. ***Elastic and quasi-static structures.*** *The global behaviour of the structures is supposed to be elastic and quasi-static.*

Moreover, every location of a structure gives rise to a proper relation between the force and the stress tensor, depending on the geometry and on the material. In any structures incurring loads, crack initiation is more likely at the critical points of a structure. The durability of the components completely depends on the behaviour of these critical points. We

will concentrate on them in this study. The first critical point reaching a damage equal to one is called A_c. At the critical point A_c, we will consider that the stress tensor is uniaxial.

Assumption 3.2. ***Uniaxial stress tensor.*** *At the critical point A_c of the structures, the stress tensor $\mathbf{\Sigma}(A_c, F)$ is supposed to be uniaxial,*

$$\mathbf{\Sigma}(A_c, F) = \sigma(A_c, F) \begin{pmatrix} 1 & 0 & 0 \\ 0 & 0 & 0 \\ 0 & 0 & 0 \end{pmatrix}.$$

The use of the uniaxial EFL has been restricted to the structures that fulfill Assumption 3.1 and Assumption 3.2.

3.2.1 Evaluation of the damage from the forces

The damage is usually expressed from the stress component $\sigma(A_c, F)$. In the equivalent fatigue approach, the geometry of the structures is supposed to be unknown. Consequently, in order to build a uniaxial EFL, we need to evaluate the damage from the forces, instead.

As is shown in Fig. 3.2, the evaluation of the damage from the forces is split into two different steps. The first step is devoted to finding a general expression of the stress component from the force F (as indicated by $\{\mathbf{1}\}$ in Fig. 3.2). With the help of a fatigue criterion, we can evaluate the damage from components of the stress tensor (step denoted as $\{\mathbf{2}\}$). We finally get a model to evaluate damage from variable amplitude loading (denoted by $\{\mathbf{1}+\mathbf{2}\}$).

General expression of stress from the uniaxial force (step $\{\mathbf{1}\}$ in Fig. 3.2)

Under the hypothesis of elastic structure, the stress component $\sigma(A_c, F)$ is proportional to the force F.

$$\sigma(A_c, F) = k(A_c)\, F. \tag{3.1}$$

The coefficient $k(A_c)$ depends on the geometry and on the material.

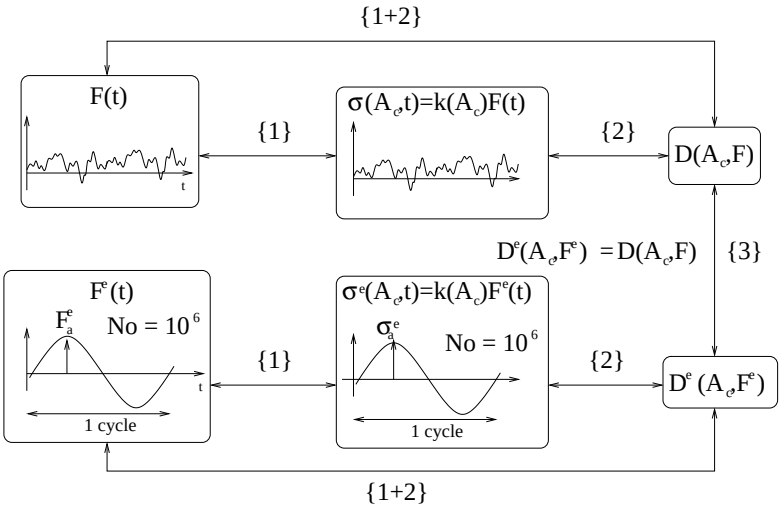

Figure 3.2: Steps of the one-input equivalent fatigue approach.

Evaluation of the damage from variable amplitude stress (step $\{2\}$ in Fig. 3.2)

The aim is now to evaluate the number of cycles before failure from variable amplitude stress. This will be done at the critical point A_c of a structure, defined by its proper $k(A_c)$. Basquin's curve has been chosen to evaluate the damage from $\sigma(A_c, F)$ and is shown in Eq. (2.1). Parameters B and β are the parameters of Basquin's criterion, and depend on the material. We usually approximate the exponent $\beta \simeq 8$, for steels. Let's consider a zero mean cycle of stress, with an amplitude $\sigma_a(A_c, F)$. The number of cycles N and $\sigma_a(A_c, F)$ is linked by,

$$N_j \ (\sigma_a(A_c, F))^{\beta} = B(A_c). \tag{3.2}$$

Mean value effect

In order to take into account the impact of the mean value, a correction on the amplitude σ_{aj} into σ'_{aj} is made, so that the couples $(\sigma_{aj}, \sigma_{mj}, n_j)$ and $(\sigma'_{aj}, 0, n_j)$ are equivalent in terms of damage [8, 9]. The extension of the

Gerber's parabola to any non-zero mean stress cycle is used. It is restricted to mean values σ_{mj} under the tensile strength σ_u.

$$\sigma'_{aj}(A_c, F) = \frac{\sigma_{aj}(A_c, F)}{\left(1 - \left(\frac{\sigma_{mj}(A_c,F)}{S_u}\right)^2\right)} \quad \text{with} \quad |\sigma_{mj}(A_c, F)| < \sigma_u. \tag{3.3}$$

Damage accumulation

Let's consider as N_j the number of cycles to failure under the stress amplitude σ'_{aj}. From Eq. (3.2), we get,

$$N_j \left(\sigma'_{aj}(A_c, F)\right)^\beta = B(A_c)$$

The Palmgren-Miner accumulation of damage is adopted. So, Eq. (2.4) holds. From Eq. (3.2) and Eq. (3.3), we get,

$$D(A_c, F) = \sum_j n_j \frac{1}{B(A_c)} \left(\frac{\sigma_{aj}(A_c, F)}{1 - \left(\frac{\sigma_{mj}(A_c,F)}{\sigma_u}\right)^2} \right)^\beta. \tag{3.4}$$

Evaluation of the damage from uniaxial force (step $\{\mathbf{1}+\mathbf{2}\}$ in Fig. 3.2)

From the extraction of rainflow cycles from F, we get cycles defined by (F_{aj}, F_{mj}, n_j). From Eq. (3.1),

$$\begin{aligned} \sigma_{aj}(A_c, F) &= k(A_c) F_{aj}, \\ \sigma_{mj}(A_c, F) &= k(A_c) F_{mj}. \end{aligned} \tag{3.5}$$

Thus, from Eq. (3.3), we get,

$$F'_{aj} = \frac{F_{aj}}{1 - \left(\frac{k(A_c)F_{mj}}{S_u}\right)^2}. \tag{3.6}$$

If we refer to a standard S-N curve, as shown in Fig. 2.3, the endurance limit is reached at 10^6 cycles. Consequently, as F^e is supposed to be a sinusoidal zero mean force, the ratio between σ_d and F^e_a is the coefficient $k(A_c)$,

$$\sigma_d = k(A_c)\, F^e_a.$$

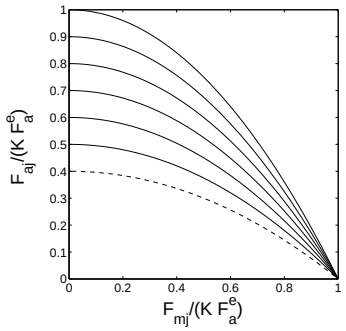

Figure 3.3: Network of Gerber parabola.

An approximation of the ratio between the tensile strength σ_u and the fatigue limit σ_d has been proposed in [9],

$$K = \frac{\sigma_u}{\sigma_d} \simeq 2.5 \quad \text{(for steel [65])}. \tag{3.7}$$

From Eq. (3.6) and Eq. (3.7),

$$F'_{aj} = \frac{F_{aj}}{1 - \left(\frac{F_{mj}}{K F_a^e}\right)^2}. \tag{3.8}$$

In Fig. 3.3, Gerber's parabola correspond to different values of $1/(K F_a^e)$. So, from Equations (3.4, 3.5, 3.8),

$$D(A_c, F) = \frac{1}{B(A_c)} \left(k(A_c)\right)^\beta \sum_j n_j \left(\frac{F_{aj}}{1 - \left(\frac{F_{mj}}{K F_a^e}\right)^2} \right)^\beta. \tag{3.9}$$

3.2.2 Equivalence of damage and characterization the equivalent fatigue loading

The number of rainflow cycles of F^e is N_0 and the amplitude of all of them is F_a^e. The mean of the uniaxial EFL is zero. The damage induced by the F^e can be evaluated,

$$D^e(A_c, F^e) = \frac{1}{B(A_c)} \left(k(A_c)\right)^\beta N_0 \ (F_a^e)^\beta. \tag{3.10}$$

The last step (denoted as {3} in Fig. 3.2) is deduced from Eq. (3.9) and Eq. (3.10),

$$D^e(A_c, F^e) = D(A_c, F),$$

then,

$$\sum_j n_j \left(\frac{F_{aj}}{1 - \left(\frac{F_{mj}}{K F_a^e}\right)^2} \right)^\beta = N_0 \, (F_a^e)^\beta \, . \tag{3.11}$$

We can conclude that no parameter depending on the geometry intervenes in the expression of Eq. (3.11). It is valid for any structure, fulfilling Assumption 3.1 and Assumption 3.2. Two constants depending on the material are present, K, given in Eq. (3.7), and the Basquin's exponent β. A numerical value has been proposed, which is appropriate for steels.

3.3 Conclusion

The evaluation of the damage from the variable amplitude force F is based on the rainflow content of the variable amplitude force. The Gerber's parabola are used in order to take into account the impact of the mean values of the rainflow cycles on the damage. An extra assumption about the ratio between the tensile strength and the fatigue limit was needed. Basquin's criterion and Palmgren-Miner accumulation of damage are used in order to evaluate the damage from the variable amplitude loads. The determination of the amplitude of the zero-mean equivalent fatigue force is governed by the equality of the damage induced by the measurements and the damage induced by the one-input EFL. The calculation of the amplitude of the EFL requires numerical solving.

Chapter 4

High cycle fatigue life prediction under multiaxial loading

Life prediction in multiaxial fatigue is a wide, recent and complex domain of fatigue. This has been discussed in numerous research work, in order to understand, analyze and predict life of structures under constant and variable amplitude multiaxial stresses. In general, in high cycle fatigue, no plastic deformation is visible at the macroscopic scale. Fatigue is governed by initiation and growth of cracks. In automotive industry, the life is mostly covered by the initiation of cracks, because the crack growth duration is relatively short.

The first studies in multiaxial fatigue are empirical approaches, based on experimental results (e.g. Gough and Pollard). Then, the macroscopic approaches have been developed. The proposed criteria are based on macroscopic quantities. Some of them are based on stresses, like shear stresses or invariant (e.g. Mc Diarmid, Sines, Crossland). Synthesis of the empirical and the macroscopic approach can be found e.g. in [19, 47, 61, 63]. A historical state of art of multiaxial fatigue is presented in [25]. Other macroscopic criteria are based on the energy dissipated by the strain work (e.g. Palin-Luc [4]). Micro-macro approaches are closely related to the microscopic phenomenon of fatigue, (e.g. Dang Van [12], Papadopoulos [47, 48], Morel [39, 40, 41]). The evaluation of the damage is computed

from macroscopic stresses, using a model of the fatigue phenomenon at the scale of the grains of the metal.

Two classes of criteria can be differentiated. One class contains the high cycle multiaxial fatigue criteria. In this case, we aim to define the loading for which the life of the structure is infinite and the loading for which the life is finite. For each loading, we can estimate if the structure will break or not. The other class of fatigue criteria predicts the life of components in a finite life domain of multiaxial fatigue, i.e. it provides a way of computing damage from constant amplitude and variable amplitude loading. In the general framework of multi-input EFL, these criteria are needed.

4.1 A high cycle fatigue criterion for infinite life, Dang Van's criterion

The micro-macro approach in high cycle fatigue seems to be the most advanced approach in the last few years. We will describe the Dang Van's criterion, precursor of this approach, see [12]. Criteria based on the micro-macro approach of the fatigue phenomenon follow the same idea that the nucleation of microcracks is at the origin of the fatigue phenomenon. These small cracks grow until they are detected on the macroscopic scale.

The macroscopic stress tensor is defined in the minimum volume where no heterogeneity is observable. This is called the representative elementary volume (REV). At the macroscopic scale, the REV is homogeneous. The macroscopic stress tensor is defined at this scale. In high cycle fatigue, near the fatigue limit, the elastic shakedown is reached after a few cycles and consequently the material remains elastic.

The REV is composed of many grains. At the scale of a grain, the material is not homogeneous. Even if the macroscopic behaviour of the material is elastic, plastic flow can appear in some grains of the REV where the elastic limit has been reached. It is at the origin of the crack initiation in the grain. Although we associate this approach with the micro-macro approach, in contrast to the macroscopic approach, all the phenomena at the origin of the fatigue phenomenon are described at the grain scale. The scale of a grain is rather called the mesoscopic scale. We will use this scale in the following.

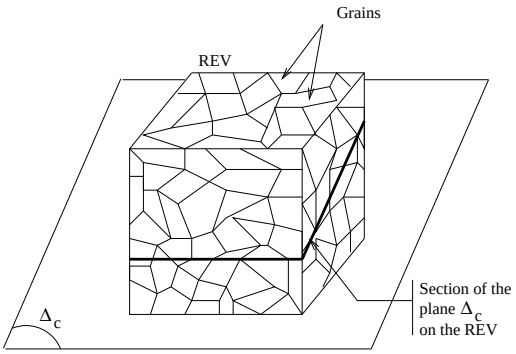

Figure 4.1: Representation of a REV and a plane Δ_c.

The criterion aims to characterize the macroscopic loading that induces the crack initiation in the REV. Papadopoulos has also formulated a criterion based on the same principle as Dang Van. It is easier to use, and also provides good results, see [50].

Each metal grain, also called crystal, has its own orientation, where plastic strain is more likely to appear when incurring loading. This orientation is called the easy glide direction. In an REV, we suppose that the grains are randomly orientated. Thus, the REV is made up of grains of many different orientations. Some grains will experience more plastic strains than others, and will be more damaged. Crack initiation is more likely to appear first in those grains. The plasticity in some grains is due to the mesoscopic shear stress. We will be interested in the plane Δ_c of the REV, which incurs the maximum amplitude of mesoscopic shear stress, see Fig. 4.1. The grains with an orientation that coincides with Δ_c will be damaged first. At the macroscopic level, stresses applied to a plane are decomposed into two parts, the shear stress, defined as a column vector $\boldsymbol{C}(t)$ and the normal stress $\boldsymbol{N}(t)$, see Fig. 4.2. The shear stress describes the amplitude over time of the cyclic stress resulting from the projection of $\boldsymbol{\Sigma}(t)$, on a plane of normal unit vector $\boldsymbol{n}$:

$$\boldsymbol{N}(\boldsymbol{n},t) = \left(\boldsymbol{n}^T \cdot \boldsymbol{\Sigma}(t) \cdot \boldsymbol{n}\right)\, \boldsymbol{n}, \tag{4.1}$$

and

$$\boldsymbol{C}(\boldsymbol{n},t) = \boldsymbol{\Sigma}(t) \cdot \boldsymbol{n} - \left(\boldsymbol{n}^T \cdot \boldsymbol{\Sigma}(t) \cdot \boldsymbol{n}\right)\, \boldsymbol{n}. \tag{4.2}$$

In Fig. 4.2, the normal stress and the shear stress are represented, applied to any plane Δ of the REV. A metallic structure incurs elastic shakedown

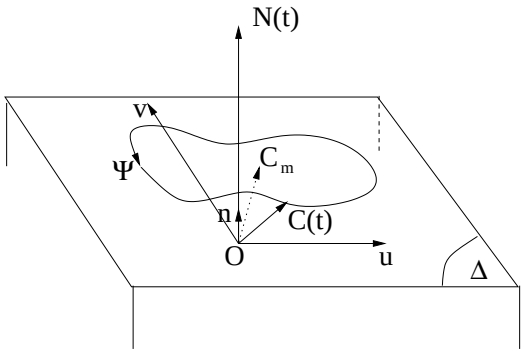

Figure 4.2: The loading on a shear plane are defined by the shear stress $\boldsymbol{C}(t)$ and the normal stress $\boldsymbol{N}(\boldsymbol{n}, t)$. The axis system related to the plane is $(0, u, v)$.

when, after several cycles inducing plasticity, the response of the structure becomes elastic. Dang Van has assumed that the structure must incur elastic shakedown at the mesoscopic and the macroscopic scale to be in an infinite life regime. The structure tends to adapt. The mesoscopic shear stress in the adapted conditions is called $\boldsymbol{c}(\boldsymbol{n}, t)$. It can be expressed from the macroscopic shear stress $\boldsymbol{C}(\boldsymbol{n}, t)$, under the conditions of adaptation as:

$$\boldsymbol{c}(\boldsymbol{n}, t) = \boldsymbol{C}(\boldsymbol{n}, t) - C_m(\boldsymbol{n}), \tag{4.3}$$

where $C_m(\boldsymbol{n})$ is the center of the minimum circumscribed circle to $\boldsymbol{C}(\boldsymbol{n}, t)$.

Dang Van's criterion is based on the hydrostatic pressure $P(t)$ and shear stress $\boldsymbol{c}(\boldsymbol{n}, t)$. No plasticity appears in the most damaged grains of the REV if,

$$\max_{\boldsymbol{n}} \left[\max_{t} \left[\|\boldsymbol{c}(\boldsymbol{n}, t)\| + \alpha_d P(t) \right] \right] \leq \beta_d. \tag{4.4}$$

The parameters α_d and β_d are called Dang Van's parameters and depend on the material. Plasticity in the most damaged grains appears if Eq. (4.4) is violated. We need to evaluate the plane Δ_c for which the maximum amplitude of the shear stress is reached. Consequently, we need to maximize the shear stress over the different plane, and over the time t.

Dang Van's criterion is usually represented in graphs, relating the shear stress $\boldsymbol{c}(\boldsymbol{n}, t)$ and $p(t)$.

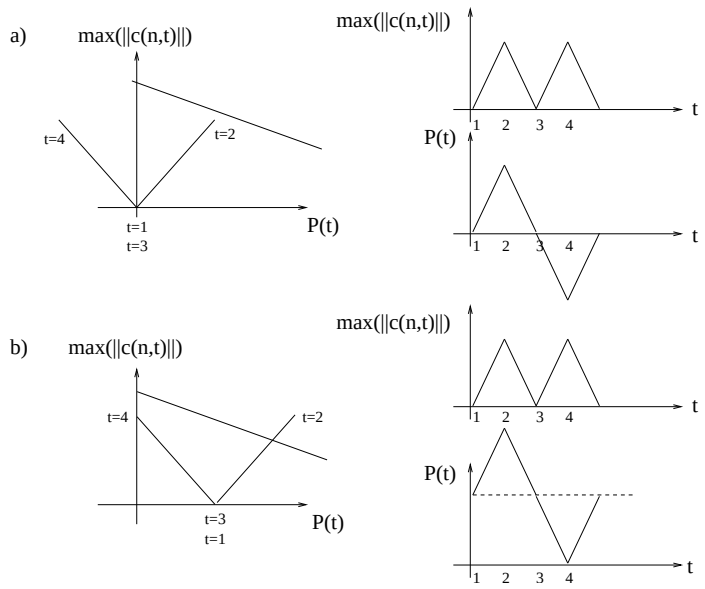

Figure 4.3: Examples of representation of the Dang Van's criterion. In case a), no crack initiation predicted. In case b), crack initiation predicted.

Crack initiation appears if the cyclic loading crosses Dang Van's limit, defined by a line with intercept β_d and slope α_d. This corresponds to the case b) in Fig. 4.3. In graph a), crack initiation will not happen.

4.2 Multiaxial criterion for finite life prediction

Dang Van's criterion and many other criteria have been developed and tested so far. However, they concern the infinite life domain of high cycle fatigue. We can not access finite life prediction and damage. There exists several different criteria, leading to the prediction of life. We can distinguish two different ways of predicting life. The macroscopic approach allows us to evaluate damage from macroscopic magnitudes, related to the macroscopic stress tensor. For example, criteria from Macha and Robert (see [23, 37, 43]) are based on the macroscopic approach. The second approach is based on the micro-macro approach, and on the elastic shakedown phenomenon. Morel and Papadopoulos are examples of them. Morel's criterion will be discussed in the following.

4.3 Morel's model

Morel's criterion is based on the micro-macro approach introduced and developed by Dang Van and Papadopoulos. In the high cycle fatigue regime, some grains can undergo plasticity, while the macroscopic behaviour of the REV remains elastic. Cracks initiate at the scale of the grains of the REV. Crack initiation in a grain is due to accumulated plastic strain appearing at the mesoscopic scale. The passage from the macroscopic scale to the mesoscopic scale has been modeled, in order to predict the fatigue phenomena in the mesoscopic scale, with magnitudes related to the REV.

In each metal grain or crystal, the plastic strain is due to plastic glide appearing along a particular direction, called the easy glide direction. In a REV, we suppose that the grains are randomly orientated. Thus, the REV is made up of grains of many different orientations. Some grains will experience more plastic strains than others, and will be more damaged. Crack initiation is more likely to appear first in those grains. Morel uses the accumulated mesoscopic plastic strain Γ, as a variable of damage.

Plastic strain in a grain is due to plastic mesoscopic shear stress, occurring along the easy glide direction of a grain. The easy glide direction of a grain belongs to the easy glide plane. An easy glide plane is defined by its normal vector $\boldsymbol{n}$. It is located by its spherical co-ordinates, by the angles θ and ϕ. An easy glide direction on it is defined by its unit vector $\boldsymbol{m}$. It is located by the angle ψ. The couple $(\boldsymbol{n}, \boldsymbol{m})$ is the easy glide system. Only one easy glide system is assumed to be active in a grain. This is illustrated in Fig. 4.4. The vector $\boldsymbol{C}$, the macroscopic shear stress, is defined by Eq. (4.2). The mesoscopic shear plastic strain γ_p is due to the mesoscopic shear stress $\boldsymbol{\tau}$, acting on $\boldsymbol{m}$. Papadopoulos, in [47, 49], has established that the mesoscopic shear stress is related to the macrosopic resolved shear stress $\boldsymbol{\mathcal{T}}$ by Eq. (4.5),

$$\boldsymbol{\tau} = \boldsymbol{\mathcal{T}} - \mu \gamma_p \boldsymbol{m}. \tag{4.5}$$

The factor μ is material dependent. The magnitudes $\boldsymbol{\tau}$ and $\boldsymbol{\mathcal{T}}$ are the mesoscopic and macroscopic resolved shear stresses, respectively. They are deduced from the projection of the $\boldsymbol{\sigma}$ and $\boldsymbol{\Sigma}$, the mesoscopic and macroscopic stress tensors, respectively, on $\boldsymbol{m}$,

$$\begin{aligned} \boldsymbol{\tau} &= (\boldsymbol{m}^T \cdot \boldsymbol{\sigma} \cdot \boldsymbol{n})\, \boldsymbol{m}, \\ \boldsymbol{\mathcal{T}} &= (\boldsymbol{m}^T \cdot \boldsymbol{\Sigma} \cdot \boldsymbol{n})\, \boldsymbol{m}, \\ &= \mathcal{T}\, \boldsymbol{m}. \end{aligned}$$

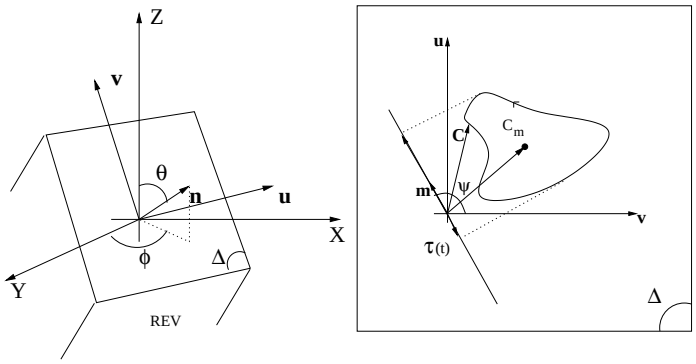

Figure 4.4: Location of a slip band of a grain, through the gliding system (***n***,***m***). The unit vector ***n*** is normal to the plane Δ. The unit vector ***m*** belongs to the plane Δ.

The norm of $\boldsymbol{\tau}$ is called τ.

4.3.1 Constant amplitude loads

The method of fatigue life prediction for constant amplitude similar and non-similar loading has been developed and discussed in [39, 40, 42]. In the case of constant amplitude loads, the components of the stress tensor $\boldsymbol{\Sigma}$ can be expressed with an amplitude, a mean value, and a phase shift.

Location of the critical plane and the critical direction

The aim is to predict the location of the critical plane and the critical direction. The quantities $\boldsymbol{\tau}$ and $\boldsymbol{\tau}$ are both sinusoidal, with amplitudes τ_a and $\boldsymbol{\tau}_a$, respectively. Let's consider $T_\sigma(\theta, \phi)$ such that,

$$T_\sigma(\theta, \phi) = \sqrt{\int_0^{2\pi} \boldsymbol{\tau}_a^2(\theta, \phi, \psi) d\psi}.$$

Papadopoulos, in [48], has shown that $T_\sigma(\theta, \phi)$ on a plane $\boldsymbol{\Delta}$ is proportional to an upper bound estimation of the plastic mesostrain accumulated

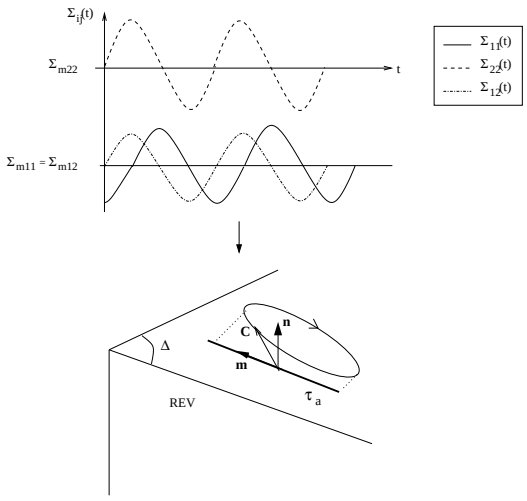

Figure 4.5: Elliptic path of the macroscopic shear stress $\boldsymbol{C}$, on a plane $\boldsymbol{\Delta}$, defined by $\boldsymbol{n}$. The amplitude $\boldsymbol{\tau}_a$ of the macroscopic resolved shear stress $\boldsymbol{\tau}$ results from the projection of $\boldsymbol{C}$ on the direction $\boldsymbol{m}$.

on the grains of the REV, so orientated that their easy glide planes are parallel to the plane defined by the couple (θ, ϕ). The Papadopoulos criterion gives,

$$\max_{\theta,\phi}\{T_\sigma(\theta,\phi)\} + \alpha_p P_{max} \leq \beta_p,$$

where α_p and β_p are constants related to the material. They can be linked to the Dang Van's constant α_d and β_d,

$$\alpha_p = \alpha_d\sqrt{\pi},$$

$$\beta_p = \beta_d\sqrt{\pi}. \tag{4.6}$$

The magnitude P_{max} is the maximum of the hydrostatic pressure over a sequence of loading. The critical plane $\boldsymbol{\Delta_c}$ is defined by the couple (θ_c, ϕ_c), for which the variable $T_\sigma(\theta,\phi)$ reaches the maximum T_Σ,

$$T_\Sigma = \max_{\theta,\phi}(T_\sigma(\theta,\phi)).$$

Grains with easy glide direction contained in Δ_c experience more plasticity than the grains with other orientation and easy glide direction. Under constant amplitude loading, the most critical direction on it is defined by

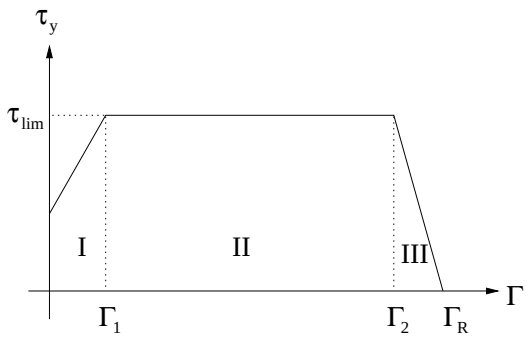

Figure 4.6: Evolution of the yield limit.

the maximum amplitude of the macroscopic resolved shear stress τ_a,

$$\tau_A = \max_{\psi} \tau_a(\theta, \phi, \psi).$$

The direction with maximum amplitude of macroscopic resolved shear stress τ_A is located by ψ_c. Since the metal is isotropic at the macroscopic scale, there always exists some grains less favorably orientated, i.e. grains with an easy glide direction that coincides with the direction defined by $(\theta_c, \phi_c, \psi_c)$. Consequently, the crack initiation may appear along this critical plane, experiencing T_Σ and along the direction defined by ψ_c.

Accumulation of plastic mesoscopic strain

A crystal starts to deform plastically when $\boldsymbol{\tau}$ fulfills,

$$f(\boldsymbol{\tau}, \gamma_p, \tau_y) = (\boldsymbol{\tau} - c\gamma_p \boldsymbol{m}) \cdot (\boldsymbol{\tau} - c\gamma_p \boldsymbol{m}) - \tau_y^2 = 0,$$

where c is a constant dependent on the material, and τ_y is called the yield limit. Associated with Eq. (4.5), we get,

$$f(\boldsymbol{\tau}, \gamma_p, \tau_y) = (\boldsymbol{\tau} - (c+\mu)\gamma_p \boldsymbol{m}) \cdot (\boldsymbol{\tau} - (c+\mu)\gamma_p \boldsymbol{m}) - \tau_y^2 = 0,$$

Three successive phases describe the crystal, from the first yielding to failure, see Fig. 4.6. During these three phases, the yield limit evolves. The crystal reaches failure when the accumulated plastic mesostrain Γ reaches a critical value Γ_R and the yield limit becomes negligible. Phases I and

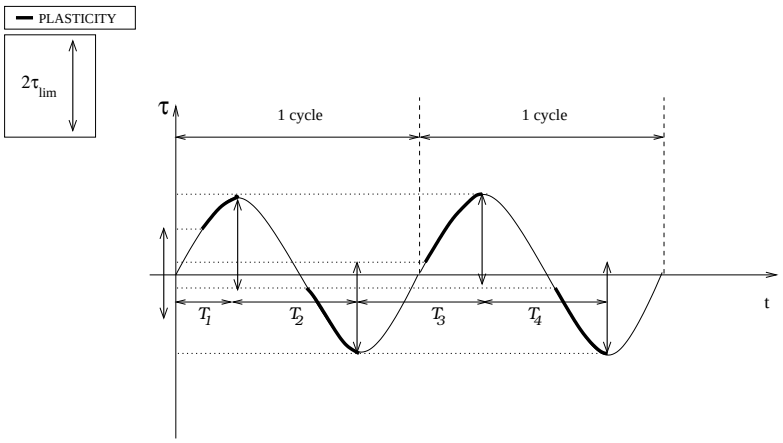

Figure 4.7: Accumulation of plastic strain.

III are the hardening and the softening phases, where the yield limit increases and decreases, respectively. Phase II is called the saturation phase. At this stage, the yield limit is considered as constant. The phase II is often predominant, see [41]. Thus, we will consider here that the saturation phase represents the life of a grain. The yield limit is equal to τ_{lim}, at the saturation phase. The plasticity cumulates as illustrated in Fig. 4.7. Plastic strain cumulates in each transition, defined by the period of time T_k. We suppose that the metal is virgin for $t < 0$, i.e. no plastic strain has been accumulated at $t < 0$. Plastic deformation appears when the macroscopic resolved shear stress crosses the interval of $2\tau_{lim}$, as illustrated in Fig. 4.7. The plastic deformation accumulated during a transition is proportional to the length of the segment Ω_{T_k},

$$\begin{aligned} \Omega_{T_1} &= (\boldsymbol{\tau}_A - \tau_{lim}), \\ \Omega_{T_k} &= 2(\boldsymbol{\tau}_A - \tau_{lim}) = (\boldsymbol{\tau}_R - 2\tau_{lim}), \quad \forall k \geq 2, \end{aligned}$$

where $\boldsymbol{\tau}_R$ is the range of the cycles of $\boldsymbol{\tau}$. Under the assumptions that the saturation phase is predominant, the plastic strain Γ can be deduced from them, for each transition T_k,

$$\Gamma_k = L_1 \Omega_{T_k} \quad \text{for} \quad k \geq 1.$$

The plastic strain accumulated until failure is called Γ_R,

$$\Gamma_R = \frac{\tau_{lim}}{L_2}. \tag{4.7}$$

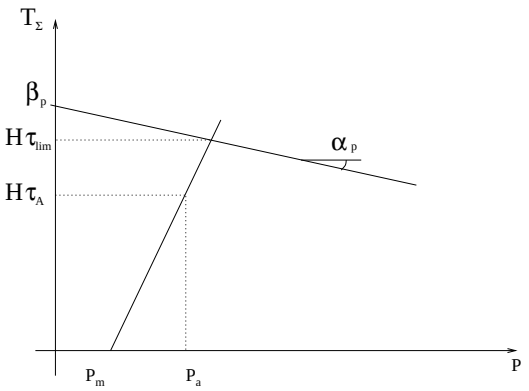

Figure 4.8: Evaluation of τ_{lim}. The variable P_a represents the amplitude of the hydrostatic pressure, and P_m the mean value. The variable τ_a is the amplitude of the resolved shear stress.

The constants L_1 and L_2 depend on the material.

Morel has proposed an expression of τ_{lim}, as illustrated in Fig. 4.8,

$$\tau_{lim} = \frac{1}{H}\left(\frac{-\alpha_p P_m + \beta_p}{\alpha_p + \frac{T_\Sigma}{P_a}}\frac{T_\Sigma}{P_a}\right),$$

where P_a and P_m are the amplitude and the mean value of the hydrostatic pressure on the sequence. The constant α_p and β_p are material constant from Papadopoulos criterion, see Eq. (4.6). The coefficient H represents the ratio between $\boldsymbol{\tau}_A$ and T_Σ, see Fig. 4.5,

$$H = \frac{T_\Sigma}{\boldsymbol{\tau}_A}, \quad \sqrt{\pi} \leq H \leq \sqrt{2\pi}.$$

In the case of proportional stress tensors, the coefficient H is equal to $\sqrt{\pi}$.

The life is expressed as the number of cycles, N, until the grains with an easy glide direction that coincides with the most damaging direction, reaches failure. From Fig. 4.7, one cycle of $\boldsymbol{\tau}$ includes two transitions. Therefore, the plastic strain accumulated during one cycle is,

$$\begin{aligned} \Gamma_{cy} &= 4L_1(\boldsymbol{\tau}_A - \tau_{lim}), \\ &= 2L_1(\boldsymbol{\tau}_R - 2\tau_{lim}). \end{aligned} \tag{4.8}$$

The number of cycles cycles N is,

$$N = \frac{\Gamma_R}{\Gamma_{cy}}.$$

From Equations (4.7,4.8),

$$N = q\frac{\tau_{lim}}{(\boldsymbol{\tau}_A - \tau_{lim})_+},$$

with

$$q = \frac{1}{4L_1L_2}, \tag{4.9}$$

and,

$$x_+ = \begin{cases} x & \text{if} \quad x > 0 \\ 0 & \text{if} \quad x \leq 0. \end{cases}$$

The variable q is a constant related to the material. It is determined from a Wöhler curve of the material. The damage induced by n cycles (or 2n reversals) of amplitudes and ranges $\boldsymbol{\tau}_A$ and $\boldsymbol{\tau}_R$ is,

$$\begin{aligned} D = \frac{n}{N} \quad &= \frac{n(\boldsymbol{\tau}_A - \tau_{lim})_+}{\tau_{lim}q} \\ &= \frac{n(\boldsymbol{\tau}_R - 2\tau_{lim})_+}{2\tau_{lim}q}. \end{aligned} \tag{4.10}$$

4.3.2 Variable amplitude loading

Morel proposed to evaluate damage from multiaxial variable amplitude loading. In Fig. 4.9, an example of macroscopic shear stress $\boldsymbol{C}$ is shown. For more details, see [41].

Damage accumulation

Morel proposed to locate the critical plane by the use of the parameter $T_{\sigma rms}$,

$$T_{\sigma rms}(\theta, \phi) = \sqrt{\int_0^{2\pi} \boldsymbol{\tau}_{rms}^2(\theta, \phi, \psi) d\psi}.$$

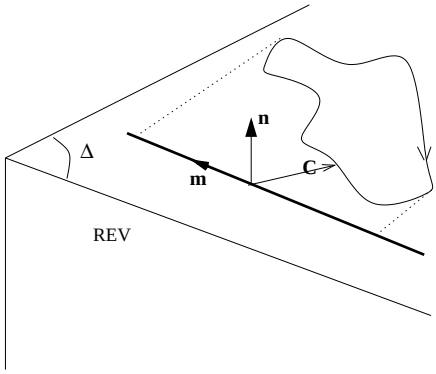

Figure 4.9: Variable amplitude macroscopic shear stress $\boldsymbol{C}$ on a plane $\boldsymbol{\Delta}$.

The variable $\boldsymbol{\tau}_{rms}$ is the standard deviation of $\boldsymbol{\tau}$. The critical plane $\boldsymbol{\Delta_c}$ is located at the maximum of $T_{\sigma_{rms}}(\theta, \phi)$,

$$T_{\Sigma rms} = \max_{\theta,\phi}(T_{\sigma rms}(\theta, \phi)).$$

We will assume that the material is virgin, i.e. no microscopic plastic deformation exists before submitting the loading. The damage reaches one when the accumulated plastic deformation reaches Γ_R. We will assume that the saturation is predominant. Thus, τ_y is constant, see Fig. 4.6,

$$\tau_y = \tau_{lim}.$$

In Fig. 4.10, the method of evaluation of the plastic strain Γ from the macroscopic resolved shear stress is described. It is based on the extrema of the history of the macroscopic resolved shear stress. At time point $t = 0$, the interval $[-\tau_{lim}, \tau_{lim}]$ is centered around 0, as shown in Fig. 4.10. Once the signal crosses the segment of $2\tau_{lim}$, plastic strain accumulates. It stops accumulating when the first next turning point is reached. The segment of length $2\tau_{lim}$ moves to this turning point. The time period during each accumulation of the plastic strain is called a transition. In Fig. 4.10, four different transitions are illustrated.

The plastic deformation induced by the transition k during the time period T_k is proportional Ω_k,

$$\Omega_k = |\boldsymbol{\tau}_k - \boldsymbol{\tau}_{k-1} - 2\tau_{lim}|.$$

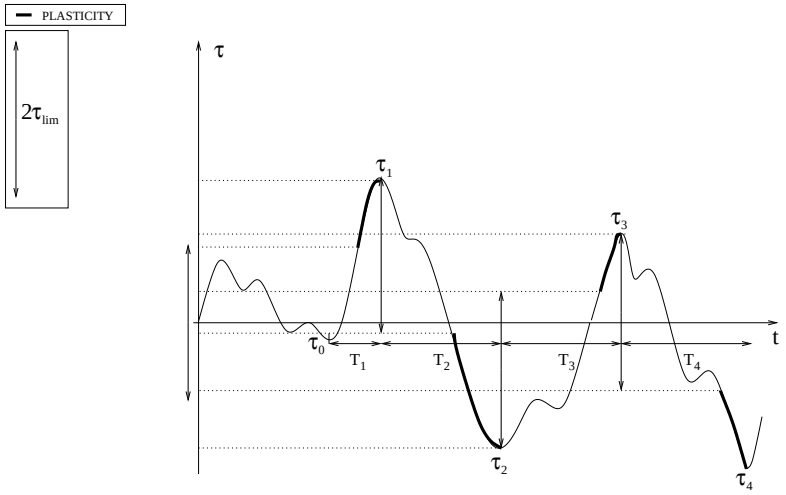

Figure 4.10: Accumulation of plasticity in grains in the case of variable amplitude macroscopic resolved shear stress.

Moreover,

$$\Gamma_k = L_1 \Omega_k.$$

The plastic strain accumulated during the four transitions is,

$$\Gamma = L_1 \sum_{k=1}^{4} \Omega_k.$$

We have deduced that the way of evaluating the accumulated mesoscopic plastic strain is very close to the rainflow filter counting. Thus, we will consider that the evaluation of Γ on a sequence of loading follows Theorem 4.1,

Theorem 4.1. ***Evaluation of the plastic mesoscopic strain*** Γ**.** *Under the assumption that the saturation phase is predominant, Morel's way of evaluating the accumulated plastic mesoscopic strain* Γ *from variable amplitude macroscopic resolved shear stress can be expressed from the rainflow cycles counting method. The mesoscopic plastic strain is induced by the reversals of rainflow cycles with ranges greater than* $2\tau_{lim}$*, and the reversals of the residual with ranges greater than* $2\tau_{lim}$*. The ranges of the reversals inducing damage are called* τ_{ri}*, and,*

$$\Gamma = L_1 \sum_{k} (\tau_{ri} - 2\tau_{lim})_+.$$

Evaluation of life

A simple way of computing a good approximation of τ_{lim} is to express it with the standard deviations of the hydrostatic pressure and the resolved shear stress,

$$\tau_{lim} = \frac{1}{H}\left(\frac{-\alpha_p P_m + \beta_p}{\alpha_p + \frac{T_{\Sigma rms}}{P_{rms}}}\frac{T_{\Sigma rms}}{P_{rms}}\right). \tag{4.11}$$

The variable P_{rms} is the standard deviation of the hydrostatic pressure P. In [39], Morel proposed to evaluate H,

$$H = \frac{T_{\Sigma rms}}{C_{rms}},$$

with

$$C_{rms} = \max_{\psi}(\boldsymbol{\tau}_{rms}(\psi)).$$

For the sake of simplicity Morel proposed, in [41], to use the most conservative value $\sqrt{2\pi}$, in the case of non-proportional loading.

The damage induced by a reversal of $\boldsymbol{\tau}$ is expressed from τ_{lim} and the ranges of the reversals, called $\boldsymbol{\tau}_{ri}$. We assume that the saturation phase is predominant. Thus, the accumulation of damage over a sequence of loading is linear. Let's consider as $N_{seq,R}$, the number of sequences of loading, inducing the plastic strain Γ_R, before crack initiation. From Eq. (4.7), we get

$$N_{seq,R} = \frac{\tau_{lim}}{L_2 L_1 \sum_k (\boldsymbol{\tau}_{ri} - 2\tau_{lim})_+}.$$

From Eq. (4.9),

$$N_{seq,R} = \frac{4q\tau_{lim}}{\sum_k (\boldsymbol{\tau}_{ri} - 2\tau_{lim})_+}, \tag{4.12}$$

where $\boldsymbol{\tau}_{ri}$ is defined in Theorem 4.1. Let $\boldsymbol{\tau}_{ai}$ be the amplitude of the reversals of $\boldsymbol{\tau}$. Then,

$$N_{seq,R} = \frac{2q\tau_{lim}}{\sum_k (\boldsymbol{\tau}_{ai} - \tau_{lim})_+}. \tag{4.13}$$

The aim is to locate the critical direction on the critical plane. Let's consider as D_{seq}, the damage induced by N_{seq} sequences of cyclic loading. We

will consider that the direction $\boldsymbol{m}$ for which the damage D_{seq} is the greatest one is the critical direction,

$$\begin{aligned} D_{seq} &= \frac{N_{seq}}{N_{seq,R}} \\ &= N_{seq} \frac{\Sigma_k (\boldsymbol{\tau}_{ai} - \tau_{lim})_+}{2q\tau_{lim}}. \end{aligned} \tag{4.14}$$

4.4 Conclusion

Morel's criterion provides a method of life prediction in multiaxial high cycle fatigue for finite life. The damage is due to plastic strain appearing in some grains of the REV. The damage is based on the mesoscopic plastic strain accumulated on the less favorably orientated grains of the REV. The plastic strain is due to the macroscopic resolved shear stress, acting on one of the directions of the critical plane. We observed that Morel's way of evaluating the plastic strain from the macroscopic resolved shear stress is close to the rainflow filter method.

Part II

An approach to multi-input equivalent fatigue loads

Chapter 5

Multi-input equivalent fatigue loads: Motivations and needs

It is commonly observed that structures in service are not only exposed to one-input external forces, but also to multi-input external forces. Suspensions of cars are a good example of structures submitted to such loads. In this case, loads usually come from the wheels. They are vertical, transversal and longitudinal variable amplitude forces, coupled or not, acting on the suspension at the same time. Structures like axles are even submitted to forces from the two front (or two rear) wheels. Consequently, six different forces act on them, three from each of the wheels.

It is evident that some interactions exist within the forces. Right and left front (or rear) vertical forces are often either in phase (e.g. in the case of straight line roads), or in opposite phase (e.g. in curves). In order to analyze these forces in fatigue, we have to take into account these interactions. The fatigue analysis of each component of the multi-input forces, considered separately, would not take into account the interaction that may have an important impact on the life prediction.

Most of the components of the vehicle incur multiaxial fatigue, i.e. fatigue induced by multiaxial stress tensors. This is mostly due to the geometry of the structures. The aim of the multi-input equivalent fatigue approach

is to build simple multi-input forces, equivalent in terms of damage, to some variable amplitude loads, like measurements. This has to be performed without information about the geometry they are applied to. Thus, we need a model to evaluate damage from variable amplitude multiaxial stresses, in the framework of the high-cycle fatigue for finite life prediction.

5.1 Prediction of life from forces and characterization of the equivalent forces

First of all, in order to evaluate damage from the forces, we need to know the stress fields generated by multi-input variable amplitude loads. The structures are exposed to forces that do not depend on the point of the structure we look at. They are global magnitudes. Conversely, stress fields are defined at points of the structures, and can be different from one point to another. They are local magnitudes. The damage is also locally defined. Thus, we need to evaluate local magnitudes, as damage, with global magnitudes, as forces. We will restrict the study to points of structures where cracks are more likely to appear. These points are called the critical points of the structures.

We also need to predict the life from the stress fields. Different criteria predicting finite life can be used. Are they all usable in the method of multi-input equivalent fatigue approach? Are there any restrictions or properties that the criterion has to fulfill, in order to be used in the equivalent fatigue approach? Uniaxial EFL is applicable to uniaxial stress field, and Basquin's curve for life prediction was chosen. How can we evaluate the damage from multiaxial stress fields? How do we extract the damage from the forces directly?

In the context of the EFL, the geometrical properties of the structures are unknown. Therefore, we need to get information about the damage from the forces, without information about the structures. In the expression of the damage from the forces, some parameters may be linked to the geometry. Some extra assumptions about the structures may be necessary, in order to evaluate them.

The study of the multi-input EFL aims to define the equivalent forces. We have to choose the shape of the equivalent loads. The choice can be motivated by different factors, like the simplicity in their shape or in their

generation. The choice can be also motivated by the ability to evaluate damage from the parameters defining the EFL. For instance, in the case of sinusoidal multi-input EFL, amplitudes and phase shifts are essential to describe the EFL entirely. We need to know the interaction of these parameters on the damage and to express the damage from them.

The unknown parameters of the EFL that influence the damage are contained in the parameter vector $\boldsymbol{\theta}$. In order to characterize the parameters that will influence the damage, for each types and shapes of EFL, we need to evaluate $\boldsymbol{\theta}$. The vector of parameters $\boldsymbol{\theta}$ is defined in the parameter space $\boldsymbol{\Theta}$ and is determined from the equivalence of damage.

Notation 5.1. ***Parameter vector $\boldsymbol{\theta}$.*** *The vector $\boldsymbol{\theta}$ contains the parameters defining the EFL and influencing the damage induced by them.*

In the case of uniaxial EFL, only sinusoidal loads have been experienced, essentially because of their simplicity in their application to test benches and characterization of severity of customers. An extension to other types of EFL will be explored, such as deterministic and probabilistic equivalent forces. Deterministic forces such as sinusoidal equivalent forces have been studied, see Fig. 5.1. Probabilistic loads like narrow band Gaussian and Markov chain loads have also been investigated. They are illustrated in Fig. 5.2 and Fig. 5.3. On the basis of these three models, we will study the possibility to evaluate the damage as an expression of the parameters that belong to the vector $\boldsymbol{\theta}$. The sinusoidal equivalent loads are defined by their amplitudes, phase shifts and number of cycles. This model can be composed by either one block, or several blocks of sinusoids.

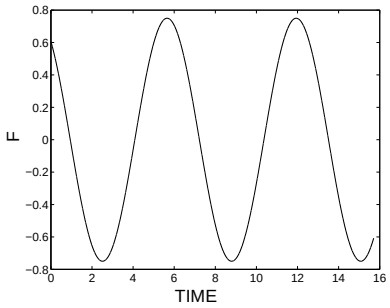

Figure 5.1: Illustration of sinusoidal loads.

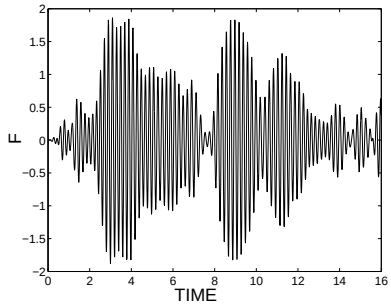

Figure 5.2: Illustration of Gaussian loads.

The Gaussian EFL is interesting as it reproduces, with greater accuracy, the different measurements we attempt to model. The rainflow content of the loads can be closer to the measurements, compared to the Markov or sinusoidal multi-input EFL. We will be particularly interested in the narrow-band Gaussian processes.

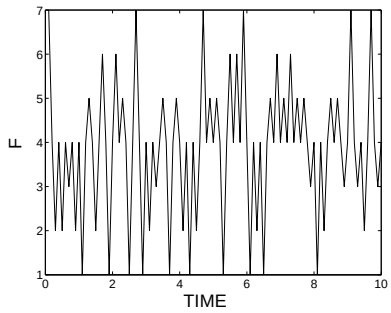

Figure 5.3: Illustration of Markov chain loads.

The Markov chain model is interesting to develop because of its flexibility. We can choose to define the Markov chain EFL with a large number of states. It allows us to model some rare and damaging events with a high amplitude of loads as well. These rare events induce a great part of the damage over the life of the structure. After describing a simple model of Markov chain EFL, a model of Markov chain with peaks has been studied.

5.2 Synopsis

In Fig. 5.4, a synopsis of the general problem of the multi-input EFL is proposed (see [26, 27]).

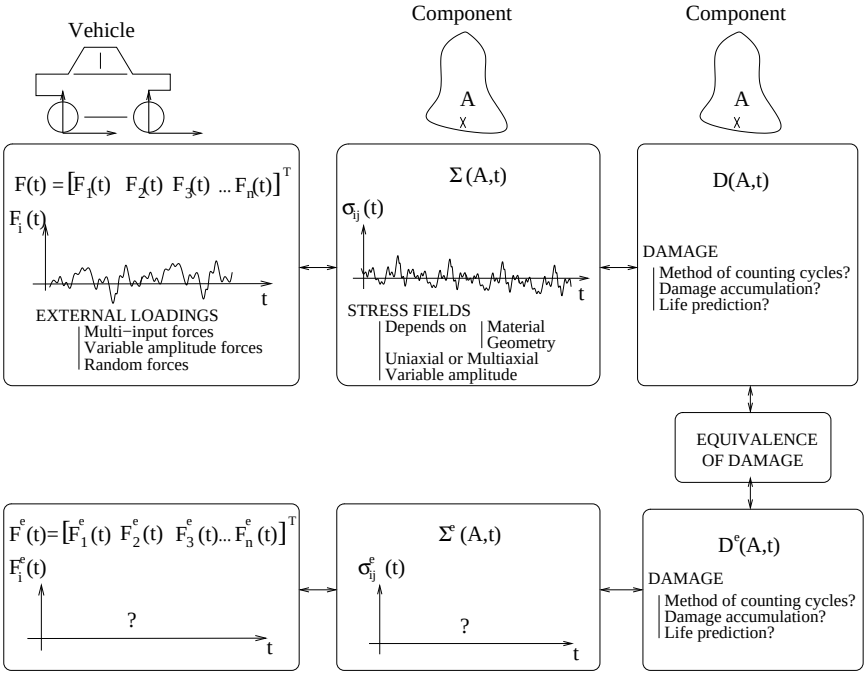

Figure 5.4: Synopsis of the Multi-input EFL.

This synopsis deals with an example of suspensions of cars. The component illustrated is exposed to the forces from the wheels. The passage from the forces to the stress fields depends on the geometry and the material properties of the component. In the case of the uniaxial stress field, the evaluation of the damage from the forces is governed by the method of extracting damaging cycles from the forces, by the relation between damage and amplitude of cycles, and finally by the accumulation of damage over the different cycles.

In the case of multiaxial variable amplitude stress fields, Basquin's criterion is not appropriate. We need a criterion of multiaxial high cycle fatigue

that predicts life of structures. In the previous part, a large number of fatigue criteria has been presented. However, criteria based on the micro-macro approach of damage are the most advanced. Morel's criterion, described in the previous part has been chosen to evaluate the damage from multiaxial stress fields. It is based on the microscopic approach and provides a rather good assessment of life.

Chapter 6

Evaluation of the damage from multi-input loads

The aim of this chapter is to evaluate damage from multi-input variable amplitude forces. Different parameters related to the geometry will have an impact on the expression of the damage. However, if we do not know the geometry of the structures, we will see how it is possible to get rid of these constants. In the case it is not possible, we will attempt to evaluate them.

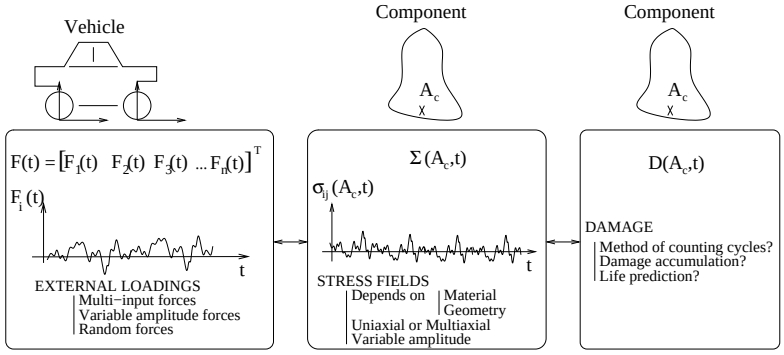

Figure 6.1: Synopsis of the evaluation of the damage from multi-input forces

As explained in the previous chapter, the damage is expressed at a point of a structure, from the stress tensor, see Fig. 6.1. Thus, it is locally defined. However, the forces are applied to a structure and are globally defined. How can we evaluate a local parameter, like damage, with a global parameter, like forces, without information about the geometry? This question seems to be impossible to answer, since every structure is different, and consequently incurs different damage, even if they are exposed to the same loads.

In the case of uniaxial stress tensor, the evaluation of the damage from the loads can be expressed by Basquin's curve, see [65], [8] or [9]. Several reports and articles have explored the evaluation of the damage from the forces, in the framework of multidimensional stress tensors, like in [7, 17]. Criteria like the critical plane approach have been used. The evaluation of the damage is usually based on an equivalent stress, called σ^e. The first task is to evaluate σ^e from the forces. In [18], a normalized equivalent stress has been chosen as a linear combination of the forces:

$$\sigma^e = \sum_{i=1}^{n} c_i F_i \qquad \text{with} \qquad \sum_{i=1}^{n} c_i^2 = 1.$$

The damage is based on the rainflow content of σ^e, which is defined as a linear combination of the forces. The RiaD concept (or the rainflow-in-all-direction) is based on the rainflow counting of linear combinations of multiaxial and non-proportional forces.

In the following, we aim to evaluate the damage from Morel's and Basquin's criteria. What these criteria have in common is that they are based on the rainflow content of the components of the stress tensors. Once the evaluation of the damage from the forces is settled, we will define the equivalence of damage in order to determine the multi-input EFL.

6.1 Assumptions on the behaviour of metal components

Let's consider $\boldsymbol{F}(t)$, a vector of n-input forces, over the time period T_0,

$$\boldsymbol{F} = \left\{ \begin{pmatrix} F_1(t) \\ F_2(t) \\ \vdots \\ F_n(t) \end{pmatrix} : t \in [0, T_0] \right\}. \tag{6.1}$$

First, we will assume that the global behaviour of the structure is elastic. This assumption is in accordance with the framework of high cycle fatigue. Moreover, these structures are quasi-static. We will consider that the effect of the frequency of the different loads on the fatigue life is negligible, in accordance with Basquin's and Morel's criteria.

Assumption 6.1. ***Elastic and quasi-static structures.*** *We will assume that the global behaviours of the structures are elastic and quasi-static, when exposed to cyclic loads* $\boldsymbol{F}$*.*

Every location of a structure gives rise to a proper relation between loads and multiaxial stresses that depends on the geometry and on the material. In any structure exposed to loads, crack initiation is more likely at the critical points of the structure. The durability of the components completely depends on the behaviour of these critical points. The multi-input forces give rise to one or more critical points. Structures reach failure if the damage reaches one at one of its critical points. The first critical point reaching a damage equal to one is called A_c. The location of the critical point depends on the structure and on the sequence of multi-input loads applied to it.

Remark 6.1. *The critical point* A_c *on a structure should be written as a function of* $\boldsymbol{F}$ *and of the geometry* $\boldsymbol{G}$*, like* $A_c(\boldsymbol{F}, \boldsymbol{G})$*. However, for the sake of simplicity, we will consider that the dependency of the critical point to the loads* $\boldsymbol{F}$ *and the geometry* $\boldsymbol{G}$ *is implicit.*

It has been frequently observed that, in car components, when the loads $\boldsymbol{F}$ are applied to the structure, the principal directions of stress tensors at the critical points often do not rotate in time. Let's consider these two assumptions.

Assumption 6.2. ***Proportional stress tensors.*** *Let's consider* $\boldsymbol{F}$*, applied to a structure. The multi-input forces give rise to a critical point* A_c*. It is assumed that, at* A_c*, the principal directions do not move in time.*

Assumption 6.3. ***Unidirectional stress tensors.*** *This assumption is a special case of the proportional stress tensor. We will assume that the stress tensor is unidirectional at* A_c*.*

Under Assumption 6.1 and Assumption 6.3, Basquin's criterion is applicable. However, if we consider Assumption 6.1 and Assumption 6.2, Basquin's criterion is not appropriate. Morel's criterion can be used for life prediction from multiaxial proportional and non- proportional stress tensors. In

the following, we will express the stress tensors from the loads under the different assumptions. Let's consider $\boldsymbol{\Sigma}(A_c, \boldsymbol{F}, t)$, the multiaxial stress tensor at the point A_c. It can be written as a symmetric matrix,

$$\boldsymbol{\Sigma}(A_c, \boldsymbol{F}, t) = \begin{pmatrix} \sigma_{11}(A_c, \boldsymbol{F}, t) & \sigma_{12}(A_c, \boldsymbol{F}, t) & \sigma_{13}(A_c, \boldsymbol{F}, t) \\ \sigma_{12}(A_c, \boldsymbol{F}, t) & \sigma_{22}(A_c, \boldsymbol{F}, t) & \sigma_{23}(A_c, \boldsymbol{F}, t) \\ \sigma_{13}(A_c, \boldsymbol{F}, t) & \sigma_{23}(A_c, \boldsymbol{F}, t) & \sigma_{33}(A_c, \boldsymbol{F}, t) \end{pmatrix}.$$

Under Assumption 6.1, we can conclude that,

$$\boldsymbol{\Sigma}(A_c, \boldsymbol{F}, t) = \sum_{i=1}^{n} \boldsymbol{K_i}(A_c) F_i(t), \tag{6.2}$$

with

$$\boldsymbol{K_i}(A_c) = \begin{pmatrix} K_{i,11}(A_c) & K_{i,12}(A_c) & K_{i,13}(A_c) \\ K_{i,12}(A_c) & K_{i,22}(A_c) & K_{i,23}(A_c) \\ K_{i,13}(A_c) & K_{i,23}(A_c) & K_{i,33}(A_c) \end{pmatrix}.$$

Let's consider $\boldsymbol{\Sigma_d}(A_c, \boldsymbol{F}, t)$ the diagonalized stress tensor, at the time point t,

$$\boldsymbol{\Sigma_d}(A_c, \boldsymbol{F}, t) = \boldsymbol{R}^T(A_c, t) \boldsymbol{\Sigma}(A_c, \boldsymbol{F}, t) \boldsymbol{R}(A_c, t), \tag{6.3}$$

where $\boldsymbol{R}$ defines the change of basis from $\boldsymbol{\Sigma}(A_c, \boldsymbol{F}, t)$ to $\boldsymbol{\Sigma_d}(A_c, \boldsymbol{F}, t)$,

$$\boldsymbol{\Sigma_d}(A_c, \boldsymbol{F}, t) = \begin{pmatrix} \sigma_{d,11}(A_c, \boldsymbol{F}, t) & 0 & 0 \\ 0 & \sigma_{d,22}(A_c, \boldsymbol{F}, t) & 0 \\ 0 & 0 & \sigma_{d,33}(A_c, \boldsymbol{F}, t) \end{pmatrix},$$

with

$$\sigma_{d,11} \geq \sigma_{d,22} \geq \sigma_{d,33}.$$

Under Assumption 6.2, the principal directions of the stress tensor do not rotate in time. We will therefore conclude that the principal directions of $\boldsymbol{R}$ do not change in time,

$$\boldsymbol{R}(A_c, t) = \boldsymbol{R}(A_c).$$

As a consequence, we can normalize the vector $\boldsymbol{\Sigma}_d(A_c, \boldsymbol{F}, t)$,

$$\boldsymbol{\Sigma}_d(A_c, \boldsymbol{F}, t) = \sigma(A_c, \boldsymbol{F}, t) \begin{pmatrix} 1 & 0 & 0 \\ 0 & \alpha(A_c) & 0 \\ 0 & 0 & \beta(A_c) \end{pmatrix}, \tag{6.4}$$

with

$$-1 \leq \beta(A_c) \leq \alpha(A_c) \leq 1.$$

For the sake of simplicity, we will consider tensors $\boldsymbol{\Sigma}_d(A_c, \boldsymbol{F}, t)$ as row vectors,

$$\boldsymbol{\Sigma}_d(A_c, \boldsymbol{F}, t) = \sigma(A_c, \boldsymbol{F}, t) \begin{pmatrix} 1 \\ \alpha(A_c) \\ \beta(A_c) \end{pmatrix} \text{ with } -1 \leq \beta(A_c) \leq \alpha(A_c) \leq 1. \tag{6.5}$$

The structures for which Assumption 6.1 and Assumption 6.3 are fulfilled, the diagonalized stress tensor can be deduced from Eq. (6.5), with particular values of $\alpha(A_c)$ and $\beta(A_c)$,

$$\alpha(A_c) = \beta(A_c) = 0. \tag{6.6}$$

6.2 Damage from multi-input forces using Morel's criterion

Morel's criterion aims to define the critical plane and the most critical direction on it. For each direction of the critical plane, we associate the macroscopic resolved shear stress. The damage is based on the cycles and the residual of the macroscopic resolved shear stress, computed from rainflow filter counting method. Morel's criterion is applicable for variable amplitude multiaxial stress tensors. We will use it for proportional multiaxial stress tensors, for points of structures where Assumption 6.1 and Assumption 6.2 are satisfied.

6.2.1 Expression of the resolved shear stress

Let's call $\boldsymbol{\tau}(A_c, \boldsymbol{F}, t)$ the resolved shear stress on the most damaging direction of the critical plane, when multi-input forces $\boldsymbol{F}$ are applied. The resolved shear stress is a linear combination of the different components of the stress tensor. The stress components are linear combinations of the forces. So, the norm $\tau(A_c, \boldsymbol{F}, t)$ is a linear combination of the components of $\boldsymbol{F}$. Hence, under Assumption 6.1,

$$\tau(A_c, \boldsymbol{F}, t) = \sum_{i=1}^{n} c_i(A_c, \boldsymbol{F}, t)\, F_i(t). \tag{6.7}$$

Moreover, we have previously assumed that the stress tensor at the critical point A_c is proportional. Consequently, the linear combination between

the forces and the components of the stress tensor, at the point A_c, depends only on the location of A_c, as shown in Eq. (6.2). The critical plane and the most damaging direction on it do not move in time, [61]. Under Assumption 6.1 and Assumption 6.2, and from Eq. (6.2), Eq. (6.7) becomes,

$$\tau(A_c, \boldsymbol{F}, t) = \sum_{i=1}^{n} c_i(A_c) F_i(t).$$

After normalizing it, we get,

$$\tau(A_c, \boldsymbol{F}, t) = C(A_c) \sum_{i=1}^{n} a_i(A_c) F_i(t), \tag{6.8}$$

The coefficients $a_i(A_c)$ and the parameter $C(A_c)$ are defined as follows,

$$\sum_{i=1}^{n} [a_i(A_c)]^2 = 1 \quad \text{and} \quad C(A_c) > 0.$$

The row vector $\mathbf{a}(A_c)$ is the vector containing the coefficients $a_i(A_c)$,

$$\mathbf{a}(A_c) = (a_1(A_c), \ldots, a_n(A_c)). \tag{6.9}$$

We will also define,

$$\begin{aligned} F^*(A_c, \boldsymbol{F}, t) &= \sum_{i=1}^{n} a_i(A_c) F_i(t), \\ &= \mathbf{a}(A_c)\, \boldsymbol{F}(t). \end{aligned}$$

Thus,

$$\tau(A_c, \boldsymbol{F}, t) = C(A_c) F^*(A_c, \boldsymbol{F}, t).$$

We can therefore conclude that each pair of $C(A_c)$ and $\mathbf{a}(A_c)$ refers to a structure exposed to the forces $\boldsymbol{F}$ and to the localization of A_c, on it. Moreover, τ is expressed in MPa. The coefficients $a_i(A_c)$ do not have a unit. As $\boldsymbol{F}$ is expressed in Newton, the parameter $C(A_c)$ is expressed in mm^{-2}. For the sake of simplicity, we will adopt Eq. (6.10), in the following,

$$\tau(A_c, \boldsymbol{F}) = C(A_c) F^*(A_c, \boldsymbol{F}). \tag{6.10}$$

6.2.2 Evaluation of the damage

The damage is defined at the point A_c, the most critical point of a structure. It is induced by the loads $\boldsymbol{F}$, applied to it. From Eq. (4.12) and Eq. (4.14),

the damage induced by Morel's criterion depends on the reversals of the rainflow cycles and the residual of the resolved shear stress τ,

$$D(A_c, \boldsymbol{F}) = \frac{1}{4q\tau_{lim}(A_c, \boldsymbol{F})} \left[\sum_i (\tau_{ri}(A_c, \boldsymbol{F}) - 2\tau_{lim}(A_c, \boldsymbol{F}))_+ \right],$$

where

$$x_+ = \begin{cases} x & \text{if} \quad x > 0 \\ 0 & \text{otherwise.} \end{cases}$$

The parameter q depends on the material of the structure, $\tau_{ri}(A_c, \boldsymbol{F})$ is the range of the i-th reversal (or half cycle) of the rainflow cycles or the residual. The parameter $\tau_{lim}(A_c, \boldsymbol{F})$, defined in Eq. (4.11), depends on the resolved shear stress, on the hydrostatic pressure and on Dang Van's coefficients. Hence, it also depends on the multi-input loads $\boldsymbol{F}$. From Eq. (6.10), we deduce that,

$$D(A_c, \boldsymbol{F}) = \frac{1}{4q\tau_{lim}(A_c, \boldsymbol{F})} \left[\sum_i (C(A_c) F^*_{ri}(A_c, \boldsymbol{F}) - 2\tau_{lim}(A_c, \boldsymbol{F}))_+ \right],$$

where $F^*_{ri}(A_c, \boldsymbol{F})$ is the range of the i-th reversal of the rainflow cycle or the residual of $F^*(A_c, \boldsymbol{F})$. Hence

$$D(A_c, \boldsymbol{F}) = \frac{C(A_c)}{4q\tau_{lim}(A_c, \boldsymbol{F})} \left[\sum_i \left(F^*_{ri}(A_c, \boldsymbol{F}) - 2\frac{\tau_{lim}(A_c, \boldsymbol{F})}{C(A_c)} \right)_+ \right].$$

Let's consider the change of variable,

$$T(A_c, \boldsymbol{F}) = 2\frac{\tau_{lim}(A_c, \boldsymbol{F})}{C(A_c)}. \tag{6.11}$$

We get,

$$D(A_c, \boldsymbol{F}) = \frac{1}{2qT(A_c, \boldsymbol{F})} \left[\sum_i (F^*_{ri}(A_c, \boldsymbol{F}) - T(A_c, \boldsymbol{F}))_+ \right].$$

The parameter $T(A_c, \boldsymbol{F})$ depends on the geometry, on the material and on the loads, the parameter $\mathbf{a}(A_c)$, on the geometry and q is a material constant.

Theorem 6.1. ***Life prediction from multi-input forces F, for proportional stress tensors.*** *The damage induced by the multi-input forces* $\boldsymbol{F}$ *at the points of a structure, where* Assumption 6.1 *and* Assumption 6.2 *are fulfilled, is,*

$$D(A_c, \boldsymbol{F}) = \frac{1}{2qT(A_c, \boldsymbol{F})} \left(\sum_i (F^*_{ri}(A_c, \boldsymbol{F}) - T(A_c, \boldsymbol{F}))_+ \right), \tag{6.12}$$

with

$$T(A_c, \boldsymbol{F}) = 2\frac{\tau_{lim}(A_c, \boldsymbol{F})}{C(A_c)}, \quad T(A_c, \boldsymbol{F}) > 0. \tag{6.13}$$

The entity $F^*_{ri}(A_c, \boldsymbol{F})$ is the range of the reversal of the i-th rainflow cycle of $F^*(A_c, \boldsymbol{F})$,

$$F^*(A_c, \boldsymbol{F}) = \mathbf{a}(A_c)\,\boldsymbol{F}, \quad ||\mathbf{a}(A_c)|| = 1. \tag{6.14}$$

Remark 6.2. ***Life prediction from one-input force** F**, for proportional stress tensors.*** *For one-input EFL,*

$$F^*(A_c, F) = F.$$

Hence,

$$D(A_c, F) = \frac{1}{2qT(A_c, F)} \sum_i (F_{ri} - T(A_c, F))_+ ,$$

with F_{ri}, the range of the reversal of the i-th rainflow cycle of F.

Each critical point is characterized by the row vector $\mathbf{a}(A_c)$, $T(A_c, \boldsymbol{F})$ and the material constant q. Two critical points can be defined with the same $T(A_c, \boldsymbol{F})$ and $\mathbf{a}(A_c)$, even if the geometry is different. Consequently, they will reach the same damage when they are exposed to the same loads.

6.3 Damage from multi-input forces using Basquin's criterion

Basquin's criterion is valid if Assumption 6.1 and Assumption 6.3 are fulfilled. In this case, the stress tensor is unidirectional. After expressing the stress tensor from the forces, we will evaluate the damage from the forces.

6.3.1 Expression of the stress tensor from the forces

In the case of unidirectional stress tensor, the diagonalized stress tensor is reduced to one component. From Eq. (6.5) and Eq. (6.6),

$$\Sigma_d(A_c, \boldsymbol{F}, t) = \sigma(A_c, \boldsymbol{F}, t) \begin{pmatrix} 1 \\ 0 \\ 0 \end{pmatrix}.$$

When Assumption 6.1 and Assumption 6.3 are valid, $\sigma(A_c, \boldsymbol{F}, t)$ can be written as a linear combination of the forces.

$$\sigma(A_c, \boldsymbol{F}, t) = C_b(A_c) \sum_{i=1}^{n} a_i(A_c) F_i(t).$$

The coefficients $a_i(A_c)$ and the parameter $C_b(A_c)$ are defined by,

$$C_b(A_c) > 0, \quad \text{and} \quad \sum_{i=1}^{n} [a_i(A_c)]^2 = 1.$$

The linear combination of the forces $F^*(A_c, \boldsymbol{F})$ is defined as,

$$F^*(A_c, \boldsymbol{F}, t) = \sum_{i=1}^{n} a_i(A_c) F_i(t).$$

Thus,

$$\Sigma_d(A_c, \boldsymbol{F}, t) = C_b(A_c) F^*(A_c, \boldsymbol{F}, t) \begin{pmatrix} 1 \\ 0 \\ 0 \end{pmatrix}. \tag{6.15}$$

6.3.2 Evaluation of the damage

From Eq. (2.1), the damage is expressed from the rainflow cycles of the stress component. Together with the Palmgren-Miner accumulation, we can deduce the damage from variable amplitude forces $\boldsymbol{F}$, as a function of the amplitudes of the rainflow cycles of the stress component. Thus,

$$D(A_c, \boldsymbol{F}) = \frac{1}{B(A_c)} \sum_i (\sigma_{ai}(A_c, \boldsymbol{F}))^\beta,$$

where σ_{ai} is the amplitude of the i-th rainflow cycle, and $B(A_c)$ is a constant depending on the geometry. Hence,

$$D(A_c, \boldsymbol{F}) = \frac{1}{B(A_c)} \sum_i \left(\frac{\sigma_{ri}(A_c, \boldsymbol{F})}{2} \right)^\beta,$$

where σ_{ri} is the range of the i-th reversal. From Eq. (6.15), we obtain,

$$D(A_c, \boldsymbol{F}) = \frac{C_b(A_c)}{B(A_c)} \sum_i \left(\frac{F^*_{ri}(A_c, \boldsymbol{F})}{2} \right)^\beta.$$

The entity $F^*_{ri}(A_c, \boldsymbol{F})$ is the range of the i-th reversal of $F^*(A_c, \boldsymbol{F})$. In the following, we will consider that,

$$C_B(A_c) = \frac{C_b(A_c)}{B(A_c)}.$$

Theorem 6.2. ***Life prediction from multi-input forces F, from uniaxial stress tensors.*** *When* Assumption 6.1 *and* Assumption 6.3 *are fulfilled, the damage induced by the multi-input forces* $\boldsymbol{F}$ *can be expressed from Basquin's criterion.*

$$D(A_c, \boldsymbol{F}) = C_B(A_c) \sum_i \left(\frac{F^*_{ri}(A_c, \boldsymbol{F})}{2} \right)^{\beta}, \tag{6.16}$$

with,

$$C_B(A_c) > 0.$$

The entity $F^*_{ri}(A_c, \boldsymbol{F})$ *is the range of the reversal of the i-th rainflow cycle of* $F^*(A_c, \boldsymbol{F})$.

$$F^*(A_c, \boldsymbol{F}) = \mathbf{a}(A_c)\, \boldsymbol{F}, \quad ||\mathbf{a}(A_c)|| = 1.$$

Remark 6.3. ***Life prediction from one-input force*** F***, from uniaxial stress tensors.*** *For one-input EFL,*

$$F^*(A_c, F) = F.$$

Hence,

$$D(A_c, F) = C_B(A_c) \sum_i \left(\frac{F_{ri}}{2} \right)^{\beta}.$$

The range of the i-th reversal of F is called F_{ri}.

In the study, the Gerber's parabola have not been included in the evaluation of the damage from the forces.

6.4 Equivalence of damage

Let's consider the measurements $\boldsymbol{F}$, as defined in Eq. (6.1). The aim is to characterize the EFL $\boldsymbol{F^e}$, equivalent in terms of damage to the measurements $\boldsymbol{F}$,

$$\boldsymbol{F^e} = \left\{ \begin{pmatrix} F^e_1(t) \\ F^e_2(t) \\ \vdots \\ F^e_n(t) \end{pmatrix} : t \in [0, T_0] \right\}. \tag{6.17}$$

The loads $\boldsymbol{F^e}$ can be chosen as deterministic or probabilistic. Once the model of $\boldsymbol{F^e}$ has been chosen, the aim is to evaluate the parameter vector $\boldsymbol{\theta}$, characterized in Notation 5.1, containing all the parameters defining $\boldsymbol{F^e}$ influencing the damage.

The damage on a structure, at its critical point A_c, induced by the measurements, is called $D(A_c, \boldsymbol{F})$. The damage induced by the EFL is called $D^e(A_c, \boldsymbol{F^e})$. The damage induced by $\boldsymbol{F^e}$ is expressed with the parameters of the EFL, contained in $\boldsymbol{\theta}$. From Basquin's or Morel's criterion, the damage is deduced from the rainflow content of the linear combinations of the components of the forces, $F^*(A_c, \boldsymbol{F})$. Therefore, we need to determine the rainflow content from parameters defining the EFL. We need to evaluate the expected damage $E[D(A_c, \boldsymbol{F^e})]$, i.e. the expected rainflow content of each linear combination from parameters characterizing $\boldsymbol{F^e}$,

$$E[D(A_c, \boldsymbol{F^e})] = D^e(A_c, \boldsymbol{\theta}), \tag{6.18}$$

where $\boldsymbol{F^e}$ is expressed in Eq. (6.17).

The equivalence has to be performed whatever the structures fulfilling Assumption 6.1 and Assumption 6.2 or Assumption 6.1 and Assumption 6.3.

6.4.1 Equivalence of damage for one-input EFL

For the one-input EFL, the equivalence between the measurements and the EFL is fulfilled when the equality between $D(A_c, \boldsymbol{F})$ and $D^e(A_c, \boldsymbol{F^e})$ is satisfied.

Definition 6.3. ***Equivalence of damage for one-input force.*** *The one-input EFL F^e is equivalent to the one-input deterministic force F defined on the time period T_0, if,*

$$D(A_c, F) = D^e(A_c, \boldsymbol{\theta}). \tag{6.19}$$

From Remark 6.2, the equivalence of damage can be given in details, using Morel's criterion,

$$\frac{1}{T(A_c, F)} \sum_i (F_{ri} - T(A_c, F))_+ = E\left[\frac{1}{T(A_c, \boldsymbol{\theta})} \sum_j \left(F^e_{rj} - T(A_c, \boldsymbol{\theta}) \right)_+ \right]. \tag{6.20}$$

The components F_{ri} and F^e_{rj} are the i-th and j^{th} ranges of the rainflow cycles of F and F^e, respectively. We deduce that the equality between $D(A_c, \boldsymbol{F})$

and $D^e(A_c, \boldsymbol{\theta})$ is not independent of the structure, as we cannot get rid of the thresholds $T(A_c, F)$ and $T(A_c, \boldsymbol{\theta})$. This means that the equivalence of damage can be fulfilled for a particular known structure.

From Remark 6.3, the equivalence of damage can be given in details, using Basquin's criterion.

$$\sum_i (F_{ri})^\beta = \sum_j [E\ (F_{rj})^\beta]. \tag{6.21}$$

The equality of damage is valid whatever the structures they are applied to. However, the exponent β, dependent on the material, has to be evaluated.

6.4.2 Equivalence of damage for multi-input EFL

Let $F^{e*}(A_c, \boldsymbol{F^e})$ be the linear combination of the components of the multi-input forces $\boldsymbol{F^e}$,

$$F^{e*}(A_c, \boldsymbol{F^e}) = \mathbf{a}(A_c)\, \boldsymbol{F^e}.$$

The magnitudes $D(A_c, \boldsymbol{F})$ and $D^e(A_c, \boldsymbol{\theta})$ are dependent on $F^*(A_c, \boldsymbol{F})$ and $F^{e*}(A_c, \boldsymbol{F^e})$. The coefficients of the linear combinations are contained in the unit vector $\mathbf{a}(A_c)$, dependent on the geometry of the structure.

In order for $\boldsymbol{F^e}$ to be equivalent, we need to find the parameter vector $\boldsymbol{\theta}$ so that $\boldsymbol{F^e}$ and $\boldsymbol{F}$ give the same damage whatever the structures. As soon as the number of structures is infinite and the number of parameters contained in $\boldsymbol{\theta}$ is finite, we can not fulfill the equality of damage for any structure. Thus, we will identify the parameter vector $\boldsymbol{\theta}$ so that the two forces $\boldsymbol{F^e}$ and $\boldsymbol{F}$ are almost equivalent, whatever the structures. In order to assure that $\boldsymbol{F^e}$ and $\boldsymbol{F}$ are almost equivalent, we have chosen to evaluate $\boldsymbol{\theta}$ so that the square distances between $D^e(A_c, \boldsymbol{\theta})$ and $D(A_c, \boldsymbol{F})$ are minimized, whatever the structures and critical points A_c on them. The least square method is used.

Definition 6.4. ***Equivalence of damage for multi-input forces F.*** *The EFL are said to be equivalent to measurements $\boldsymbol{F}$ if the parameter vector $\boldsymbol{\theta}$ defining $\boldsymbol{F^e}$ fulfills,*

$$\boldsymbol{\theta} = arg \min_{\boldsymbol{\theta} \in \boldsymbol{\Theta}} \left(\int_{||\mathbf{a}||=1} \left(D^e(A_c, \boldsymbol{\theta}) - D(A_c, \boldsymbol{F})\right)^2 dS \right), \tag{6.22}$$

where dS is a small element of the surface of the n-dimensional unit sphere.

Using Morel's criterion and from Theorem 6.1 and Eq. (6.22), we can deduce that,

$$\boldsymbol{\theta} = arg \min_{\boldsymbol{\theta}\in\boldsymbol{\Theta}} \left(\int_{||\mathbf{a}||=1} \left(E\left[\frac{1}{T(A_c,\boldsymbol{\theta})} \left(\sum_i (F_{ri}^{e*}(A_c,\boldsymbol{\theta}) - T(A_c,\boldsymbol{\theta}))_+ \right) \right] \right.\right.$$
$$\left.\left. - \frac{1}{T(A_c,\boldsymbol{F})} \left(\sum_j \left(F_{rj}^{*}(A_c,\boldsymbol{F}) - T(A_c,\boldsymbol{F}) \right)_+ \right) \right)^2 dS \right). \quad (6.23)$$

We will assume that the EFL and the measurements are applied to the same structures. The location of the critical point is the same when $\boldsymbol{F}$ or $\boldsymbol{F}^e$ applied. Consequently, the vector $\mathbf{a}(A_c)$ will be the same, from $\boldsymbol{F}$ to $\boldsymbol{F}^e$. The equivalence of damage with Morel's criterion is dependent of constants related to the geometry at the critical point.

Using Basquin's criterion and from Theorem 6.2 and Eq. (6.22), we get,

$$\boldsymbol{\theta} = arg \min_{\boldsymbol{\theta}\in\boldsymbol{\Theta}} \left(\int_{||\mathbf{a}||=1} \left(\sum_i \left[E\left(F_{ri}^{e*}(A_c,\boldsymbol{\theta}) \right)^{\beta} \right] - \sum_j \left(F_{rj}^{*}(A_c,\boldsymbol{F}) \right)^{\beta} \right)^2 dS \right). \quad (6.24)$$

In Basquin's case, contrary to the equivalence of damage for one input case, the equivalence of damage from multi-input forces depends on the geometry of the structures, through the unit vector $\mathbf{a}(A_c)$.

6.4.3 Evaluation of a threshold of non-damaging ranges of rainflow cycles in Morel's criterion

The parameters $T(A_c,\boldsymbol{F})$ and $\mathbf{a}(A_c)$ both depend on the geometry and on the location of the critical points on the structures. They are essential for evaluating damage from loads. In order to evaluate the multi-input EFL, using Morel's criterion, we still need to evaluate the thresholds $T(A_c,\boldsymbol{F})$ that correspond to each $\mathbf{a}(A_c)$ and the forces $\boldsymbol{F}$, i.e. each critical point A_c.

The threshold $T(A_c,\boldsymbol{F})$ depends on A_c, and on the forces. Cycles of F^* or F^{e*} do not induce damage if their ranges do not exceed $T(A_c,\boldsymbol{F})$ or $T(A_c,\boldsymbol{\theta})$ respectively. In Theorem 6.5, we will investigate the influence of the forces on the threshold and provide an analytical expression of it, for proportional stress tensors.

Theorem 6.5. ***Expression of the threshold*** $T(A_c, \boldsymbol{F})$**.** *The stress field fulfilling* Assumption 6.1 *and* Assumption 6.2 *can be written as,*

$$\boldsymbol{\Sigma}_d(A_c, \boldsymbol{F}, t) = C_s(A_c) \sum_{i=1}^{n} d_i(A_c)\, F_i(t) \begin{pmatrix} 1 \\ \alpha(A_c) \\ \beta(A_c) \end{pmatrix},$$

with

$$C_s(A_c) > 0, \quad -1 \leq \beta(A_c) \leq \alpha(A_c) \leq 1.$$

The threshold $T(A_c, \boldsymbol{F})$ *of any structure and point fulfilling* Assumption 6.1 *and* Assumption 6.2*, has an analytical expression,*

$$T(A_c, \boldsymbol{F}) = \frac{M_1}{M_2},$$

The variables M_1 *and* M_2 *are defined by,*

$$\begin{aligned} M_1 &= 2\left(\frac{\beta_d}{C_s(A_c)} - \frac{\alpha_d}{3}(1 + \alpha(A_c) + \beta(A_c))\, F_m^*(A_c, \boldsymbol{F})\right) \\ M_2 &= \frac{\alpha_d}{3}|1 + \alpha(A_c) + \beta(A_c)| + \frac{1 - \beta(A_c)}{2}, \end{aligned} \tag{6.25}$$

where α_d *and* β_d *are Dang Van's coefficients, dependent on the material. The variable* $F_m^*(A_c, \boldsymbol{F})$ *is the mean value of the* $F^*(A_c, \boldsymbol{F})$*.*

Proof. The proof is detailed in Appendix A. □

Equivalence of damage

We deduce from Theorem 6.5 that the threshold $T(A_c, \boldsymbol{F})$ depends on the mean value of the loads, and on the location of the critical point. The mean values of the components of $\boldsymbol{F^e}$ belong to the parameter vector $\boldsymbol{\theta}$, as it influences the damage induced by $\boldsymbol{F^e}$ (see Notation 5.1). We will consider that the mean of the components of the EFL is equal to the mean of the components of $\boldsymbol{F}$,

$$\text{mean}\ (F_i) = E[F_i^e]$$

Therefore, if the loads $\boldsymbol{F}$ and $\boldsymbol{F^e}$ are applied to the same critical points of the same structures,

$$T(A_c, \boldsymbol{F}) = T(A_c, \boldsymbol{\theta}) = T(A_c). \tag{6.26}$$

From Eq. (6.20), we get,

$$\sum_j E\left[\left(F^e_{rj} - T(A_c)\right)_+\right] = \sum_i \left(F_{ri} - T(A_c)\right)_+ . \tag{6.27}$$

From Eq. (6.23), we get,

$$\boldsymbol{\theta} = arg \min_{\boldsymbol{\theta}\in\boldsymbol{\Theta}} \left(\int_{||\mathbf{a}||=1} \left(\left(\sum_j E\left(F^{e*}_{rj}(A_c, \boldsymbol{\theta}) - T(A_c)\right)_+ \right) - \left(\sum_i \left(F^*_{ri}(A_c, \boldsymbol{F}) - T(A_c)\right)_+ \right) \right)^2 dS \right). \tag{6.28}$$

Threshold for one-input EFL

Moreover, the threshold $T(A_c)$ can also be evaluated for unidirectional stress tensor, when $\alpha(A_c) = \beta(A_c) = 0$.

Theorem 6.6. ***Threshold*** $T(A_c)$ ***for unidirectional proportional stress tensors.*** *In the case of unidirectional stress tensor, the threshold* $T(A_c)$ *is,*

$$T(A_c, \boldsymbol{F}) = \frac{4}{C_s(A_c)} \frac{3\beta_d - C_s(A_c)\alpha_d F^*_m(A_c, \boldsymbol{F})}{2\alpha_d + 3}. \tag{6.29}$$

Proof. The particular values $\alpha(A_c) = \beta(A_c) = 0$ are replaced in Eq. (A.1). □

We can conclude with regard to this approach that we can get a theoretical expression of the threshold. However, parameters like $C_s(A_c)$ are unknown. We do not end up with numerical useful results of the threshold. However, in the framework of equivalent fatigue approach, and from the equivalence of damage, clarified in Eq. (6.22), we can not get rid of the threshold. We need a numerical evaluation of it to determine the equivalent loads $\boldsymbol{F}^e$.

6.5 Optimal structures

The problem of finding a suitable threshold $T(A_c, \boldsymbol{F})$ whatever the geometry, seems to be impossible to solve without additional assumptions on the components we are working on. In a number of industrial cases, structures are designed to fulfill reliability requirements, imposed by the manufacturer. These requirements can take different forms. We consider that the forces that the structures are supposed to incur without reaching failure, are known. These forces are measured and stored during test tracks, and are representative of the design life of the structures. The structures fulfilling the reliability requirements have damage below or equal to one, at their critical point, once these predefined sequences of forces are applied to them. The predefined loads are called $\boldsymbol{F_{dl}}$.

We will consider the optimal structures, for which the damage reaches exactly one, at their critical point, after the forces $\boldsymbol{F_{dl}}$ have been applied, and satisfying Assumption 6.1 and Assumption 6.3. The critical points of the optimal structures are called $\widehat{A_c}$.

Definition 6.7. ***Optimal structures.*** *A structure is optimally designed if, after applying the predefined multi-input forces,*

$$\boldsymbol{F_{dl}} = \left\{ \begin{pmatrix} F_{dl,1}(t) \\ \vdots \\ F_{dl,n}(t) \end{pmatrix} \, : \, t \in [0, T_{dl}] \right\},$$

we get,

$$D(\widehat{A_c}, \boldsymbol{F_{dl}}) = 1,$$

where $\widehat{A_c}$ is the critical point of the optimal structure.

Using Morel's criterion, a critical point $\widehat{A_c}$ on an optimal structure is defined by its threshold $T(\widehat{A_c}, \boldsymbol{F_{dl}})$ and linear combination $\mathbf{a}(\widehat{A_c})$. For each point, from Eq. (6.12), the following equation is fulfilled:

$$\frac{1}{2qT(\widehat{A_c})} \sum_i \left(F^*_{ri}(\widehat{A_c}, \boldsymbol{F_{dl}}) - T(\widehat{A_c}) \right)_+ = 1. \tag{6.30}$$

In consequence, we will be able to characterize the critical points, through $\mathbf{a}(\widehat{A_c})$ and $T(\widehat{A_c}, \boldsymbol{F_{dl}})$, of all the different optimal structures. In practice, we will only choose to treat a finite number of optimal structures.

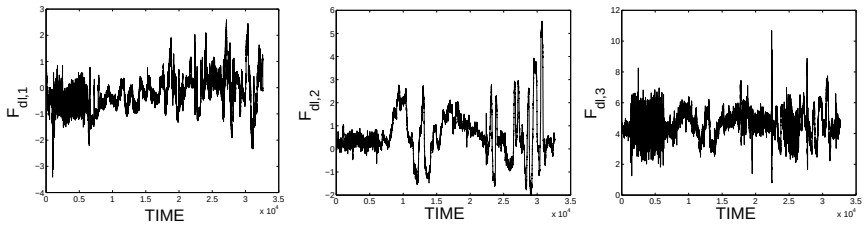

Figure 6.2: Loadings $F_{dl,1}$, $F_{dl,2}$, $F_{dl,3}$.

Moreover the threshold depends on the mean value of the linear combinations of the loads $F^*(A_c, \boldsymbol{F})$. It means that the evaluation of the thresholds with the loads $\boldsymbol{F_{dl}}$ is available for the mean values of the components of $\boldsymbol{F_{dl}}$. This means that the numerical thresholds we have computed is not usable for multi-input forces with different mean values.

Example 6.5.1. Several examples of characterization of optimal geometries will be proposed. The aim is to characterize the structures, optimally designed for predefined $\boldsymbol{F_{dl}}$. In Fig. 6.2, forces from wheels, stored on test tracks are presented. The longitudinal, transversal and the vertical forces are called $F_{dl,1}$, $F_{dl,2}$ and $F_{dl,3}$, respectively. The structures exposed to these loads are designed so that the damage at their critical points reaches one after N times a predefined loading. Let's call D_T the damage induced by one lap of track. The force $\boldsymbol{F_{dl}}$ is composed by N sequences stored during a lap. For optimal structures, we get,

$$N\, D_T(\widehat{A_c}, \boldsymbol{F_{dl}}) = 1. \tag{6.31}$$

Some structures are exposed to two-input loads, or three-input loads $F_{dl,1}$, $F_{dl,2}$ and $F_{dl,3}$. First, we will determine $\mathbf{a}(\widehat{A_c})$ and $T(\widehat{A_c}, \boldsymbol{F_{dl}})$, so that Eq. (6.31) is fulfilled, and for

$$\boldsymbol{F_{dl}} = \begin{pmatrix} F_{dl,1} \\ F_{dl,2} \end{pmatrix}.$$

We will consider that, in the case of bidimensional vector $\mathbf{a}(\widehat{A_c})$,

$$\mathbf{a}(\widehat{A_c}) = \Big(\cos(\gamma(\widehat{A_c})), \sin(\gamma(\widehat{A_c}))\Big).$$

The evaluation of the thresholds $T(\widehat{A_c}, \boldsymbol{F})$ will be done for a finite number of $\gamma(\widehat{A_c})$, called γ_k. In Fig. 6.3, the different thresholds $T(\widehat{A_c}, \boldsymbol{F_{dl}})$ are

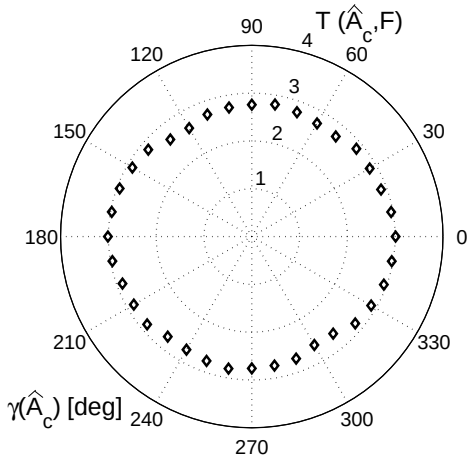

Figure 6.3: Pairs $(T(\widehat{A_c}, F), \mathbf{a}(\widehat{A_c}))$ defining the optimal designed structures, exposed to longitudinal and transversal loads $F_{dl,1}$ and $F_{dl,2}$.

represented in a polar plot, for,

$$\gamma_k = \frac{k\pi}{18} \quad 1 \leq k \leq 18. \tag{6.32}$$

Each γ_k corresponds to a linear combination $\mathbf{a}(\widehat{A_c})$ and a threshold $T(\widehat{A_c}, \boldsymbol{F})$.

Another example is illustrated in Fig. 6.4. Forces $F_{dl,1}$ and $F_{dl,3}$ were taken into account.

$$\boldsymbol{F_{dl}} = \begin{pmatrix} F_{dl,1} \\ F_{dl,3} \end{pmatrix}.$$

The threshold $T(\widehat{A_c}, \boldsymbol{F_{dl}})$ has been computed, for the same values of γ_k in Eq. (6.32).

The next example is computed from the three loads, $F_{dl,1}$, $F_{dl,2}$ and $F_{dl,3}$,

$$\boldsymbol{F_{dl}} = \begin{pmatrix} F_{dl,1} \\ F_{dl,2} \\ F_{dl,3} \end{pmatrix}.$$

The different vectors $\mathbf{a}(\widehat{A_c})$ are generated randomly and uniformly. In Fig. 6.5, the threshold is represented in a polar plot. □

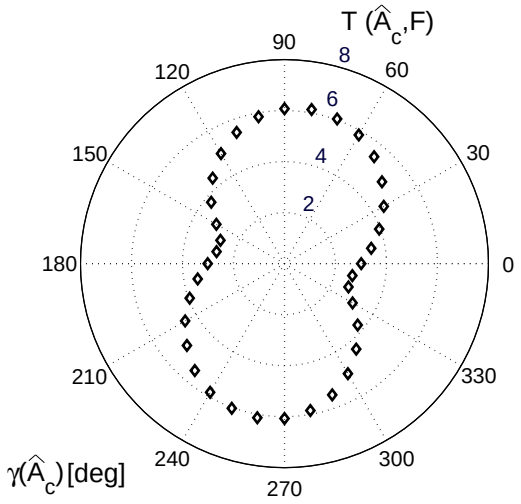

Figure 6.4: Pairs $(T(\widehat{A_c}, \boldsymbol{F}), \mathbf{a}(\widehat{A_c}))$ defining optimal designed structures, exposed to longitudinal and vertical loads $F_{dl,1}$ and $F_{dl,3}$.

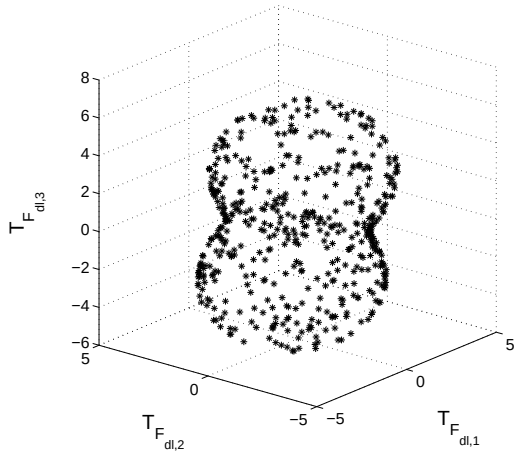

Figure 6.5: Pairs $(T(\widehat{A_c}, \boldsymbol{F}), \mathbf{a}(\widehat{A_c}))$ defining optimal designed structures, exposed to longitudinal, transversal and vertical loads $F_{dl,1}$, $F_{dl,2}$ and $F_{dl,3}$.

6.6 Conclusion

This part is devoted to the evaluation of the damage from one-input and multi-input forces. We succeed in evaluating the damage, under different assumptions. The structures are supposed to be elastic and quasi-static. Under the assumption of uniaxial stress tensor, we use Basquin's criterion to predict the life of the components. In the case of multiaxial stress tensor, Morel's criterion is used. We assume that the stress tensor is proportional.

We end up with different expressions of life prediction. Using Basquin's or Morel's case, the damage is dependent on the rainflow content of linear combinations of the forces. The coefficients defining the linear combinations depend on the geometry of the structures. Other constants appear in the expression of the damage from forces. They are linked to the geometry, the material and the loads.

In the case of Morel's model, the constant $T(A_c, \boldsymbol{F})$, needs to be evaluated. When Assumption 6.2 is valid, a theoretical expression of the threshold is proposed. It can be evaluated numerically for optimal structures, for which the damage reaches one at their critical points, once $\boldsymbol{F_{dl}}$ is applied. In the case of Basquin's criterion, the exponent β, dependent on the material, needs to be determined. The Gerber's parabola have not been used in this application.

For one-input force, the equivalence of damage between F and F^e is fulfilled if the equality in damage is satisfied. However, for multi-input forces, the forces $\boldsymbol{F}$ and $\boldsymbol{F}^e$ are equivalent if the distances between $D(A_c, \boldsymbol{F})$ and $D^e(A_c, \boldsymbol{\theta})$ are minimized, over the different structures.

Chapter 7

Sinusoidal equivalent fatigue loads

In this chapter, a deterministic EFL is studied. Each component of the EFL is considered as a sinusoidal load. Thus, an extension of the uniaxial approach, described in Chapter 3, to the multi-input equivalent fatigue approach, is proposed. The sinusoidal EFL will be developed with Basquin's and Morel's criteria for the evaluation of the damage. The EFL and the measurements are denoted as in Equations (6.1,6.17).

First, we will evaluate the sinusoidal EFL with one block. The measurements are modeled by constant amplitude EFL. Then, we will extend this model. The EFL are not only defined by one block of sinusoid, but several blocks. Each block is characterized by amplitudes, phase shifts, and a number of cycles.

7.1 A model of sinusoidal EFL

A first model of sinusoidal EFL is proposed. Each component is defined by one block of sinusoids. The components of $\boldsymbol{F}^e$ are expressed as,

$$F_i^e(t) = A_i \cos(\omega t + \phi_i),\ 1 \leq i \leq n.$$

Several assumptions are made. The mean of each component of $\boldsymbol{F}^e$ is equal to the one of each component of $\boldsymbol{F}$. Then,

$$\text{mean}(F_i^e) = \text{mean}(F_i).$$

We have chosen to fix the phase shift ϕ_1, otherwise the condition of equivalence does not admit of a unique solution. Hence,

$$\phi_1 = 0. \tag{7.1}$$

Moreover, we have fixed the number of cycles of $\boldsymbol{F}^e$ to N_0. The angular frequency of each component is fixed to ω,

$$\omega = 2\pi \frac{N_0}{T_0}, \tag{7.2}$$

where T_0 is defined in Eq. (6.17).

In the case of one-input EFL,

$$F^{e*}(A_c, t) = F^e(t) = A_1 \cos(\omega t).$$

The variable we need to evaluate from the equivalence of damage is contained in the vector $\boldsymbol{\theta}_s$, as in Notation 5.1. For one-input EFL, we get,

$$\boldsymbol{\theta}_s = (A_1).$$

The vector $\boldsymbol{\theta}_s$ is defined in the parameter space $\boldsymbol{\Theta}_s$,

$$\boldsymbol{\Theta}_s = \{A_1 > 0\}.$$

In the case of multi-input EFL, the different parameters that should be found are the amplitudes and the phase shifts of the different components of $\boldsymbol{F}^e$. We deduce the parameter vector $\boldsymbol{\theta}_s$,

$$\boldsymbol{\theta}_s = (A_1, \ldots, A_n, \phi_2, \ldots, \phi_n). \tag{7.3}$$

The parameter vector $\boldsymbol{\theta}_s$ belongs to the parameters space $\boldsymbol{\Theta}_s$,

$$\boldsymbol{\Theta}_s = \{A_1 > 0, \ldots, A_n > 0, 0 \leq \phi_2 < 2\pi, \ldots, 0 \leq \phi_n < 2\pi\}.$$

7.2 Damage from multi-input sinusoidal loads

In the case of sinusoidal loads, the linear combination of the components, F^{e*}, can be written as,

$$\begin{aligned} F^{e*}(A_c, \boldsymbol{F^e}) &= \mathbf{a}(A_c)\, \boldsymbol{F^e} \\ &= A^*(A_c, \boldsymbol{\theta}_s)\cos(\omega t + \phi^*(A_c, \boldsymbol{\theta}_s)). \end{aligned} \tag{7.4}$$

The vector $\mathbf{a}(A_c)$ is defined by Eq. (6.9) and by its coefficients $a_i(A_c)$. The amplitude $A^*(A_c, \boldsymbol{\theta}_s)$ and the phase $\phi^*(A_c, \boldsymbol{\theta}_s)$ can be derived from the amplitudes and phase shifts of the components of $\boldsymbol{F^e}$,

$$\begin{aligned} A^*(A_c, \boldsymbol{\theta}_s) = \Bigg(& \sum_{i=1}^{n} a_i^2(A_c) A_i^2 \\ & + 2 \sum_{i=1}^{n-1} \sum_{j=i+1}^{n} A_i A_j a_i(A_c) a_j(A_c) \cos(\phi_i - \phi_j) \Bigg)^{\frac{1}{2}}, \end{aligned} \tag{7.5}$$

$$\cos(\phi^*(A_c, \boldsymbol{\theta}_s)) = \frac{\sum_{i=1}^{n} a_i(A_c) A_i \cos\phi_i}{A^*(A_c, \boldsymbol{\theta}_s)}, \quad \text{with} \quad 0 \le \phi^*(A_c, \boldsymbol{\theta}_s) < 2\pi. \tag{7.6}$$

The damage induced by Morel's or Basquin's criterion is based on the rainflow content of $F^{e*}(A_c, \boldsymbol{F^e})$. The rainflow content of $F^{e*}(A_c, \boldsymbol{F^e})$ is reduced to a cycle with the amplitude $A^*(A_c, \boldsymbol{\theta}_s)$ and N_0 number of occurrences ($2N_0$ reversals).

From Theorem 6.1, the damage induced by $F^{e*}(A_c, \boldsymbol{F^e})$, using Morel's criterion, is,

$$D^e(A_c, \boldsymbol{\theta}_s) = \frac{N_0}{2qT(A_c)} (2A^*(A_c, \boldsymbol{\theta}_s) - T(A_c))_+. \tag{7.7}$$

From Theorem 6.2, the damage induced by Basquin's criterion is,

$$D^e(A_c, \boldsymbol{\theta}_{sb}) = C_B(A_c) N_0 (A^*(A_c, \boldsymbol{\theta}_s))^{\beta}. \tag{7.8}$$

7.3 Equivalence of damage

Basquin's and Morel's criteria allow us to evaluate the damage from the parameter vector $\boldsymbol{\theta}_s$. We find a solution $\boldsymbol{\theta}_s$ from the condition of equivalence of damage, described in the previous chapter. For one-input EFL,

the equivalence of damage is governed by Definition 6.3. The damage induced by $\boldsymbol{F}$ is deduced from Remark 6.2 and Remark 6.3 when using Morel's or Basquin's criterion. Using Morel's criterion, from Remark 6.2, the damage induced by the $2N_0$ reversals of the one-input EFL F^e is,

$$D^e(A_c, \boldsymbol{\theta}_s) = \frac{1}{2qT(A_c)} N_0 (2A_1 - T(A_c))_+.$$

Hence, the amplitude of the equivalent load becomes,

$$A_1 = \frac{1}{2}\left(T(A_c) + \frac{1}{N_0}\sum_i (F_{ri} - T(A_c))_+ \right). \tag{7.9}$$

From Basquin's criterion, the damage is expressed from the N_0 rainflow cycles of F^e.

$$D^e(A_c, \boldsymbol{\theta}_s) = C_B(A_c) N_0 A_1^{\beta}. \tag{7.10}$$

The amplitude A_1 is deduced by,

$$A_1 = \frac{1}{N_0} \sqrt[\beta]{\sum_i \left(\frac{F_{ri}}{2}\right)^{\beta}}. \tag{7.11}$$

Note that Eq. (7.9) and Eq. (7.11) involved material and geometrical parameters like $T(A_c)$ and β.

In the case of multi-input loads, the equivalence of damage between $\boldsymbol{F}$ and $\boldsymbol{F^e}$ is expressed in Definition 6.4. The expression of the damage from Morel's or Basquin's criteria are deduced from Theorem 6.2 and Theorem 6.1. The damage induced by the sinusoidal EFL from Morel's criterion is,

$$D^e(A_c, \boldsymbol{\theta}_s) = \frac{1}{2qT(A_c)} N_0 (2A^*(A_c, \boldsymbol{\theta}_s) - T(A_c))_+.$$

The amplitude $A^*(A_c, \boldsymbol{\theta}_s)$ is deduced from the parameters belonging to $\boldsymbol{\theta}_s$, from Equations (7.5,7.6). Basquin's model gives,

$$D^e(A_c, \boldsymbol{\theta}_s) = C_B(A_c) N_0 (A^*(A_c, \boldsymbol{\theta}_s))^{\beta}.$$

The vector $\boldsymbol{\theta}_s$ fulfills Definition 6.4.

Example 7.3.2. An example of sinusoidal two-input EFL is presented here. We choose to model the sequence of variable amplitude forces by a sinusoidal EFL, with $N_0 = 500$ cycles. The EFL and the measurements are

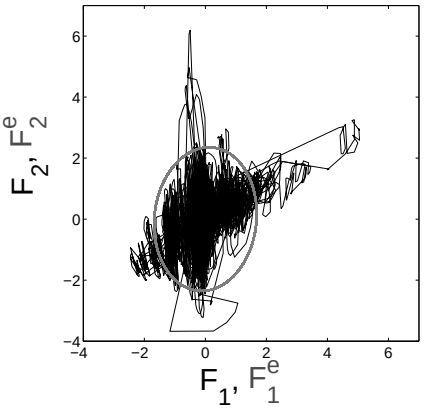

Figure 7.1: Simulation of sinusoidal EFL with Basquin's model.

illustrated in Fig. 7.1. Moreover, we choose Basquin's criterion to evaluate $\boldsymbol{F^e}$, with $\beta = 8$. The parameter vector $\boldsymbol{\theta}_s(A_c)$ is,

$$\boldsymbol{\theta}_s = (1.68, 2.34, 1.47),$$

The phase shift ϕ_2 is expressed in radians, which means 84°. □

7.4 Sinusoidal EFL with several blocks

In this section, the multi-input EFL with several blocks of sinusoids is developed. Each component of $\boldsymbol{F^e}$ is defined by K different blocks. We assume that the number of cycles of each block is the same.

For

$$\frac{(k-1)T_0}{K} \leq t < \frac{kT_0}{K},$$

the k-th block of the component F_i^e is defined as,

$$F_i^e(t) = A_{ki} \cos(\omega t + \phi_{ki}), \quad 1 \leq i \leq n, \quad 1 \leq k \leq K, \tag{7.12}$$

where ω is defined by Eq. (7.2).

7.4.1 Model of sinusoidal EFL with several blocks

For the same reason as in the sinusoidal EFL with one block, we assume that,

$$\phi_{k1} = 0, \quad \forall 1 \leq k \leq K.$$

The parameters defining multi-input sinusoidal EFL with several blocks are contained in the vector $\boldsymbol{\theta}_{sb}$. Amplitudes and phase shifts of each block are contained in $\boldsymbol{\theta}_{sb}$,

$$\begin{aligned}\boldsymbol{\theta}_{sb} = (&A_{11}, \ldots, A_{K1}, A_{12}, \ldots, A_{K2}, \ldots, A_{1K}, \ldots, A_{nK}, \\ &\phi_{12}, \ldots, \phi_{K2}, \ldots, \phi_{1n}, \ldots, \phi_{Kn}).\end{aligned} \tag{7.13}$$

The parameter vector $\boldsymbol{\theta}_{sb}$ belongs to the parameter space $\boldsymbol{\Theta}_{sb}$,

$$\begin{aligned}\boldsymbol{\Theta}_{sb} = \{&A_{11} > 0, \ldots, A_{K1} > 0, \ldots, A_{1K} > 0, \ldots, A_{nK} > 0, \\ &0 \leq \phi_{12} < 2\pi, \ldots, 0 \leq \phi_{K2} < 2\pi, \ldots, \\ &0 \leq \phi_{1n} < 2\pi, \ldots, 0 \leq \phi_{Kn} < 2\pi\}.\end{aligned} \tag{7.14}$$

The damage induced by Morel's or Basquin's criteria is a function of the parameters in $\boldsymbol{\theta}_{sb}$.

7.4.2 Damage from sinusoidal EFL with several blocks

For one-input EFL, the equivalence of damage is governed by Definition 6.3. In the case of one-input EFL with several blocks, we use the equation of equivalence of damage to determine more than one parameter. We do not get a unique solution, due to the number of unknown parameters, greater than the number of equations used to determine them.

In the multi-input case, the damage from Morel's and Basquin's models is deduced from the linear combinations of $\boldsymbol{F^e}$, $F^{e*}(A_c, \boldsymbol{F^e})$. From Eq. (7.12), we deduce $F^{e*}(A_c, \boldsymbol{F^e})$,

$$F^{e*}(A_c, \boldsymbol{F^e}) = A_k^*(A_c, \boldsymbol{\theta}_{sb}) \cos\left(\omega t + \phi_k^*(A_c, \boldsymbol{\theta}_{sb})\right), \quad 1 \leq k \leq K,$$

with

$$\frac{(k-1)T_0}{K} \leq t < \frac{kT_0}{K}.$$

The parameters $A_k^*(A_c, \boldsymbol{\theta}_{sb})$ and $\phi_k^*(A_c, \boldsymbol{\theta}_{sb})$ are deduced from Equations (7.5,7.6).

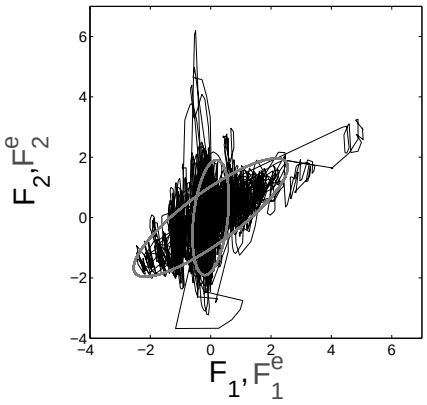

Figure 7.2: Simulation of sinusoidal EFL with Basquin's model.

From Morel's model, the damage induced by $F^{e*}(A_c, \boldsymbol{F^e})$ is deduced from the amplitudes of each block of sinusoids of $F^{e*}(A_c, \boldsymbol{F^e})$,

$$D^e(A_c, \boldsymbol{\theta}_{sb}) = \frac{1}{2qT(A_c)} \frac{N_0}{K} \sum_{k=1}^{K} \left(2A_k^*(A_c, \boldsymbol{\theta}_{sb}) - T(A_c)\right)_+ . \tag{7.15}$$

From Basquin's model, the damage induced by $F^{e*}(A_c, \boldsymbol{F^e})$ is,

$$D^e(A_c, \boldsymbol{\theta}_{sb}) = C_B(A_c) \frac{N_0}{K} \sum_{k=1}^{K} \left(A_k^*(A_c, \boldsymbol{\theta}_{sb})\right)^{\beta} . \tag{7.16}$$

In order for $\boldsymbol{F^e}$ and $\boldsymbol{F}$ to be equivalent in terms of damage, the vector $\boldsymbol{\theta}_{sb}$ has to fulfill Definition 6.4.

Example 7.4.3. In Fig. 7.2, a simulation of sinusoidal EFL with two blocks is presented. The measurements $\boldsymbol{F}$ are the same as in Example 7.3.2. Basquin's model has been chosen, with $\beta = 8$. The number of cycles of each block is 250 cycles. The parameter vector is,

$$\boldsymbol{\theta}_{sb} = (0.6, 2.56, 1.91, 1.96, 1.63, 0.82)$$

The phase shifts are expressed in radians, which means 93.4° and 47°. □

Chapter 8

Gaussian equivalent fatigue loads

In contrast to the sinusoidal EFL, the Gaussian loads are random processes. Morel and Basquin's model will be used. Details about the construction of one-input and multi-input narrow-band Gaussian EFL will be described. In order to use Gaussian processes as EFL, we need to evaluate the expected intensity of rainflow cycles of linear combinations of the components of the forces. In the following, we will see how it is possible to access the distribution of the rainflow amplitudes of Gaussian processes.

We first recall some definitions and properties of Gaussian loads. For more details, see [33] and [29]. Let's consider a random process X,

$$X = \{X(t) : t \in \mathbb{R}\}.$$

The process X is stationary if it satisfies Definition 8.1.

Definition 8.1. *A random process X is stationary if the expectation $E[X(t)]$ does not depend on the time point t,*

$$E[X(t)] = E[X(0)] = m,$$

and if the covariance $C(X(t), X(t+\tau))$ only depends on τ, i.e.

$$\begin{aligned} C(X(t), X(t+\tau)) &= E\left[(X(t) - m)(X(t+\tau) - m)\right] \\ &= E\left[(X(0) - m)(X(\tau) - m)\right] \\ &= r(\tau), \end{aligned} \tag{8.1}$$

where $r(\tau)$ is the covariance function .

Thus,

$$r(0) = Var(X(t)).$$

From the covariance function, the power spectrum can be derived. When the spectrum is continuous,

$$r(t) = \int_{-\infty}^{+\infty} S(f) \exp(2i\pi ft) df.$$

The function S is called the spectral density or the power spectrum of X. Moreover,

$$Var(X(t)) = \int_{-\infty}^{+\infty} S(f) df$$

We can also define the spectral moment λ_m, as a function of the spectral density S,

$$\lambda_m = (2\pi)^m \int_{-\infty}^{+\infty} f^m S(f) df.$$

Thus,

$$\lambda_0 = Var(X(t)).$$

The random process X is a Gaussian random process if it satisfies Definition 8.2,

Definition 8.2. *A random process X is a Gaussian process if, for each n and each time point $t_1, t_2 \ldots, t_n$, every linear combination $\alpha_1 X(t_1) + \ldots + \alpha_n X(t_n)$ has a Gaussian distribution.*

A stationary Gaussian process X is characterized by its spectrum S and its mean value m. We can distinguish two types of Gaussian processes, narrow and broad-band processes, as shown in Fig. 8.1 and Fig. 8.2. The narrow-band Gaussian process is described by a narrow-band power spectrum, as shown in Fig. 8.1. The spectrum is concentrated around some close frequencies. An example of the function $S(f)$ for a narrow-band Gaussian process is, e.g. ,

$$S(f) = \begin{cases} 0 & \text{for } f < f_0 - \frac{\Delta f}{2}, \\ \text{Var}(X(t))/\Delta f & \text{for } f_0 - \frac{\Delta f}{2} < f < f_0 + \frac{\Delta f}{2}, \\ 0 & \text{for } f > f_0 + \frac{\Delta f}{2}. \end{cases}$$

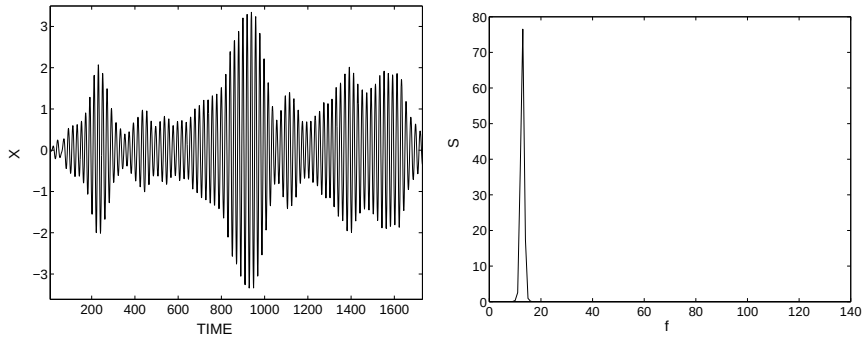

Figure 8.1: Simulation of narrow-band Gaussian process (left) and its estimated spectrum (right).

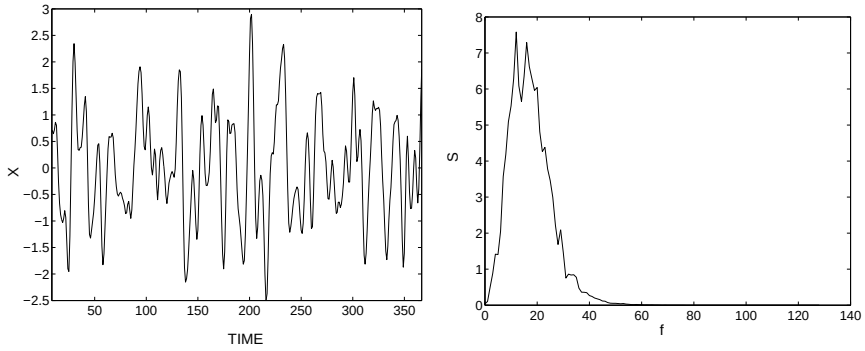

Figure 8.2: Simulation of broad-band Gaussian process (left) and its estimated spectrum (right).

In this case, the spectrum is concentrated around f_0. The irregularity factor, $0 \leq \alpha \leq 1$, is commonly used, taking values close to 1 for narrow-band processes, and close to 0 for broad-band processes,

$$\alpha = \frac{\text{Intensity of upcrossings of the mean of } X}{\text{Intensity of local maxima of X}}.$$

In this study, we are particularly interested in the intensity of rainflow cycles. Much work has been done on the distribution of cycles of Gaussian processes, like [6, 36, 56, 58, 66].

Let's consider the cumulative intensity of rainflow cycles of a Gaussian process, $\mu^{rfc}(u, v)$, as the expected number of rainflow cycles per time unit, with the minimum below the level u and the maximum above the level v, with $u < v$. In [56], it is proved that the cumulative intensity of rainflow cycles is the intensity of upcrossings of the interval $[u, v]$, which was independently found in [59]. Let's consider $N^{osc}_{T_0}(u, v)$, the number of interval upcrossings of the process X, during the time period T_0,

$$N^{osc}_{T_0}(u, v) = \sharp\{\text{upcrossings of } [u, v] \text{ by } \{X_t : t = [0, T_0]\}\},$$

where $\sharp\{.\}$ represents the number of elements in the set $\{.\}$. The variable $N^{rfc}_{T_0}(u, v)$ is the number of rainflow cycles with a minimum below u and a maximum above v, of the process X, during the time period T_0. Thus, from [56],

$$N^{rfc}_{T_0}(u, v) = N^{osc}_{T_0}(u, v).$$

Moreover, if,

$$\mu^{osc}(u, v) = \lim_{T_0 \to +\infty} \frac{E[N^{osc}_{T_0}(u, v)]}{T_0},$$

and,

$$\mu^{rfc}(u, v) = \lim_{T_0 \to +\infty} \frac{E[N^{rfc}_{T_0}(u, v)]}{T_0},$$

then,

$$\mu^{rfc}(u, v) = \mu^{osc}(u, v). \tag{8.2}$$

The Theorem 8.3 is found in [57].

Theorem 8.3. ***Bounding the cumulative intensity of rainflow cycles.*** *Let's consider a continuous random process X, with a finite number of turning points in a bounded time interval. The cumulative intensity of rainflow cycles is bounded from below by the intensity of cycles using the range counting method (or min-max counting cycles, see subsection 2.2.1), which is called $\mu^{rc}(u, v)$. Moreover,*

$\mu^{rfc}(u,v)$ does not exceed the minimum intensity of upcrossings of levels u and v, called $\mu^{+}(u)$ and $\mu^{+}(v)$. Thus,

$$\mu^{rc}(u,v) \leq \mu^{rfc}(u,v) \leq \min\left(\mu^{+}(u), \mu^{+}(v)\right). \tag{8.3}$$

Let's consider $\mu^{+}_{nb}(u)$ and $\mu^{+}_{nb}(v)$, the expected numbers of upcrossings of the levels u and v, per time unit, of a narrow-band Gaussian process. Then the expected number of rainflow cycles with the minimum below u and the maximum above v, $\mu^{rfc}_{nb}(u,v)$ is,

$$\mu^{rfc}_{nb}(u,v) \approx \min\left(\mu^{+}_{nb}(u), \mu^{+}_{nb}(v)\right).$$

In [6, 66], Eq. (8.3) was used to investigate an approximation of the joint probability distribution $h_{rfc}(u,v)$ of rainflow cycles with the minimum at level u and the maximum at level v for a class of Gaussian process. It is expressed by the cycle distribution of a Gaussian process using the range counting method, called $h_{rc}(u,v)$ and the distribution of cycles of a narrow-band Gaussian process, $h_{nb}(u,v)$,

$$h_{rfc}(u,v) = b h_{nb}(u,v) + (1-b) h_{rc}(u,v). \tag{8.4}$$

The parameter b depends on spectral moments λ_0, λ_1, λ_2 and λ_4. Several approximations of the distribution $h_{rc}(u,v)$ have been proposed. One of them is described in [6],

$$h_{rc}(u,v) = \frac{1}{\lambda_0 \alpha^2 2\sqrt{2\pi}} \left(\frac{u-v}{\sqrt{4\lambda_0(1-\alpha^2)}} \right) \exp\left(-\frac{u^2+v^2}{4\lambda_0(1-\alpha^2)} - \frac{(u-v)^2(1-2\alpha^2)}{4\lambda_0(1-\alpha^2)2\alpha^2} \right), \tag{8.5}$$

with

$$\alpha = \frac{\lambda_2}{\sqrt{(\lambda_0 \lambda_4)}},$$

which is the irregularity factor. The coefficient α tends to one for narrow-band Gaussian process, and tends to zero for broad-band Gaussian process. From [66], the distribution $h_{nb}(u,v)$ can be written as,

$$h_{nb}(u,v) = \begin{cases} [p_P(u) - p_V(u)]\delta(u+v) + p_V(u)\delta(u-v) & u > 0 \\ p_P(u)\delta(u-v) & u \leq 0, \end{cases} \tag{8.6}$$

with δ denoted as the dirac function, and $p_P(u)$ and $p_V(v)$ the probability density functions of peaks at the level u and valleys at the level v, respectively. For narrow-band zero-mean Gaussian process X,

$$\begin{aligned} p_P(u) &= p_V(-v) \\ &= \frac{\sqrt{(1-\alpha^2)}}{\sqrt{2\pi\lambda_0}} \exp\left(-\frac{u^2}{2\lambda_0(1-\alpha^2)}\right) \\ &\quad + \frac{\alpha u}{\lambda_0} \exp\left(-\frac{u^2}{2\lambda_0}\right) \Phi\left(\frac{\alpha u}{\sqrt{\lambda_0(1-\alpha^2)}}\right). \end{aligned}$$

The function Φ is the cumulative standard normal distribution function,

$$\Phi(u) = \frac{1}{\sqrt{(2\pi)}} \int_{-\infty}^{u} \exp\left(-\frac{t^2}{2}\right) dt.$$

Equations (8.4, 8.5, 8.6) lead to a complicated approximation of the distribution of the amplitude of rainflow cycles for Gaussian processes. As a first approach of multi-input EFL, and for the sake of simplicity, we will restrict our work to narrow-band Gaussian processes. Thus,

$$h_{rfc}(u,v) = h_{nb}(u,v) \quad \text{and} \quad \alpha = 1.$$

Thus,

$$p_P(u) = \frac{u}{\lambda_0} \exp\left(-\frac{u^2}{2\lambda_0}\right) = p_V(-v).$$

The density function of peaks and valleys is the Rayleigh density function. The marginal distribution of amplitude of rainflow cycles with amplitude h, called $p_H(h)$, is Rayleigh,

$$p_H(h) = \frac{h}{\lambda_0} \exp\left(-\frac{h^2}{2\lambda_0}\right).$$

8.1 Expected damage from one-input stationary narrow-band Gaussian process

In order to evaluate the expected damage from a Gaussian process, we need to obtain information about the intensity of rainflow cycles, when using Basquin's or Morel's criteria. Much work has been done concerning

the evaluation of the rainflow content of narrow-band Gaussian processes. Let's consider a narrow-band stationary Gaussian process X, such as,

$$X = \{X(t) : 0 \leq t \leq T_0\},$$

with mean $E[X(t)] = m$ and variance $Var(X(t)) = \sigma_X^2$. The intensity of level crossings is the expected number of passages of the level u per time unit (see Eq. (2.5)). It is called $\mu^+(u)$. The expected number of upcrossings of the level u by the process X during the time period T_0 is called $\mu^+_{T_0}(u)$,

$$\mu^+_{T_0}(u) = T_0 \mu^+(u).$$

Rice's formula allows us to determine the expected number of level crossings of the level u by a Gaussian process, see [53, 54].

Theorem 8.4. ***Rice's formula.*** *Let's consider a stationary Gaussian process $\{X(t) : 0 \leq t \leq T_0\}$ with mean $E(X(t)) = m$ and variance $Var(X(t)) = \sigma_X^2$ and variance of the derivative $Var(\dot{X}(t)) = \sigma_{\dot{X}}^2$. The expected number of level upcrossings of a level u is:*

$$\mu^+_{T_0}(u) = \frac{T_0}{2\pi} \frac{\sigma_{\dot{X}}}{\sigma_X} \exp\left(-\frac{(u-m)^2}{2\,\sigma_X^2}\right).$$

The expected number of level crossings of the mean m is,

$$\mu^+_{T_0}(m) = \frac{T_0}{2\pi} \frac{\sigma_{\dot{X}}}{\sigma_X}.$$

For a narrow-band Gaussian process, the expected number of cycles during the time period T_0 is approximated by $\mu^+_{T_0}(m)$. The Rayleigh approximation provides an estimation of the intensity of rainflow cycles for narrow-band Gaussian processes, [57].

Theorem 8.5. ***Rayleigh approximation.*** *Let's consider a stationary narrow-band Gaussian process $\{X(t) : 0 \leq t \leq T_0\}$, with the variance σ_X^2 and the variance of the derivative $\sigma_{\dot{X}}^2$. The intensity of rainflow cycles, per time unit, with amplitude h is:*

$$\mu(h) \approx \mu^+(m) p_H(h) = \frac{1}{2\pi} \frac{\sigma_{\dot{X}}}{\sigma_X} \frac{h}{\sigma_X^2} \exp\left(-\frac{h^2}{2\sigma_X^2}\right). \tag{8.7}$$

where $p_H(h)$ is the Rayleigh probability density function of the rainflow cycles with amplitude h.

The expected damage per time unit, induced by rainflow cycles of X, depends on the intensity of rainflow cycles with amplitude h. The expected damage on a time period T_0, computed at a critical point A_c of a geometry, is called $D^e(A_c, X)$, and is defined by Eq. (6.18),

$$D^e(A_c, X) = E[D(A_c, \{X(t) : t \in [0, T_0]\})].$$

8.1.1 Morel's model of life prediction

Let's consider a critical point A_c with the threshold $T(A_c)$. The expected damage on a time period T_0, induced by X, is defined in Remark 6.2. In the case of one-input Gaussian process,

$$\begin{aligned} D^e(A_c, X) &= T_0 \frac{1}{q\, T(A_c)} \int_{\frac{T(A_c)}{2}}^{+\infty} (2h - T(A_c))\, \mu(h)\, dh \qquad (8.8) \\ &= T_0 \frac{1}{q\, T(A_c)} d^e(A_c, X), \qquad (8.9) \end{aligned}$$

where h is the amplitude of the rainflow cycle of X. Let's develop the expression of the damage:

$$\begin{aligned} d^e(A_c, X) &= 2 \int_{\frac{T(A_c)}{2}}^{+\infty} \left(h - \frac{T(A_c)}{2}\right) \mu(h)\, dh \\ &= \frac{1}{\pi} \frac{\sigma_{\dot{X}}}{\sigma_X} \int_{\frac{T(A_c)}{2}}^{+\infty} \left(h - \frac{T(A_c)}{2}\right) \frac{h}{\sigma_X^2} \exp\left(\frac{-h^2}{2\sigma_X^2}\right) dh \\ &= \frac{1}{\pi} \frac{\sigma_{\dot{X}}}{\sigma_X} \left(\left[-\left(h - \frac{T(A_c)}{2}\right) \exp\left(\frac{-h^2}{2\sigma_X^2}\right) \right]_{\frac{T(A_c)}{2}}^{+\infty} \right. \\ &\quad \left. + \int_{\frac{T(A_c)}{2}}^{+\infty} \exp\left(-\frac{h^2}{2\sigma_X^2}\right) dh \right) \\ &= \frac{1}{\pi} \frac{\sigma_{\dot{X}}}{\sigma_X} \left(\int_{\frac{T(A_c)}{2\sigma_X}}^{+\infty} \exp\left(-\frac{v^2}{2}\right) \sigma_X\, dv \right) \\ &= \sigma_{\dot{X}} \sqrt{\frac{2}{\pi}} \int_{\frac{T(A_c)}{2\sigma_X}}^{+\infty} \frac{1}{\sqrt{2\pi}} \exp\left(-\frac{v^2}{2}\right) dv \\ &= \sigma_{\dot{X}} \sqrt{\frac{2}{\pi}} \left(1 - \Phi\left(\frac{T(A_c)}{2\sigma_X}\right)\right). \qquad (8.10) \end{aligned}$$

The function Φ is the normal cumulative distribution. Consequently the expected damage induced by X is finally:

$$D^e(A_c, X) = T_0 \frac{1}{q\, T(A_c)} \sigma_{\dot{X}} \sqrt{\frac{2}{\pi}} \left(1 - \Phi\left(\frac{T(A_c)}{2\sigma_X}\right)\right).$$

Theorem 8.6. ***Expected damage from one-input narrow-band Gaussian process with Morel's criterion.*** *Let A_c be a critical point on a structure fulfilling* Assumption 6.1 *and* Assumption 6.2*, defined by the threshold $T(A_c)$. The stationary Gaussian process $X = \{X(t) : t \in [0, T_0]\}$ is a one-input force, applied to the structure, with the standard deviation σ_X and the standard deviation of the derivative $\sigma_{\dot{X}}$. The damage induced by Morel's criterion at A_c is,*

$$D^e(A_c, X) = T_0 \frac{1}{q\, T(A_c)} \sigma_{\dot{X}} \sqrt{\frac{2}{\pi}} \left(1 - \Phi\left(\frac{T(A_c)}{2\sigma_X}\right)\right). \tag{8.11}$$

8.1.2 Basquin's model of life prediction

Basquin's model of damage is also based on the intensity of rainflow cycles of the process X. Let's consider a critical point of a structure, called A_c. From Remark 6.3, we can deduce the expected damage induced by X, called $D^e(A_c, X)$ over a time period T_0,

$$D^e(A_c, X) = T_0 \int_0^{+\infty} C_B(A_c)\, h^\beta\, \mu(h)\, \mathrm{dh}.$$

From the Rayleigh approximation, we get:

$$D^e(A_c, X) = C_B(A_c)\, \frac{T_0\, \sigma_{\dot{X}}}{2\,\pi\sigma_X} \int_0^{+\infty} h^\beta\, \frac{h}{\sigma_{\dot{X}}^2}\, \exp\left(-\frac{h^2}{2\,\sigma_{\dot{X}}^2}\right) \mathrm{dh}$$

Thus,

$$\begin{aligned} D^e(A_c, X) &= C_B(A_c)\, \frac{T_0\, \sigma_{\dot{X}}}{2\,\pi\sigma_X} \int_0^{+\infty} (2r)^{\beta/2}\, \sigma_X^\beta\, \exp(-r)\mathrm{dr}\,, \qquad \left(r = \frac{h^2}{2\,\sigma_{\dot{X}}^2}\right), \\ &= C_B(A_c)\, \frac{T_0\, \sigma_{\dot{X}}}{2\,\pi\sigma_X}\, 2^{(\beta/2)}\, \sigma_X^\beta \Gamma\left(\frac{\beta}{2} + 1\right). \end{aligned}$$

The gamma function is defined as:

$$\Gamma(t) = \int_0^{+\infty} x^{t-1} \exp(-x) dx.$$

Theorem 8.7. ***Expected damage from one-input narrow-band Gaussian process with Basquin's criterion.*** *Let A_c be a critical point on a structure, fulfilling* Assumption 6.1 *and* Assumption 6.3. *The stationary Gaussian process $X = \{X(t) : t \in [0, T_0]\}$ is a one-input force, applied to the structure, with the standard deviation σ_X and the standard deviation of the derivative $\sigma_{\dot{X}}$. The damage induced by Basquin's criterion at A_c is,*

$$D^e(A_c, X) = C_B(A_c)\, \frac{T_0\, \sigma_{\dot{X}}}{2\, \pi \sigma_X}\, 2^{(\beta/2)}\, \sigma_X^{\beta} \Gamma\left(\frac{\beta}{2} + 1\right). \tag{8.12}$$

8.2 A model of Gaussian EFL

In the following, the one-input Gaussian EFL will be described first. The model will then be extended to multi-input Gaussian EFL, where different difficulties will appear. It mostly concerns the correlation that can appear between the measurements.

Let's consider multi-input stationary narrow-band Gaussian EFL $\boldsymbol{F^e}$, defined by Eq. (6.17). The variance matrix of $\boldsymbol{F^e}$ is called $Var(\boldsymbol{F^e})$,

$$Var(\boldsymbol{F^e}) = \begin{pmatrix} \sigma_1^2 & \dots & \sigma_{1n} \\ \vdots & \ddots & \vdots \\ \sigma_{n1} & \dots & \sigma_n^2 \end{pmatrix}. \tag{8.13}$$

The covariance function of stationary Gaussian processes F_i^e and F_j^e, with mean value m_i and m_j respectively, is called $r_{i,j}$,

$$\begin{aligned} r_{i,j}(\tau) &= C(F_i^e(t), F_j^e(t+\tau)) \\ &= E\left[(F_i^e(t) - m_i)(F_j^e(t+\tau) - m_j)\right]. \end{aligned}$$

The covariance matrix $\boldsymbol{R}(\tau)$ contains all the covariance function of $\boldsymbol{F^e}$,

$$\boldsymbol{R}(\tau) = \begin{pmatrix} & \vdots & \\ \dots & r_{i,j}(\tau) & \dots \\ & \vdots & \end{pmatrix}_{i=1,\dots,n, j=1,\dots,n.}$$

From the covariance function $r_{i,j}(\tau)$, the cross spectrum can be computed,

$$s_{i,j}(f) = \int_{-\infty}^{+\infty} r_{i,j}(\tau) \exp^{-2i\pi f \tau}\, d\tau,$$

when the integral converges. We can deduce the matrix of cross spectra $\boldsymbol{S}(f)$,

$$\boldsymbol{S}(f) = \begin{pmatrix} & \vdots & \\ \dots & s_{i,j}(f) & \dots \\ & \vdots & \end{pmatrix}_{i=1,\dots,n, j=1,\dots,n.}$$

8.2.1 Assumptions

The multi-input Gaussian EFL are assumed to be stationary narrow-band Gaussian processes. The EFL are equivalent in terms of damage to the measurements $\boldsymbol{F}$, defined in Eq. (6.1). We will assume that the expected number of cycles is fixed to N_0, for each component of the EFL. Let's call $\sigma_{\dot{F}_i^e}$, with $1 \leq i \leq n$, the standard deviation of its derivative. Then, from Theorem 8.4, and using,

$$\mu_{T_0}^+(m) = N_0,$$

we get,

$$\sigma_{\dot{F}_i^e} = N_0\, \sigma_i\, \frac{2\pi}{T_0}, \quad i = 1, \dots, n, \tag{8.14}$$

where T_0 is the time period of the process $\boldsymbol{F}^e$. Moreover, we will also consider that, for each component, the mean values of the equivalent loads are equal to the ones of the measurements.

8.2.2 One-input Gaussian EFL

Let's consider the one-input narrow-band stationary Gaussian load F^e, equivalent in terms of damage to the one-input measurement F. The parameter we have to find in order to define F^e entirely is σ_1. Let's consider the parameter vector,

$$\boldsymbol{\theta}_g = (\sigma_1),$$

belonging to the parameter space $\boldsymbol{\Theta}_g$,

$$\boldsymbol{\theta}_g \in \boldsymbol{\Theta}_g = \{\sigma_1 > 0\}.$$

8.2.3 Two-input Gaussian EFL

In Fig. 8.3, a simple example of measurements is presented. In this case, $F_1(t)$ and $F_2(t)$ are correlated in the axis system (A). However, in the axis system (B), the forces do not seem to be correlated anymore.

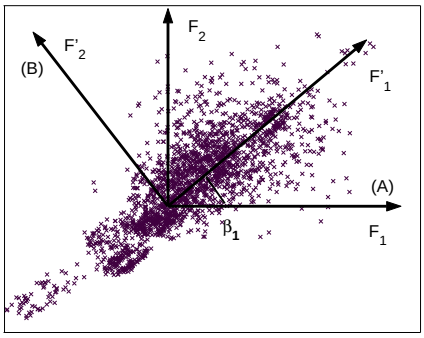

Figure 8.3: Example of correlation between two loads F_1 and F_2, where β_1 is the angle between F_1 and F_1'.

Let's consider the matrix $\boldsymbol{R}_{(A)}$, the estimated covariance matrix of F_1 and F_2. For every time point t, the diagonalized matrix is called $\boldsymbol{R}_{(B)}$,

$$\boldsymbol{R}_{(B)} = \boldsymbol{M}^T \boldsymbol{R}_{(A)} \boldsymbol{M}. \tag{8.15}$$

Therefore, we can define an axis system B, such as the projections of $F_1(t)$ and $F_2(t)$ in B are almost independent. Let's consider $F_1'(t)$ and $F_2'(t)$, resulting from the projection of $F_1(t)$ and $F_2(t)$ in (B),

$$C(F_1'(t), F_2'(t)) \approx 0. \tag{8.16}$$

Let's consider stationary and narrow-band Gaussian EFL $\boldsymbol{F}^e$ such as,

$$\boldsymbol{F}^e = \left\{ \begin{pmatrix} F_1^e \\ F_2^e \end{pmatrix} : t \in [0, T_0] \right\}$$

and,

$$F_i^e = \{F_i^e(t) : 0 \leq t \leq T_0\}, \quad \text{with} \quad i = 1, 2.$$

The construction of the Gaussian EFL will be based on the two-input independent stationary narrow-band Gaussian processes X_1 and X_2, components of $\boldsymbol{X}$,

$$\boldsymbol{X} = \left\{ \begin{pmatrix} X_1(t) \\ X_2(t) \end{pmatrix} : t \in [0, T_0] \right\},$$

and

$$X_i = \{X_i(t) : 0 \leq t \leq T_0\}, \quad \text{with} \quad i = 1, 2.$$

Processes $\boldsymbol{X}$ and $\boldsymbol{F^e}$ are linked by the matrix $\boldsymbol{M}$,

$$\boldsymbol{F^e} = \boldsymbol{M}\boldsymbol{X}. \tag{8.17}$$

The variance of the components of $\boldsymbol{F^e}$ and $\boldsymbol{X}$ are denoted as,

$$Var(\boldsymbol{F^e}) = \begin{pmatrix} \sigma_1^2 & \sigma_{12} \\ \sigma_{21} & \sigma_2^2 \end{pmatrix},$$

and

$$Var(\boldsymbol{X}) = \begin{pmatrix} \sigma_{X_1}^2 & 0 \\ 0 & \sigma_{X_2}^2 \end{pmatrix}.$$

From Eq. (8.17),

$$Var(\boldsymbol{F^e}) = \boldsymbol{M}\, Var(\boldsymbol{X})\, \boldsymbol{M}^T. \tag{8.18}$$

In the two-input case, the change of axis system is given by an angle β_1, see Fig. 8.3. Thus,

$$\boldsymbol{M} = \begin{pmatrix} \cos(\beta_1) & \sin(\beta_1) \\ -\sin(\beta_1) & \cos(\beta_1) \end{pmatrix}.$$

Consequently, we can deduce the standard deviation of the equivalent loads F_1^e and F_2^e from those of X_1 and X_2.

If Eq. (8.14) is fulfilled for the processes X_1 and X_2, we can prove that Eq. (8.14) holds for F_1^e and F_2^e. Let's consider $\sigma_{\dot{X}_1}^2$ and $\sigma_{\dot{X}_2}^2$ the variance of the derivative $\dot{X}_1$ and $\dot{X}_2$,

$$\begin{aligned} \sigma_{\dot{X}_1} &= \frac{N_0 \sigma_{X_1} 2\pi}{T_0}, \\ \sigma_{\dot{X}_2} &= \frac{N_0 \sigma_{X_2} 2\pi}{T_0}. \end{aligned}$$

So, from Eq. (8.18),

$$\begin{aligned} Var(\dot{\boldsymbol{F}}^{\boldsymbol{e}}) &= \boldsymbol{M} \begin{pmatrix} \sigma^2_{\dot{X}_1} & 0 \\ 0 & \sigma^2_{\dot{X}_2} \end{pmatrix} \boldsymbol{M}^T \\ &= \boldsymbol{M} \begin{pmatrix} \left(\frac{N_0 \sigma_{X_1} 2\pi}{T_0}\right)^2 & 0 \\ 0 & \left(\frac{N_0 \sigma_{X_2} 2\pi}{T_0}\right)^2 \end{pmatrix} \boldsymbol{M}^T \\ &= \left(\frac{N_0 2\pi}{T_0}\right)^2 \boldsymbol{M} \begin{pmatrix} \sigma^2_{X_1} & 0 \\ 0 & \sigma^2_{X_2} \end{pmatrix} \boldsymbol{M}^T, \end{aligned}$$

Hence,

$$Var(\dot{\boldsymbol{F}}^{\boldsymbol{e}}) = \left(\frac{N_0 2\pi}{T_0}\right)^2 Var(\boldsymbol{F}^{\boldsymbol{e}}). \tag{8.19}$$

If the expected number of rainflow cycles of X_1 and X_2 is fixed to N_0, the expected number of rainflow cycles for F_1^e and F_2^e is fixed to N_0 as well.

In order to define the Gaussian EFL, we finally need to evaluate the change of the axis system. The vector $\boldsymbol{\theta}_g$ contains parameters defining the equivalent loads,

$$\boldsymbol{\theta}_g = (\sigma_{X_1}, \sigma_{X_2}, \beta_1).$$

The vector $\boldsymbol{\theta}_g$ belongs to the parameter space $\boldsymbol{\Theta}_g$, see [67]:

$$\boldsymbol{\theta}_g \in \boldsymbol{\Theta}_g = \{\sigma_{X_1} > 0, \sigma_{X_2} > 0, -\frac{\pi}{2} \leq \beta_1 \leq \frac{\pi}{2}\}.$$

8.2.4 N-input Gaussian EFL

In the n-input case, the processes $\boldsymbol{X}$ are defined as follows,

$$\boldsymbol{X} = \left\{ \begin{pmatrix} X_1(t) \\ \vdots \\ X_n(t) \end{pmatrix} : 0 \leq t \leq T_0 \right\}$$

The variance of $\boldsymbol{X}$ is characterized by,

$$Var(\boldsymbol{X}) = \begin{pmatrix} \sigma^2_{X_1} & \dots & 0 \\ \vdots & \ddots & \vdots \\ 0 & \dots & \sigma^2_{X_n} \end{pmatrix}.$$

The multi-input EFL are defined in Eq. (6.17), and the variance in Eq. (8.13). Equations (8.17, 8.18) hold in the n-input case. The matrix $\boldsymbol{M}$ is the rotation matrix. Its components are expressed from the $\frac{1}{2}n(n-1)$ angles, see [2] and [67]. The orthogonal matrix $\boldsymbol{M}$ can be decomposed into several orthogonal matrices,

$$\boldsymbol{M} = (\boldsymbol{M}_{12}\boldsymbol{M}_{13}\dots\boldsymbol{M}_{1n})\,(\boldsymbol{M}_{23}\boldsymbol{M}_{24}\dots\boldsymbol{M}_{2n})\dots(\boldsymbol{M}_{(n-1)(n)}), \tag{8.20}$$

with

$$\boldsymbol{M}_{ab} = \begin{pmatrix} \boldsymbol{I} & 0 & 0 & 0 & 0 \\ 0 & \cos(\beta_{ab}) & 0 & \sin(\beta_{ab}) & 0 \\ 0 & 0 & \boldsymbol{I} & 0 & 0 \\ 0 & -\sin(\beta_{ab}) & 0 & \cos(\beta_{ab}) & 0 \\ 0 & 0 & 0 & 0 & \boldsymbol{I} \end{pmatrix} \begin{matrix} \\ \text{row a} \\ \\ \text{row b} \\ \\ \end{matrix}$$

The sines and cosines take place in the rows a and b and in the columns a and b. The different angles β_{ab} with $1 \le a < b \le n$ define the change of axis system from A to B. The components of the $n \times n$ matrix $\boldsymbol{M}$ are called m_{ij}, with $i = 1,\dots,n$ and $j = 1,\dots,n$.

Again, we will consider that $\boldsymbol{X}$ has a fixed and known expected number of cycles N_0. From Eq. (8.14),

$$\sigma_{\dot{X}_i} = \frac{N_0 \sigma_{X_i} 2\pi}{T_0} \quad \text{with} \quad i = 1,\dots,n.$$

Then,

$$\begin{aligned} Var(\dot{\boldsymbol{F}}^{\boldsymbol{e}}) &= \boldsymbol{M} \begin{pmatrix} \sigma^2_{\dot{X}_1} & \dots & 0 \\ \vdots & \ddots & \vdots \\ 0 & \dots & \sigma^2_{\dot{X}_n} \end{pmatrix} \boldsymbol{M}^T \\ &= \boldsymbol{M} \begin{pmatrix} \left(\frac{N_0 \sigma_{X_1} 2\pi}{T_0}\right)^2 & \dots & 0 \\ \vdots & \ddots & \vdots \\ 0 & \dots & \left(\frac{N_0 \sigma_{X_n} 2\pi}{T_0}\right)^2 \end{pmatrix} \boldsymbol{M}^T. \end{aligned}$$

Finally,

$$Var(\dot{\boldsymbol{F}}^{\boldsymbol{e}}) = \left(\frac{N_0 2\pi}{T_0}\right)^2 Var(\boldsymbol{F}^{\boldsymbol{e}}).$$

We can conclude that if the expected number of rainflow cycles of the multi-input process $\boldsymbol{X}$ is fixed to N_0, then $\boldsymbol{F^e}$ has also a fixed expected number of rainflow cycles N_0.

We have assumed that the means of the components of $\boldsymbol{F^e}$ are known and equal the ones of the measurements. The expected number of cycles of $\boldsymbol{F^e}$ is also known. We finally need to characterize the variance of $\boldsymbol{F^e}$ and the change of axis system, from (A) to (B), in order to define the narrow-band stationary Gaussian EFL.

In order to know the matrix $\boldsymbol{M}$, the number of β_{ab} that should be fixed is $\frac{1}{2}n(n-1)$. In addition to the n variances of the components of $\boldsymbol{F^e}$, we finally have $\frac{1}{2}n(n+1)$ different parameters to give, in order to specify the stationary narrow-band Gaussian EFL,

$$\boldsymbol{\theta}_g = (\sigma_{X_1}, \ldots, \sigma_{X_n}, \beta_{12}, \beta_{13}, \ldots, \beta_{1n}, \beta_{23}, \ldots, \beta_{2n}, \ldots, \beta_{(n-1)(n)}). \quad (8.21)$$

The vector $\boldsymbol{\theta}_g$ belongs to the parameter space $\boldsymbol{\Theta}_g$,

$$\boldsymbol{\theta}_g \in \boldsymbol{\Theta}_g = \{\sigma_{X_1} > 0, \ldots, \sigma_{X_n} > 0, -\frac{\pi}{2} \leq \beta_{12} \leq \frac{\pi}{2}, \ldots, -\frac{\pi}{2} \leq \beta_{(n-1)(n)} \leq \frac{\pi}{2}\}.$$

Remark 8.1. *It is also possible to define the orthonormal matrix $\boldsymbol{M}$. Then,*

$$\begin{aligned} &\sum_{i=1}^{n} m_{ij}^2 = 1, \quad j = 1, \ldots n, \\ &\sum_{i=1}^{n} m_{ij} m_{ik} = 0, \quad j = 1, \ldots, n, \quad k = 1, \ldots, n, \quad j \neq k. \end{aligned} \quad (8.22)$$

The total number of components of $\boldsymbol{M}$ is n^2. If we consider Eq. (8.22), the total number of parameters that should be found in order to define $\boldsymbol{M}$ entirely is $\frac{1}{2}n(n-1)$. The vector $\boldsymbol{\theta}_g$ still contains $\frac{1}{2}n(n+1)$ parameters that should be found from the equivalence of damage.

8.3 Equivalence of damage

We aim to evaluate the parameter vector $\boldsymbol{\theta}$, so that the equivalence of damage is fulfilled. From Basquin's or Morel's criterion, the damage is based on the rainflow content of linear combinations of the components of the forces. Thus, the expected damage induced by the EFL is based on the

rainflow content of a linear combination of narrow-band Gaussian processes, called $F^{e*}(A_c, \boldsymbol{F^e})$. A linear combination of narrow-band Gaussian processes is also a narrow-band Gaussian process, if they have the narrow band of their spectra in common. That is why Theorem 8.6 and Theorem 8.7 still hold for $F^{e*}(A_c, \boldsymbol{F^e})$.

8.3.1 One-input Gaussian EFL

The expected damage induced by the force F is $D(A_c, F)$, at a critical point A_c. The damage induced by F^e is called $D^e(A_c, F^e)$ and is deduced from Eq. (8.11), if using Morel's criterion, or from Eq. (8.12), if using Basquin's criterion. The aim is to find the vector $\boldsymbol{\theta}_g$, describing F^e so that the damage induced by the equivalent load is fulfilled, see Definition 6.3. The damage $D^e(A_c, \boldsymbol{\theta}_g)$ is expressed in Eq. (6.18). Hence, we need to solve the equation,

$$D(A_c, F) \quad = \quad D^e(A_c, \boldsymbol{\theta}_g). \tag{8.23}$$

From Morel's criterion, Theorem 8.6 and Eq. (8.14), we get,

$$D^e(A_c, \boldsymbol{\theta}_g) = \frac{N_0 \sigma_1}{q T(A_c)} \sqrt{\frac{2}{\pi}} \left(1 - \Phi\left(\frac{T(A_c)}{2\sigma_1}\right)\right). \tag{8.24}$$

Using Morel's criterion, the damage evaluated from a known sequence of measurement F is expressed from its rainflow content, as shown in Remark 6.2. The ranges of the reversals of the rainflow cycles and residuals of F are called F_{ri}:

$$D(A_c, F) = \frac{1}{2q T(A_c)} \sum_i \left(F_{ri} - T(A_c)\right)_+ .$$

Thus, from Eq. (8.23) and Eq. (8.24), we obtain,

$$\frac{1}{2} \sum_i \left(F_{ri} - T(A_c)\right)_+ = N_0 \sigma_1 \sqrt{\frac{2}{\pi}} \left(1 - \Phi\left(\frac{T(A_c)}{2\sigma_1}\right)\right). \tag{8.25}$$

Let's call g the function,

$$\mathbb{R}^+, \sigma_1 \longmapsto \sigma_1 \Phi\left(1 - \frac{T}{2\sigma_1}\right) \in \mathbb{R}^+,$$

where T is a positive constant. Since the function g is continuous and strictly increasing on $\mathbb{R}^+$, and,

$$g(\sigma_1) \to +\infty \quad \text{when,} \quad \sigma_1 \to +\infty,$$

$$g(\sigma_1) \to 0 \quad \text{when,} \quad \sigma_1 \to 0,$$

and assuming that,

$$0 < \sum_i (F_{ri} - T(A_c))_+ < +\infty,$$

Eq. (8.25) always has a solution.

From Basquin's criterion, Theorem 8.7 and Eq. (8.14), we get,

$$D^e(A_c, \boldsymbol{\theta}_g) = C_B(A_c)\, N_0\, 2^{(\beta/2)}\, \sigma_1^\beta \Gamma\left(\frac{\beta}{2} + 1\right). \tag{8.26}$$

The damage induced by the measurement F_1 is evaluated from Basquin's criterion as follows,

$$D(A_c, F) = C_B(A_c) \sum_i (F_{ri})^\beta. \tag{8.27}$$

From the equality of damage, we can deduce an analytical expression of σ_1,

$$\sigma_1 = \sqrt[\beta]{\frac{\sum_i (F_{ri})^\beta}{N_0\, 2^{(\beta/2)} \Gamma\left(\frac{\beta}{2} + 1\right)}}.$$

We can deduce the standard deviation of F from this expression.

8.3.2 Multi-input Gaussian EFL

In the case of multi-input equivalent fatigue loads,

$$F^{e*}(A_c, \boldsymbol{F^e}) = \mathbf{a}(A_c)\, \boldsymbol{F^e}.$$

From Eq. (8.17),

$$F^{e*}(A_c, \boldsymbol{F^e}) = \mathbf{a}(A_c)\, \boldsymbol{M}\, \boldsymbol{X}. \tag{8.28}$$

Let's call $\sigma^*(A_c, \boldsymbol{F^e})$ the standard deviation of the process $F^{e*}(A_c, \boldsymbol{F})$. We aim to express $\sigma^*(A_c, \boldsymbol{F^e})$ from the variances of the multi-input narrow-band Gaussian process $\boldsymbol{X}$, belonging to the parameter vector $\boldsymbol{\theta}$. From Eq. (8.28), it holds,

$$Var(F^{e*}(A_c, \boldsymbol{F^e})) = [\sigma^*(A_c, \boldsymbol{F^e})]^2 = \sum_{i=1}^{n} \left(\sum_{j=1}^{n} a_i(A_c) m_{ij} \right)^2 \sigma^2_{X_j}, \quad (8.29)$$

where m_{ij} are the components of $\boldsymbol{M}$. Thus, the standard deviation $\sigma^*(A_c, \boldsymbol{F^e})$ is a function of the parameters contained in $\boldsymbol{\theta}_g$. The expected damage induced by the multi-input narrow-band Gaussian EFL, with a fixed expected number of cycles N_0, is expressed from Theorem 8.6 and Eq. (8.14) using Morel's model,

$$D^e(A_c, \boldsymbol{\theta}_g) = \frac{N_0 \sigma^*(A_c, \boldsymbol{\theta}_g)}{q T(A_c)} \sqrt{\frac{2}{\pi}} \left(1 - \Phi \left(\frac{T(A_c)}{\sigma^*(A_c, \boldsymbol{\theta}_g)} \right) \right), \quad (8.30)$$

From Basquin's model and Theorem 8.7 and Eq. (8.14), we get,

$$D^e(A_c, \boldsymbol{\theta}_g) = C_B(A_c)\, N_0\, 2^{(\beta/2)} \left(\sigma^*(A_c, \boldsymbol{\theta}_g) \right)^{\beta} \Gamma \left(\frac{\beta}{2} + 1 \right). \quad (8.31)$$

The EFL are equivalent to the measurements $\boldsymbol{F}$ if $\boldsymbol{\theta}$ satisfies Definition 6.4 and if the square distance between the expected damage of $\boldsymbol{F^e}$ and the damage induced by the measurements is minimized.

Example 8.3.4. In the following example, a transformation of measurements from test tracks into Gaussian EFL has been performed. Morel's criterion has been used. The threshold $T(A_c)$ has been chosen to be constant over the critical points A_c, $T(A_c) = 1$. This example is a two-input case. We have considered that

$$\mathbf{a}(A_c) = (\cos(\gamma(A_c)), \sin(\gamma(A_c))).$$

The measurements are illustrated in Fig. 8.4.

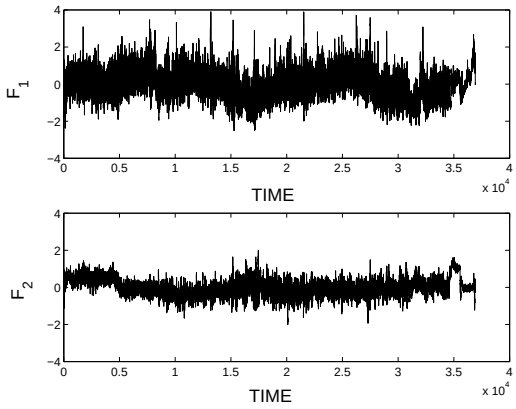

Figure 8.4: Illustration of measurements F_1 and F_2.

The number of cycles N_0 of the EFL is fixed to 1000 cycles. The parameters of the Gaussian EFL have been evaluated, see Fig. 8.5,

$$\boldsymbol{\theta}_g = (0.902, 0.518, 0.017).$$

The angle β_1 is expressed in radians, which means 1°.

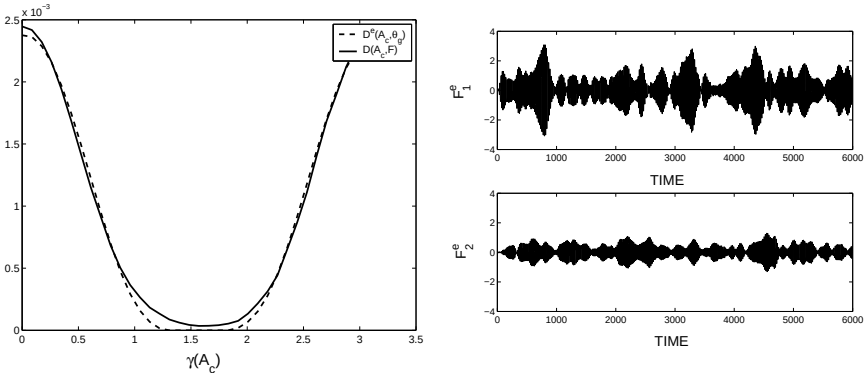

Figure 8.5: Fitting (left) and representation of a sample of F_1^e and F_2^e (right).

The comparison between the Rayleigh distribution and the cumulative frequencies of amplitudes of F_1^e and F_2^e has been calculated, see Fig. 8.6.

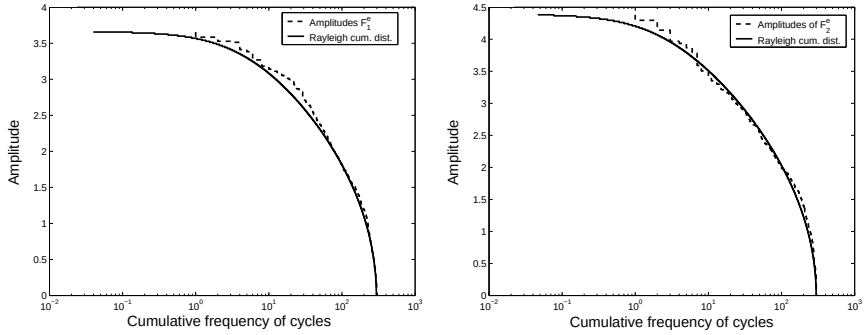

Figure 8.6: Comparison between cumulative frequencies of amplitudes of F_1^e and F_2^e and the Rayleigh cumulative distribution.

□

8.4 Conclusion

In this chapter, we have given a characterization of the stationary narrow-band Gaussian EFL. We are able to evaluate the expected damage from a narrow-band Gaussian process, using Theorem 8.7 and Theorem 8.6. The mean of the Gaussian components of EFL is assumed to be equal to the ones of the components of $\boldsymbol{F}$. The number of cycles of $\boldsymbol{F^e}$ is fixed and known.

We succeeded in translating the dependency existing between the components of the measurements $\boldsymbol{F}$. We observed that there is an axis system linked to $\boldsymbol{F}$, in which the components are almost independent. The parameter vector is composed of the standard deviation of each component of $\boldsymbol{F^e}$, and by the location of the axis system, in the nD space. The evaluation of the multi-input EFL is governed by the equivalence of damage.

Chapter 9

Markov chain equivalent fatigue loads

In the literature, Markov chains have been used to model complicated and variable amplitude sequences of turning points. As we have previously seen, the intensity of rainflow cycles is crucial in the evaluation of the damage the loads induce, when using Morel's or Basquin's criterion. The intensity of rainflow cycles from parameters of a Markov sequence is possible to evaluate, see e.g. [10, 24, 45].

In the following part, we have chosen to treat Markov chain EFL. We will first model the measurements as a simple Markov chain. The simple case of loads with three different states is considered. Moreover, some short and rare events can be identified in the measurements. These rare events usually contain a great part of the damage over the whole sequence. That is the reason why we will reproduce them in the Markov chain EFL. An extension to more than three states will be explored. The different states and the transition matrix are determined by the equivalence of damage.

A Markov chain is a discrete time random process. Every time point is associated to a state. Let's consider a time point t, referred to a state i. The state j occurring at the point $t+1$ only depends on the state at the time point t, and not on the history of the signal. The transition from i to j is governed by the probability to go from i to j. Thus, a Markov chain is defined by its states and the different conditional probabilities to go from

one state to another. These conditional probabilities are called transition probabilities. More details about Markov chains can be found in e.g. [29].

Let's consider the sequence $\{X_0, X_1, \ldots\}$ of random variables, which takes values in the finite space S, also called the state space:

$$S = \{-N, -N+1, \ldots, N-1, N\}. \tag{9.1}$$

Definition 9.1. *The process $\{X_t\}_{t=0}^{\infty}$ is a Markov chain if it satisfies the following condition:*

$$P(X_t = x_t | X_0 = x_0, \ldots, X_{t-1} = x_{t-1}) = P(X_t = x_t | X_{t-1} = x_{t-1}) \\ \forall\, t \in \mathbf{N}, \forall\, x_0, \ldots, x_t \in S. \tag{9.2}$$

The Markov chain X is homogeneous if it satisfies the following condition:

$$P(X_{t+1} = j | X_t = i) = P(X_1 = j | X_0 = i) \quad \forall\, t \in \mathbf{N}, \forall\, i, j \in S. \tag{9.3}$$

The transition matrix $\mathbf{P} = (p_{ij})$ is the matrix of transition probabilities,

$$p_{ij} = P(X_{t+1} = j | X_t = i).$$

The transition matrix $\mathbf{P}$ contains the transition probabilities (p_{ij}) which satisfies,

$$\sum_{j=-N}^{N} p_{ij} = 1. \tag{9.4}$$

Definition 9.2. *The vector $\boldsymbol{\pi}$ is called a stationary distribution of the Markov chain X if $\boldsymbol{\pi}$ has entries $\{\boldsymbol{\pi}_j : j \in S\}$ such that,*

- $\boldsymbol{\pi}_j \geq 0\, \forall j$, *and* $\sum_j \boldsymbol{\pi}_j = 1$,
- $\boldsymbol{\pi} = \boldsymbol{\pi}\mathbf{P}$, *or* $\boldsymbol{\pi}_j = \sum_i \boldsymbol{\pi}_i p_{ij}\, \forall j$.

The component i of the stationary distribution is the probability that the process X is at the state i at time point t,

$$\boldsymbol{\pi}_i = \mathbf{P}(X_t = i). \tag{9.5}$$

In the following, we will consider that the initial distribution of the Markov chain X is $\boldsymbol{\pi}$, i.e,

$$\boldsymbol{\pi}_i = \boldsymbol{P}(X_0 = i).$$

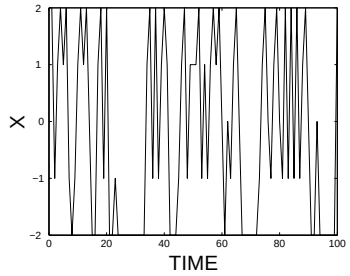

Figure 9.1: Simulation of a Markov chain X with five states.

Example 9.0.5. An example with $N = 2$ is given in detail,

$$\begin{aligned} \mathbf{P} &= \begin{pmatrix} p_{-2-2} & p_{-2-1} & p_{-20} & p_{-21} & p_{-22} \\ p_{-1-2} & p_{-1-1} & p_{-10} & p_{-11} & p_{-12} \\ p_{0-2} & p_{0-1} & p_{00} & p_{01} & p_{02} \\ p_{1-2} & p_{1-1} & p_{10} & p_{11} & p_{12} \\ p_{2-2} & p_{2-1} & p_{20} & p_{21} & p_{22} \end{pmatrix} \\ &= \begin{pmatrix} 0.8 & 0.06 & 0.05 & 0.04 & 0.05 \\ 0.1 & 0.06 & 0.04 & 0.6 & 0.2 \\ 0.5 & 0.4 & 0.05 & 0.03 & 0.02 \\ 0.05 & 0.05 & 0.1 & 0.1 & 0.7 \\ 0.1 & 0.33 & 0.03 & 0.04 & 0.5 \end{pmatrix}. \end{aligned} \tag{9.6}$$

An example of a realization of a Markov chain is given in Fig. 9.1. The stationary distribution π is,

$$\pi = (0.377, 0.153, 0.049, 0.133, 0.287)\,.$$

□

9.1 Expected damage from multidimensional Markov chain loads

The damage is evaluated from the intensity of rainflow cycles of linear combinations of the forces. The multi-input forces $\boldsymbol{F}^e$ are defined in Eq. (6.17). Even if $\boldsymbol{F}^e$ is a multi-input Markov chain, the components or the linear combinations of the components are not Markov chains. Let's call

$F^{e*}(A_c, \boldsymbol{F^e})$ a linear combination of the components of $\boldsymbol{F^e}$, defined by the row vector $\mathbf{a}(A_c) = (a_1(A_c), a_2(A_c), ..., a_n(A_c))$. The entity $\mu^{rfc}(u, v)$ represents the cumulative intensity of rainflow cycles of the process $F^{e*}(A_c, \boldsymbol{F^e})$, with a minimum below u and a maximum above v, $u \leq v$. In [56], it is proved that the cumulative intensity of rainflow cycles is the intensity of upcrossings of the interval $[u, v]$, which was found in [59]. The intensity of upcrossings is called $\mu^{osc}(u, v)$,

$$\mu^{osc}(u, v) = \mu^{rfc}(u, v).$$

The aim is to evaluate the cumulative intensity of rainflow cycles $\mu^{osc}(u, v)$, and study the upcrossings of any interval $[u, v]$, with $u \leq v$, of a linear combination $F^{e*}(A_c, \boldsymbol{F^e})$.

The different states of $\boldsymbol{F^e}$ are contained in S, and are associated with the column vector $\boldsymbol{V_i}$, going from the origin to the state i. The vector $\boldsymbol{V_i}$ is defined in an axis system with n dimensions, with the origin at 0 and axis defined with unit basis vectors $(\boldsymbol{e_1}, \boldsymbol{e_2}, \ldots, \boldsymbol{e_n})$. At the state i, $\boldsymbol{F^e}$ is equal to $\boldsymbol{V_i}$. Let's call g the following application,

$$g : S \ni i \longmapsto \boldsymbol{V_i} \in \mathbb{R}^n.$$

Each value of X in S is associated with a column vector $\boldsymbol{V_i}$,

$$g(i) = \boldsymbol{V_i}.$$

The vector $\boldsymbol{V_i}$ is illustrated in Fig. 9.2. Moreover, let's call v_i^*,

$$v_i^*(A_c) = \mathbf{a}(A_c)\, \boldsymbol{V_i}. \tag{9.7}$$

In order for the linear combination to upcross the interval $[u, v]$, the Markov chain $\boldsymbol{F^e}$ has to go from a set U to a set V, defined, in our case, as:

$$\begin{aligned} \mathrm{U} &= \{i \in S : v_i^*(A_c) < u\}, \\ \mathrm{V} &= \{i \in S : v_i^*(A_c) > v\}. \end{aligned}$$

When $\boldsymbol{F^e}$ goes from U to V, it starts at any state contained in U and can either go directly to any state in V, or may visit the set W, defined as,

$$\mathrm{W} = \{i \in S : u \leq v_i^*(A_c) \leq v\},$$

and finally go to V. The three sets are disjoint and they satisfy the property that,

$$\mathrm{U} \bigcup \mathrm{V} \bigcup \mathrm{W} = S.$$

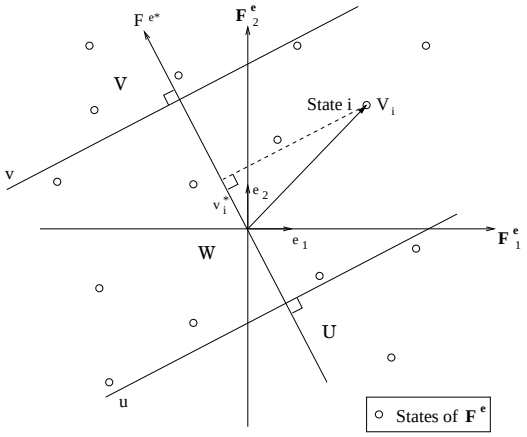

Figure 9.2: Illustration of a path of a bidimensional Markov chain EFL $\mathbf{F^e}$.

The different sets are illustrated in Fig. 9.2, in the case of a bidimensional Markov chain.

In the following, we will evaluate the probability for $\boldsymbol{F^e}$ to go from the set U to the set V, passing, or not, through the set W. The sets are different from a linear combination to another, and from an interval $[u, v]$ to another. The oscillations from U to V will occur in two different ways:

- At time point t, the Markov chain $\boldsymbol{F^e}$ starts at any state contained in U, and goes to any state of V at time point $t + 1$. We will call this first event E_0.
- If it does not go directly from U to V, the process visits the set W. Thus, $\boldsymbol{F^e}$ starts at any state in U at time point t, jumps to any state in W at time point $t + 1$, stay in W from time point $t + 1$ to $t + k$, and finally reaches V at time point $t + 1 + k$. This event is called E_k.

In Fig. 9.3, the events E_0 and E_3 are illustrated. The intensity of rainflow cycles of $F^{e*}(A_c, \boldsymbol{F^e})$, represents the probability that E_0, E_1, ..., all disjoint events, happen. We are thus interested in the probability that $\bigcup_{k=0}^{+\infty} E_k$ happens. The probability that the Markov chain $\boldsymbol{F^e}$ starts in U and goes to

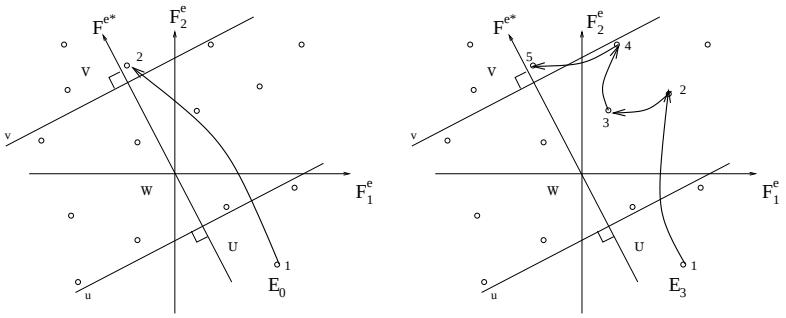

Figure 9.3: Illustration of events E_0 and E_3.

V is,

$$\begin{aligned} \mu^{rfc}(u,v) &= \mu^{rfc}(\mathrm{U},\mathrm{V}) \\ &= \sum_{k=0}^{+\infty} \mathbf{P}(E_k), \end{aligned} \tag{9.8}$$

where $\mathbf{P}(E_k)$ is the probability that the event E_k happens. The aim is to evaluate the probability $\mathbf{P}(E_k)$. Let's consider the states i_u, i_v and i_w, contained in U, V and W, respectively. Then,

$$\mathbf{P}(E_k) = \sum_{i_u \in \mathrm{U}} \mathbf{P}(E_k | X_t = i_u)\, \mathbf{P}(X_t = i_u), \tag{9.9}$$

Then, we can deduce that,

$$\mu^{rfc}(\mathrm{U},\mathrm{V}) = \sum_{k=0}^{+\infty} \sum_{i_u \in \mathrm{U}} \mathbf{P}(E_k | X_t = i_u)\, \mathbf{P}(X_t = i_u).$$

The probability $\mathbf{P}(X_t = i_u)$ is given by the stationary distribution $\boldsymbol{\pi}_{i_u}$, from Eq. (9.5),

$$\boldsymbol{\pi}_{i_u} = \mathbf{P}(X_t = i_u), \quad \forall i_u \in \mathrm{U}.$$

Thus,

$$\mathbf{P}(E_k) = \sum_{i_u \in \mathrm{U}} \mathbf{P}(E_k | X_t = i_u)\, \boldsymbol{\pi}_{i_u}.$$

Let's first consider the event E_0. We are interested in the probability to go from any state $i_u \in \mathrm{U}$ to any state $i_v \in \mathrm{V}$,

$$\mathbf{P}(E_0 | X_t = i_u) = \sum_{i_v \in \mathrm{V}} \mathbf{P}(X_{t+1} = i_v | X_t = i_u), \quad \forall i_u \in \mathrm{U}.$$

So, from Eq. (9.9), we get,

$$\mathbf{P}(E_0) = \sum_{i_u \in \mathrm{U}} \left[\sum_{i_v \in \mathrm{V}} P(X_{t+1} = i_v | X_t = i_u) \right] P(X_t = i_u).$$

Let's define the column vector $\mathbf{d}$,

$$\mathbf{d} = (q_{i_u}), \quad q_{i_u} = \sum_{i_v \in \mathrm{V}} P(X_{t+1} = i_v | X_t = i_u), \quad \forall i_u \in \mathrm{U}. \tag{9.10}$$

The row vector $\tilde{\boldsymbol{\pi}}$ is defined as,

$$\tilde{\boldsymbol{\pi}} = (\boldsymbol{\pi}_{i_u}), \quad \forall i_u \in \mathrm{U}. \tag{9.11}$$

Thus, from Eq. (9.10) and Eq. (9.11),

$$\mathbf{P}(E_0) = \tilde{\boldsymbol{\pi}} \mathbf{d}. \tag{9.12}$$

Let's now consider the event E_1, or the possibility that the signal starts at any state in U, and goes to any state in W, before reaching any state in V. Thus,

$$\begin{aligned} \mathbf{P}(E_1 | X_t = i_u) &= \sum_{i_w \in \mathrm{W}} \left[\mathbf{P}(X_{t+1} = i_w | X_t = i_u) \sum_{i_v \in \mathrm{V}} \mathbf{P}(X_{t+2} = i_v | X_{t+1} = i_w) \right] \\ &= \sum_{i_w \in \mathrm{W}} \left[\mathbf{P}(X_{t+1} = i_w | X_t = i_u) \sum_{i_v \in \mathrm{V}} \mathbf{P}(X_{t+1} = i_v | X_t = i_w) \right], \end{aligned}$$

using the property of homogeneity of the Markov chain X, in Eq. (9.3). We deduce the probability that E_1 happens,

$$\begin{aligned} \mathbf{P}(E_1) = \sum_{i_u \in \mathrm{U}} \Bigg[\sum_{i_w \in \mathrm{W}} & \mathbf{P}(X_{t+1} = i_w | X_t = i_u) \\ & \sum_{i_v \in \mathrm{V}} \mathbf{P}(X_{t+1} = i_v | X_t = i_w) \Bigg] \mathbf{P}(X_t = i_u). \end{aligned} \tag{9.13}$$

Let's first define the matrix $\mathbf{C}$, such that,

$$\mathbf{C} = (p_{i_u i_w}), \quad p_{i_u i_w} = \mathbf{P}(X_{t+1} = i_w | X_t = i_u), \quad \forall i_w \in \mathrm{W}, \forall i_u \in \mathrm{U}. \tag{9.14}$$

The column vector $\mathbf{e}$ is defined as,

$$\mathbf{e} = (q_{i_w}), \quad q_{i_w} = \sum_{i_v \in \mathrm{V}} \mathbf{P}(X_{t+1} = i_v | X_t = i_w), \quad \forall i_w \in \mathrm{W}. \tag{9.15}$$

We deduce a simpler expression of $\mathbf{P}(E_1)$, from Equations (9.11, 9.13, 9.14, 9.15),

$$\mathbf{P}(E_1) = \tilde{\boldsymbol{\pi}}\mathbf{C}\mathbf{e}.$$

The event E_2 happens when the process goes from a state in U, to two states in W, and finally goes to any states in V.

Let's consider i_{w1} and i_{w2} two different states belonging to W. The probability to start from a state i_u to any states i_v, passing by any state i_{w1} and i_{w2} is expressed as,

$$\begin{aligned}\mathbf{P}(E_2|X_t = i_u) = &\sum_{i_{w_1}\in \mathrm{W}} \mathbf{P}(X_{t+1} = i_{w_1}|X_t = i_u) \\ &\sum_{i_{w_2}\in \mathrm{W}} \left[\mathbf{P}(X_{t+2} = i_{w_2}|X_{t+1} = i_{w_1}) \sum_{i_v \in \mathrm{V}} \mathbf{P}(X_{t+3} = i_v|X_{t+2} = i_{w_2})\right] \\ = &\sum_{i_{w_1}\in \mathrm{W}} \mathbf{P}(X_{t+1} = i_{w_1}|X_t = i_u) \\ &\sum_{i_{w_2}\in \mathrm{W}} \left[\mathbf{P}(X_{t+1} = i_{w_2}|X_t = i_{w_1}) \sum_{i_v \in \mathrm{V}} \mathbf{P}(X_{t+1} = i_v|X_t = i_{w_2})\right].\end{aligned} \tag{9.16}$$

Thus, from Eq. (9.9),

$$\begin{aligned}\mathbf{P}(E_2) = \sum_{i_u\in \mathrm{U}} \Bigg[&\sum_{i_{w_1}\in \mathrm{W}} \mathbf{P}(X_{t+1} = i_{w_1}|X_t = i_u) \\ &\sum_{i_{w_2}\in \mathrm{W}} \Bigg[\underbrace{\mathbf{P}(X_{t+1} = i_{w_2}|X_t = i_{w_1}) \sum_{i_v \in \mathrm{V}} \mathbf{P}(X_{t+1} = i_v|X_t = i_{w_2})}\Bigg]\Bigg] \mathbf{P}(X_t = i_u).\end{aligned} \tag{9.17}$$

The term in the brackets is the probability to start at i_{w1} and go to any states $i_v \in \mathrm{V}$, passing by i_{w2}. Let's define the matrix $\mathbf{A}$ as,

$$\mathbf{A} = (p_{i_{w_1} i_{w_2}}), \quad p_{i_{w_1} i_{w_2}} = \mathbf{P}(X_{t+1} = i_{w_2}|X_t = i_{w_1}), \quad \forall i_{w1}, i_{w2} \in \mathrm{W}. \tag{9.18}$$

From Equations (9.11, 9.14, 9.15, 9.17, 9.18), we get,

$$\mathbf{P}(E_2) = \tilde{\boldsymbol{\pi}}\mathbf{C}\mathbf{A}\mathbf{e}.$$

By extension, we can deduce that the probability to go from U to V passing by k different states of W is $\mathbf{P}(E_k)$, so that,

$$\mathbf{P}(E_k) = \tilde{\boldsymbol{\pi}}\mathbf{C}\mathbf{A}^{k-1}\mathbf{e}, \quad k \geq 1. \tag{9.19}$$

From Equations (9.8, 9.12, 9.19), we deduce that,

$$\begin{aligned} \mu^{rfc}(\mathrm{U},\mathrm{V}) &= \tilde{\boldsymbol{\pi}}\mathbf{d} + \sum_{k=1}^{+\infty} \tilde{\boldsymbol{\pi}}\mathbf{C}\mathbf{A}^{k-1}\mathbf{e}, \\ &= \tilde{\boldsymbol{\pi}}\left(\mathbf{d} + \mathbf{C}\left(\sum_{k=1}^{+\infty}\mathbf{A}^{k-1}\right)\mathbf{e}\right). \end{aligned}$$

If the geometrical sum converges, then,

$$\begin{aligned} \sum_{k=1}^{+\infty}\mathbf{A}^{k-1} &= \sum_{k=0}^{+\infty}\mathbf{A}^{k} \\ &= (\mathbf{I}-\mathbf{A})^{-1}. \end{aligned}$$

We obtain,

$$\mu^{rfc}(\mathrm{U},\mathrm{V}) = \tilde{\boldsymbol{\pi}}(\mathbf{d} + \mathbf{C}\,(\mathbf{I}-\mathbf{A})^{-1}\,\mathbf{e}). \tag{9.20}$$

Remark 9.1. *This last expression of $\mu^{rfc}(u,v)$ is valid for infinite time. Thus, in the case of finite life processes, this is an overestimation of the cumulative intensity of rainflow cycles.*

From Eq. (9.8), we have computed the intensity of rainflow cycles of $F^{e*}(A_c, \boldsymbol{F}^e)$, with a minimum below u and a maximum above v, by computing the intensity of upcrossings of the interval $[u,v]$. We end up with an evaluation of the cumulative intensity of rainflow cycles from the transition matrix of the multidimensional Markov chain. More generally, Eq. (9.20) is valid for any disjoint sets U, V and W, and any stationary multidimensional Markov chain. This is illustrated in Fig. 9.4.

From the cumulative intensity of rainflow cycles in Eq. (9.20), we can deduce the intensity of rainflow cycles which start precisely at u and end at v. It is called $f^{rfc}(u,v)$. The amplitudes u_k represents the ordered amplitudes $v_i^*(A_c)$. Thus,

$$u_k \leq u_{k+1} \leq u_{k+2} \ldots \quad \text{with} \quad 1 \leq k \leq 2N+1. \tag{9.21}$$

Let's consider u_{k_1} and u_{k_2}, with $k_1 \leq k_2$ such that,

$$\begin{aligned} u_{k_1} &= u, \\ u_{k_2} &= v. \end{aligned} \tag{9.22}$$

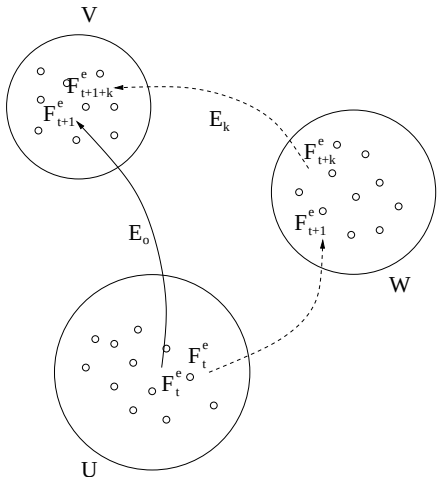

Figure 9.4: Illustration of oscillations from the set U to the set V, possibly passing by W.

Then,

$$\begin{aligned} f^{rfc}(u_{k_1}, u_{k_2}) =& \mu^{rfc}(u_{k_1+1}, u_{k_2-1}) - \mu^{rfc}(u_{k_1}, u_{k_2-1}) \\ & -\mu^{rfc}(u_{k_1+1}, u_{k_2}) + \mu^{rfc}(u_{k_1}, u_{k_2}). \end{aligned} \tag{9.23}$$

The expected number of rainflow cycles per time units, N_1, is deduced from Eq. (9.23),

$$N_1 = \sum_{u_{k_1}} \sum_{u_{k_2}} f^{rfc}(u_{k_1}, u_{k_2}). \tag{9.24}$$

Example 9.1.6. Let's consider a transition matrix $\mathbf{P}$, such as:

$$\mathbf{P} = \begin{pmatrix} 0 & 0 & 1 & 0 & 0 \\ 0 & 0 & 1 & 0 & 0 \\ p_{0-2} & p_{0-1} & 0 & p_{01} & p_{02} \\ 0 & 0 & 1 & 0 & 0 \\ 0 & 0 & 1 & 0 & 0 \end{pmatrix},$$

where

$$p_{ij} = \mathbf{P}(X_{t+1} = j | X_t = i).$$

The transition matrix $\mathbf{P}$ is related to the bidimensional process illustrated in Fig. 9.5. In this example, we will consider the intensity of oscillations

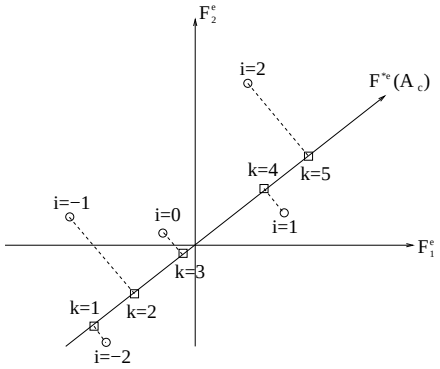

Figure 9.5: Illustration of a bidimensional process with five states.

and the intensity of rainflow cycles of the process $F^{e*}(A_c, \boldsymbol{F^e})$ as shown in Fig. 9.5. From Eq. (9.21), we get,

$$\begin{aligned} u_1 &= v^*_{-2}(A_c), \\ u_2 &= v^*_{-1}(A_c), \\ u_3 &= v^*_{0}(A_c), \\ u_4 &= v^*_{1}(A_c), \\ u_5 &= v^*_{2}(A_c). \end{aligned}$$

For all $0 < k_1 < 2N-1$, for all $0 < k_2 < 2N-1$, such as $k_1 < k_2$, the cumulative intensity of rainflow cycles of $F^{e*}(A_c, \boldsymbol{F^e})$ is,

$$\boldsymbol{\mu^{rfc}} = \begin{pmatrix} 0 & 0 & 0 & 0 & 0 \\ \frac{p_{0-2}}{2} & \frac{p_{0-2}}{2} & \frac{p_{0-2}(p_{01}+p_{02})}{2(1-p_{0-1})} & \frac{p_{0-2}p_{02}}{2(1-p_{0-1}-p_{01})} & 0 \\ \frac{p_{0-2}+p_{0-1}}{2} & \frac{p_{0-2}+p_{0-1}}{2} & \frac{(p_{0-2}+p_{0-1})(p_{01}+p_{02})}{2} & \frac{(p_{0-2}+p_{01})p_{02}}{2(1-p_{01})} & 0 \\ \frac{1-(p_{0-2}+p_{0-1})(p_{01}+p_{02})}{2} & \frac{1-(p_{0-2}+p_{0-1})(p_{01}+p_{02})}{2} & \frac{p_{01}+p_{02}}{2} & \frac{p_{02}}{2} & 0 \\ \frac{1-(p_{0-2}+p_{0-1})(p_{01}+p_{02})}{2} & \frac{1-(p_{0-2}+p_{0-1})(p_{01}+p_{02})}{2} & \frac{p_{01}+p_{02}}{2} & \frac{p_{02}}{2} & 0 \end{pmatrix},$$

The matrix of expected intensity of rainflow cycles $f^{rfc}(u_{k_1}, u_{k_2})$ can be computed from $\mu^{rfc}(u_{k_1}, u_{k_2})$, as in Eq. (9.23),

$$\boldsymbol{f^{rfc}} = \begin{pmatrix} 0 & 0 & A & B & C \\ 0 & 0 & D & E & F \\ 0 & 0 & 0 & G & H \\ 0 & 0 & 0 & 0 & 0 \\ 0 & 0 & 0 & 0 & 0 \end{pmatrix}.$$

with

$$
\begin{aligned}
A &= \frac{p_{0-2}^2}{2(1-p_{0-1})},\\
B &= \frac{p_{0-2}^2 p_{01}}{2(1-p_{0-1})(1-p_{0-1}-p_{01})},\\
C &= \frac{p_{0-2}p_{02}}{2(1-p_{0-1}-p_{01})},\\
D &= \frac{p_{0-1}(1+(p_{0-2}-1)p_{01}-p_{02}+p_{0-2}p_{02}+p_{0-1}(p_{02}+p_{01}-1))}{2(1-p_{0-1})},\\
E &= \frac{1}{2}\Big(\frac{(p_{0-2}+p_{0-1})p_{02}}{p_{01}-1}+\frac{p_{0-2}p_{02}}{p_{01}+p_{0-1}-1}\\
&\quad+\frac{p_{0-2}(p_{01}+p_{02})}{p_{0-1}-1}+(p_{0-2}+p_{0-1})(p_{01}+p_{0-1})\Big),\\
F &= \frac{-p_{0-1}p_{02}(p_{0-2}+p_{0-1}+p_{01}-1)}{2(p_{01}-1)(p_{0-1}+p_{01}-1)},\\
G &= \frac{(p_{0-2}+p_{01})p_{02}}{2(1-p_{01})},\\
H &= \frac{p_{02}(p_{0-2}+p_{0-1}+p_{01})}{2(p_{01}-1)}.
\end{aligned}
\tag{9.25}
$$

□

The Morel's and Basquin's criteria are both based on the intensity of rainflow cycles of a process. The expected damage induced by the process $\boldsymbol{F}^e$, on the time period T_0, is expressed from Eq. (6.18).

9.1.1 Morel's criterion

The range of a rainflow cycle, going from the state i to the state j is $|v_i^*(A_c) - v_j^*(A_c)|$, where $v_i^*(A_c)$ is defined in Eq. (9.7). From Theorem 6.1, we get,

$$
D^e(A_c, \boldsymbol{F}^e) = \frac{T_0}{qT(A_c)} \sum_i \sum_j \Big(|v_i^*(A_c) - v_j^*(A_c)| - T(A_c)\Big)_+ f^{rfc}(i,j).
\tag{9.26}
$$

Only rainflow cycles with ranges greater than the threshold $T(A_c)$ induce damage.

9.1.2 Basquin's criterion

The coefficients of the Basquin's curve are the parameter $B(A_c)$ and exponent β. From Theorem 6.2, the damage induced by $\boldsymbol{F}^e$ is:

$$D^e(A_c, \boldsymbol{F}^e) = C_B(A_c) T_0 \sum_i \sum_j \left(\frac{|v_i^*(A_c) - v_j^*(A_c)|}{2} \right)^\beta f^{rfc}(i,j). \quad (9.27)$$

9.2 A model of Markov chain equivalent fatigue loads

For this first attempt, we will work with the simplest case of Markov chains. The one-input and two-input cases will be developed first. The extension to more than two inputs will then be described in detail.

9.2.1 General assumptions

This study will be developped for zero mean measurements. The Markov chain EFL $\boldsymbol{F}^e$ is assumed to be symmetric around 0,

$$\boldsymbol{F}^e \overset{\mathcal{L}}{=} -\boldsymbol{F}^e. \quad (9.28)$$

This condition implies that,

$$E(\boldsymbol{F}^e) = 0.$$

For the Markov chain EFL $\boldsymbol{F}^e$, we will consider that the expected number of cycles is fixed to N_0, during the time period T_0. Hence, from Eq. (9.24), it follows,

$$N_{T_0} = T_0 \sum_i \sum_j f^{rfc}(i,j) = N_0. \quad (9.29)$$

Moreover, for the models we will develop, we need to define the unknown parameters contained in the vector $\boldsymbol{\theta}_{mc}$ and the parameter space it belongs to, so that the Markov chains EFL $\boldsymbol{F}^e$ are equivalent, in terms of damage, to measurements $\boldsymbol{F}$.

9.2.2 The one-input case

In the one-input case, we have chosen to treat a model with three different states, as shown in Fig. 9.6.

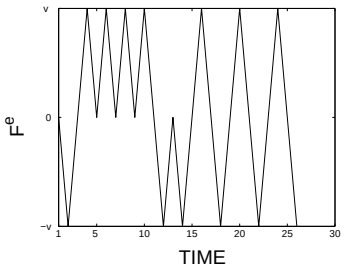

Figure 9.6: Example of realization of Markov chain for one-input equivalent loads with amplitudes $||V_1|| = ||V_{-1}|| = v$.

The levels of states 1 and -1 are defined by the amplitude v, also called the amplitude of the Markov chain F^e. The vector V_i goes from the origin 0 to a states i. Hence,

$$V_1 = -V_{-1} = v.$$

Every time we are at one of the states 1 or -1, the chain goes back to 0 with probability one, which gives:

$$\mathbf{P} = \begin{pmatrix} 0 & 1 & 0 \\ p_1 & 0 & p_{-1} \\ 0 & 1 & 0 \end{pmatrix}.$$

The parameters p_1 and p_{-1} are the transition probabilities to go from the state 0 to one of the states 1 or -1, respectively. From the property of symmetry of $\boldsymbol{F^e}$ and Eq. (9.28), we get,

$$p_{-1} = p_1 = \frac{1}{2}. \tag{9.30}$$

The vector of parameter $\theta_{mc} = v$ belongs to the parameter space Θ_{mc}:

$$\Theta_{mc} = \{v \geq 0\}.$$

We have to evaluate θ_{mc}, so that the damage induced by the one-input Markov chain EFL, $D^e(A_c, \theta_{mc})$, is equal to the damage evaluated from the one-input measurement, $D(A_c, F)$, see Eq. (6.19).

9.2.3 The two-input case

In the two-input case, the model of Markov chain adopted is presented in Fig. 9.7. The different states are corners of a rectangle. The sizes of the lengths are $2v_1$ and $2v_2$.

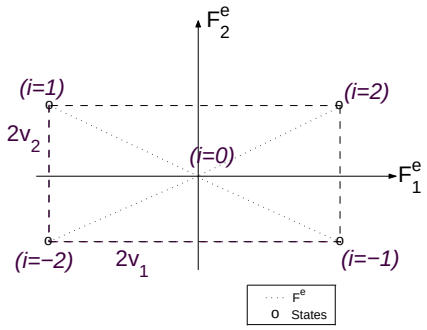

Figure 9.7: Model of Markov chain for two-input EFL.

In the Fig. 9.8, an example of realization of the two-input Markov chain EFL is illustrated.

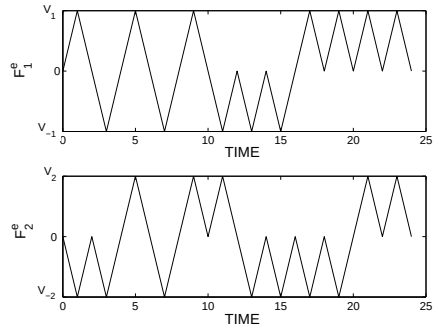

Figure 9.8: Example of a simulated two-input Markov chain EFL.

The transition probabilities to go from one of the states $i = -2, -1, 1, 2$ to the original state $i = 0$ are one. The transition probabilities to go from

the origin 0 to one of the states $i = -2, -1, 1, 2$ are called p_i. Then, the transition matrix called $\mathbf{P}$ can be written as a function of the p_i:

$$\mathbf{P} = \begin{pmatrix} 0 & 0 & 1 & 0 & 0 \\ 0 & 0 & 1 & 0 & 0 \\ p_{-2} & p_{-1} & 0 & p_1 & p_2 \\ 0 & 0 & 1 & 0 & 0 \\ 0 & 0 & 1 & 0 & 0 \end{pmatrix}.$$

Under the assumptions of a symmetric Markov chain EFL $\boldsymbol{F^e}$ and from Eq. (9.4),

$$\begin{aligned} p_{-1} &= p_1, \\ p_{-2} &= p_2. \end{aligned}$$

and

$$\begin{aligned} \boldsymbol{V_1} &= -\boldsymbol{V_{-1}}, \\ \boldsymbol{V_2} &= -\boldsymbol{V_{-2}}. \end{aligned}$$

Moreover, as shown in Fig. 9.7,

$$\boldsymbol{V_1} = -\boldsymbol{V_{-1}} = \begin{pmatrix} -v_1 \\ v_2 \end{pmatrix},$$

$$\boldsymbol{V_2} = -\boldsymbol{V_{-2}} = \begin{pmatrix} v_1 \\ v_2 \end{pmatrix}.$$

From Fig. 9.7, the situations "in phase" or "out of phase" are referred to states 2, -2 and 1, -1, respectively. Let's consider the transition probabilities p_{in} and p_{out} to be in phase or out of phase:

$$\begin{aligned} p_{in} &= p_{-2} + p_2 = 2p_{-2} \\ p_{out} &= p_{-1} + p_1 = 2p_{-1}. \end{aligned} \tag{9.31}$$

From Eq. (9.4),

$$p_{-2} = \frac{1}{2} - p_{-1}.$$

Consequently, in the two-input case, the equivalent loads are defined by parameters, given in the parameter vector $\boldsymbol{\theta}_{mc} = (p_{-1}, v_1, v_2)$. The parameter vector takes values in the parameter space $\boldsymbol{\Theta}_{mc}$:

$$\boldsymbol{\theta}_{mc} \in \boldsymbol{\Theta}_{mc} = \{0 < p_{-1} < \frac{1}{2}, v_1 > 0, v_2 > 0\}.$$

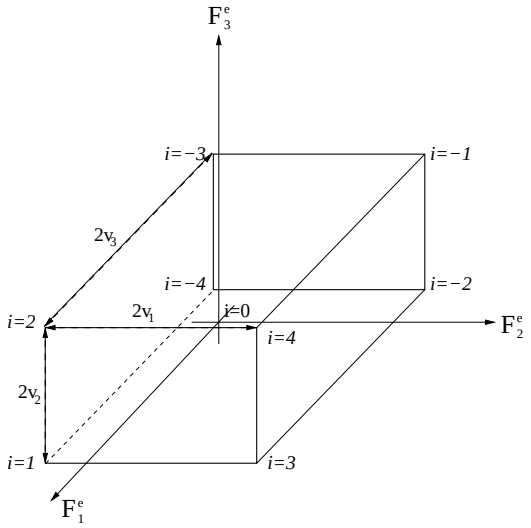

Figure 9.9: Model of Markov chain in three dimensions.

9.2.4 Generalization to the n-input case

The extension of the previous model to more than two forces is proposed. Let's consider $\boldsymbol{F}^e$ and $\boldsymbol{F}$, n-input forces. In the case of $n = 3$, the rectangle formed by the states in Fig. 9.7 is extended to a box, as illustrated in Fig. 9.9. The lengths of the sides are denoted by $2v_1$, $2v_2$ and $2v_3$. The box is centered around zero, the origin. By extensions, in the case of $n > 3$, the EFL are represented by a rectangular parallelepipe in the n dimensional space, centered around the origin 0. It is described by n sides of different lengths, and 2^n corners. Each corner represents a state. Again, every time the Markov chain is at one of the corners, it comes back to the origin. The transition probability to go from the origin to one of its corners, or to one of its states i, is denoted by p_i. The transition matrix $\mathbf{P}$ can be written as:

$$\mathbf{P} = \begin{pmatrix} 0 & \cdots & 0 & 1 & 0 & \cdots & 0 \\ \vdots & & \vdots & \vdots & \vdots & & \vdots \\ 0 & \cdots & 0 & 1 & 0 & \cdots & 0 \\ p_{-w} & \cdots & p_{-1} & 0 & p_1 & \cdots & p_w \\ 0 & \cdots & 0 & 1 & 0 & \cdots & 0 \\ \vdots & & \vdots & \vdots & \vdots & & \vdots \\ 0 & \cdots & 0 & 1 & 0 & \cdots & 0 \end{pmatrix}, \quad \text{with} \quad w = 2^{n-1}. \tag{9.32}$$

Since $\boldsymbol{F^e}$ is symmetric, we have:

$$p_i = p_{-i}.$$

From Eq. (9.4):

$$p_w = \frac{1}{2} - \sum_{i=1}^{w-1} p_i.$$

The vector of parameters $\boldsymbol{\theta}_{mc}$, defining the equivalence of damage, contains all the parameters linked to $\boldsymbol{F^e}$:

$$\boldsymbol{\theta}_{mc} = (p_1, \ldots, p_{w-1}, v_1, \ldots, v_n). \tag{9.33}$$

The vector $\boldsymbol{\theta}_{mc}$ belongs to the parameter space $\boldsymbol{\Theta}_{mc}$,

$$\boldsymbol{\Theta}_{mc} = \{0 < p_1 < \frac{1}{2}, \ldots, 0 < p_{w-1} < \frac{1}{2}, 0 < \sum_{i=1}^{w-1} p_i < \frac{1}{2}, v_1 > 0 \ldots v_n > 0\}$$

and satisfies the equivalence of damage.

9.3 Equivalence of damage

We have previously assumed that the damage is evaluated from the ranges and the intensity of the rainflow cycles. In the case of Markov chain EFL, it depends on the transition matrix, the ranges of the rainflow cycles and on the expected number of cycles $N_{T_0} = N_0$. We will evaluate $\boldsymbol{\theta}_{mcp}$ so that the Markov chain EFL and the measurements fulfill the equivalence of damage.

9.3.1 Equivalence of damage for one-input Markov chain EFL

From Eq. (9.23) and Eq. (9.30), we can deduce the matrix of intensity of rainflow cycles f^{rfc},

$$f^{rfc} = \frac{1}{8} \begin{pmatrix} 0 & 1 & 1 \\ 0 & 0 & 1 \\ 0 & 0 & 0 \end{pmatrix}. \tag{9.34}$$

Hence, from Equations (9.26,9.29,9.34),

$$D^e(A_c, \boldsymbol{\theta}_{mc}) = \frac{N_0}{3qT(A_c)} \left(2\left(v - T(A_c)\right)_+ + \left(2v - T(A_c)\right)_+\right).$$

From the equality of damage, available in the one-input case, see Eq. (6.19),

$$D^e(A_c, \boldsymbol{\theta}_{mc}) = D(A_c, \boldsymbol{\theta}_{mc}).$$

From Equations (9.27,9.29,9.34), we get, for Basquin's criterion,

$$\begin{aligned} D^e(\boldsymbol{\theta}_{mc}, A_c) &= C^B(A_c) N_0 \frac{8}{3}\left(\frac{1}{8}\left(\frac{v}{2}\right)^\beta + \frac{1}{8}(v)^\beta + \frac{1}{8}\left(\frac{v}{2}\right)^\beta\right) \\ &= C^B(A_c)\frac{N_0}{3}(v)^\beta\left(2^{1-\beta}+1\right). \end{aligned}$$

From Remark 6.3 and the equality of damage, we can deduce v, as,

$$v = \sqrt[\beta]{\frac{3\sum_i \left(\frac{F_{ri}}{2}\right)^\beta}{N_0(2^{1-\beta}+1)}}$$

9.3.2 Equivalence of damage for multi-input Markov chain EFL

We now have to find the parameter vector $\boldsymbol{\theta}_{mc}$ that fulfills Eq. (6.22). From Morel's criterion and Eq. (9.26), we can express the damage induced by $F^{e*}(A_c, \boldsymbol{F^e})$, and :

$$\begin{aligned} D^e(A_c, \boldsymbol{\theta}_{mc}) = \frac{N_0}{\sum_i \sum_j f^{rfc}(i,j)} \frac{1}{qT(A_c)} \\ \sum_i \sum_j (|v_i^*(\boldsymbol{\theta}_{mc}, A_c) - v_j^*(\boldsymbol{\theta}_{mc}, A_c)| - T(A_c))_+ f^{rfc}(i,j). \end{aligned}$$

We can express the algebraic values v_i^*, from Eq. (9.7), by the amplitudes of the states v_i, with $1 \leq i \leq n$. Again, the expected number of rainflow cycles of the Markov chain EFL is fixed to N_0.

With Basquin's definition of the damage, the damage is expressed by:

$$D^e(\boldsymbol{\theta}_{mc}, A_c) = \frac{C_B(A_c)N_0}{\sum_i \sum_j f^{rfc}(i,j)} \sum_i \sum_j \left(\frac{|v_i^*(\boldsymbol{\theta}_{mc}, A_c) - v_j^*(\boldsymbol{\theta}_{mc}, A_c)|}{2} \right)^{\beta} f^{rfc}(i,j). \quad (9.35)$$

9.4 Examples

In the first example, a case with one-input force is treated. A second example illustrates the two-input Markov chain EFL. In both of them, the damage is evaluated with Morel's criterion. A threshold $T(A_c)$ has been fixed arbitrarily.

Example 9.4.7. In Fig. 9.10, an example of transforming the measurement F_1 into Markov chain EFL F_1^e is illustrated. In this case, we have considered that $T(A_c) = 1$, for all A_c. Morels' criterion has been chosen to evaluate $D(A_c, \boldsymbol{F})$ and $D^e(A_c, \boldsymbol{\theta}_{mc})$. In this example,

$$\boldsymbol{\theta}_{mc} = (1.009).$$

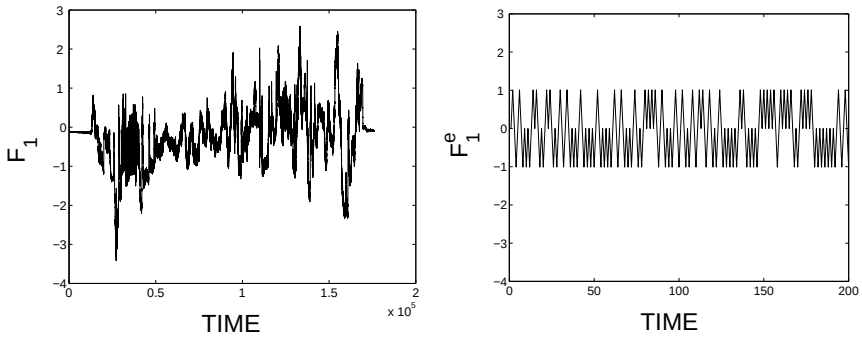

Figure 9.10: Measurement F_1 and representation of a sample of F_1^e (right).

□

Example 9.4.8. In the following pictures, an example of two-input EFL is proposed. Forces F_1 and F_2 are measurements stored during test tracks, see Fig. 9.11.

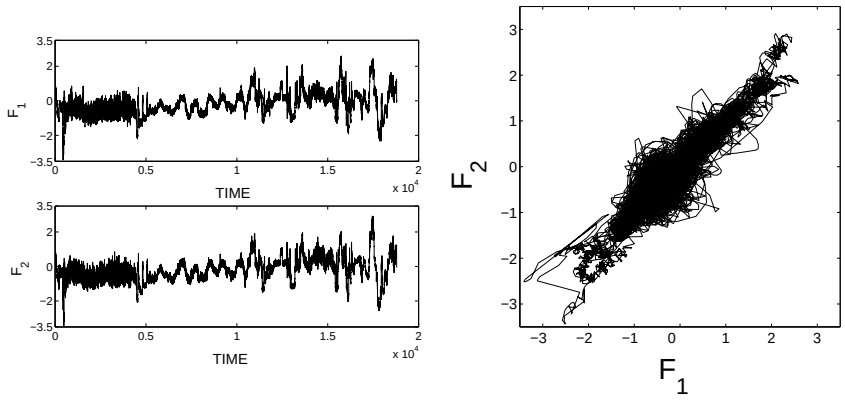

Figure 9.11: Measurements.

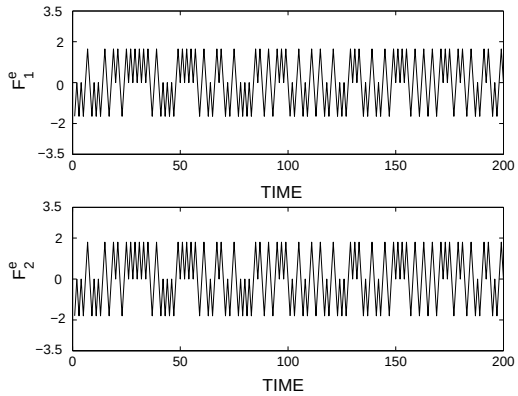

Figure 9.12: Equivalent loads using Basquin's approach.

The evaluation of the damage has been based on Basquin's approach, with Basquin's coefficient $\beta = 8$. The number of cycles $\boldsymbol{F^e}$ has been fixed to 1000. The EFL are illustrated in Fig. 9.12. The vector $\boldsymbol{\theta}_{mc}$ containing the

parameters defining F_1^e and F_2^e is,

$$\boldsymbol{\theta}_{mc} = (0.0024,\, 1.64,\, 1.8).$$

Thus, the transition matrix $\mathbf{P}$ of the example is,

$$\mathbf{P} = \begin{pmatrix} 0 & 0 & 1 & 0 & 0 \\ 0 & 0 & 1 & 0 & 0 \\ 0.4951 & 0.0024 & 0 & 0.0024 & 0.4951 \\ 0 & 0 & 1 & 0 & 0 \\ 0 & 0 & 1 & 0 & 0 \end{pmatrix}$$

From Eq. (9.31) we obtain,

$$\begin{aligned} p_{in} &= 0.9902 \\ p_{out} &= 0.0048. \end{aligned}$$

These probabilities coincides with the observation of the measurements, in Fig. 9.11. The measurements seem to be mostly in phase. □

9.5 Markov chain equivalent fatigue loads with peaks

Some short events happening during the life of components of cars contain a large part of the total damage. They are induced e.g. by bumps or pot holes. They are characterized by some peaks in the measurements of the forces, appearing during test tracks.

The aim of this work is to build a new Markov chain EFL that models these peaks. We will first give a definition of what we mean by peaks in order to detect them and evaluate the damage induced by the peaks. From the equivalence of damage, we will determine the parameter vector $\boldsymbol{\theta}_{mcp}$.

9.5.1 Characterization of peaks

Some peaks in the measurements are induced by some very damaging, short and rare events happening during the life of the components. These peaks represent the rare events. A significant damage is contained in them.

Every critical point is characterized by a linear combination of the components of the forces $\boldsymbol{F}$, and other constants depending on the fatigue criterion chosen. The critical point A_c incurs peaks during the period of time T_0 if $F^*(A_c, \boldsymbol{F})$ contains a peak during T_0. The linear combination can attenuate or magnify some peaks contained in the components of $\boldsymbol{F}$. Consequently, some geometries and critical points, incurring the same forces $\boldsymbol{F}$, can incur peaks when others do not. Hence, the temporal localization of the peaks can be different from one structure and its critical point to another. We choose to define the short events appearing as peaks in, at least, one linear combination, i.e. one critical point of a structure.

The frequency of the accidental events is usually known for structures in service. We can thus get information about the average number of occurrences during the life. The time period T_p is the life of the structures. The expected number of occurrences of peaks during T_p, for each linear combination, i.e. for each structure, is given and fixed to N_p.

Let's consider $N^+_{T_p}(u)$, the intensity of upcrossings of $F^*(A_c, \boldsymbol{F})$, of the level u, and $N^-_{T_p}(v)$, the intensity of downcrossings of the level v, during the time period T_p.

We define as peaks the maxima above a high level v_p and minima below the level u_p, where $u_p = -v_p$ and $v_p > 0$. When N_p peaks are observed during $[0, T_p]$, we have,

$$N^-_{T_p}(u_p) + N^+_{T_p}(v_p) = N_p.$$

As N_p is constant for every structure, the levels u_p and v_p are different from one structure to another, i.e. from one linear combination to another. Other factors can define the peaks in $F^*(A_c, \boldsymbol{F})$. For instance, the detection of the peaks can be supported by the expected damage accumulated by these peaks during the life of the components.

9.5.2 Damage induced by peaks

In order to evaluate the damage induced by the peaks, we need to get the part of the rainflow content of $F^*(A_c, \boldsymbol{F})$ related to them. Turning points below the level u_p or above v_p are peaks.

Definition 9.3. ***Damage induced by peaks.*** *The damage related to the peaks are induced by reversals of residual and rainflow cycles with minimum below u_p or maximum above v_p. The damage of the peaks in $\boldsymbol{F}$ is called $D_p(A_c, \boldsymbol{F})$.*

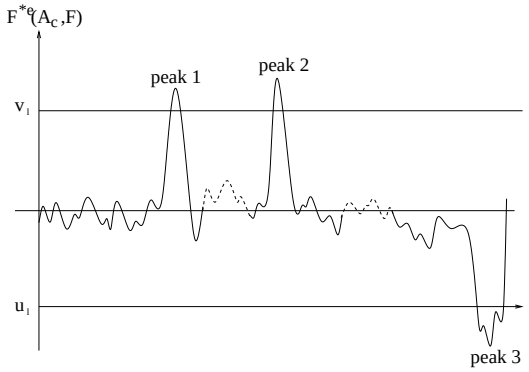

Figure 9.13: Illustration of peaks.

The damage induced by the remaining part of the rainflow content of $F^*(A_c, \boldsymbol{F})$, without the peaks, is called $D_{wp}(A_c, \boldsymbol{F})$,

$$D_{wp}(A_c, \boldsymbol{F}) = D(A_c, \boldsymbol{F}) - D_p(A_c, \boldsymbol{F}) \tag{9.36}$$

9.6 Model of Markov chain with peaks

The general assumptions of the previous model of Markov chain EFL still hold for Markov chain EFL with peaks.

- The Markov chain EFL are symmetric around 0, see Eq. (9.28),
- The expected number of rainflow cycles of the Markov chain EFL is fixed to N_0. Consequently, Eq. (9.29) is still valid.

Let's consider the state space S_p, such that,

$$S_p = \{-N', (-N+1)', \ldots, (N-1)', N'\} \backslash \{0\}.$$

It contains the states that aim to model the peaks. The states that model $\boldsymbol{F}$ without the peaks, belong to the state space S_{wp},

$$S_{wp} = S,$$

where S is defined in Eq. (9.1).

9.6.1 One-input case

We have chosen the one-input Markov chain with peaks as illustrated in Fig. 9.14.

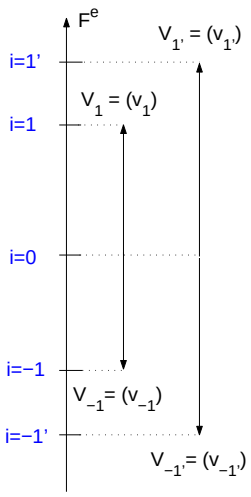

Figure 9.14: One-input Markov chain EFL with peaks.

We will assume that every time the Markov chain is at one of the states 1, -1, $1'$ or $-1'$, $\boldsymbol{F}^e$ goes back to 0. The probability for $\boldsymbol{F}^e$ to start from 0 and to go to one of the states i is called p_i. Consequently,

$$\mathbf{P} = \begin{pmatrix} 0 & 0 & 1 & 0 & 0 \\ 0 & 0 & 1 & 0 & 0 \\ p_{-1'} & p_{-1} & 0 & p_1 & p_{1'} \\ 0 & 0 & 1 & 0 & 0 \\ 0 & 0 & 1 & 0 & 0 \end{pmatrix}.$$

The two states $1'$ and $-1'$, with the greatest amplitudes, will model the damage induced by the peaks of F. They belong to S_p. The three other states 1, -1 and 0 model the remaining part of the damage induced by F. They belong to S_{wp}. The number of peaks in F^e is N_p, during the time pe-

riod T_p. Moreover, the total number of cycles is fixed to N_0. Consequently,

$$\begin{aligned} p_1 + p_{-1} &= \frac{N_0 - N_p}{N_0}, \\ p_{1'} + p_{-1'} &= \frac{N_p}{N_0}. \end{aligned} \tag{9.37}$$

Moreover, from Eq. (9.28) probabilities fulfill the following condition:

$$\begin{aligned} p_{-1'} &= p_{1'}, \\ p_{-1} &= p_1. \end{aligned} \tag{9.38}$$

From Equations(9.4, 9.37, 9.38), we can deduce the transition matrix $\mathbf{P}$,

$$\mathbf{P}(\boldsymbol{F}^e) = \begin{pmatrix} 0 & 0 & 1 & 0 & 0 \\ 0 & 0 & 1 & 0 & 0 \\ \frac{N_p}{2N_0} & \frac{N_0 - N_p}{2N_0} & 0 & \frac{N_0 - N_p}{2N_0} & \frac{N_p}{2N_0} \\ 0 & 0 & 1 & 0 & 0 \\ 0 & 0 & 1 & 0 & 0 \end{pmatrix}.$$

The transition matrix is expressed by the constants N_p and N_0. But we still need to evaluate the amplitudes of the states. From Eq. (9.28) and Fig. 9.14, we deduce,

$$\begin{aligned} v_1 &= -v_{-1}, \\ v_{1'} &= -v_{-1'}. \end{aligned} \tag{9.39}$$

The unknown parameters are contained in $\boldsymbol{\theta}_{mcp}$,

$$\boldsymbol{\theta}_{mcp} = (v_1, v_{1'}). \tag{9.40}$$

The parameter vector $\boldsymbol{\theta}_{mcp}$ belongs to the vector space $\boldsymbol{\Theta}_{mcp}$, such as,

$$\boldsymbol{\Theta}_{mcp} = \{v_1 > 0, v_{1'} > 0\}.$$

9.6.2 Multi-input case

In the case of multi-input Markov chain EFL with peaks, the general approach is the same as the multi-input Markov chain EFL previously seen. However, we will add states in order to model the peaks detected in $\boldsymbol{F}$. Consequently, the different states of the chains are represented by the

corners of two rectangular parallelepipeds, with 2^n corners each. In the three-dimensional case, the Markov chain EFL with peaks is illustrated in Fig. 9.15.

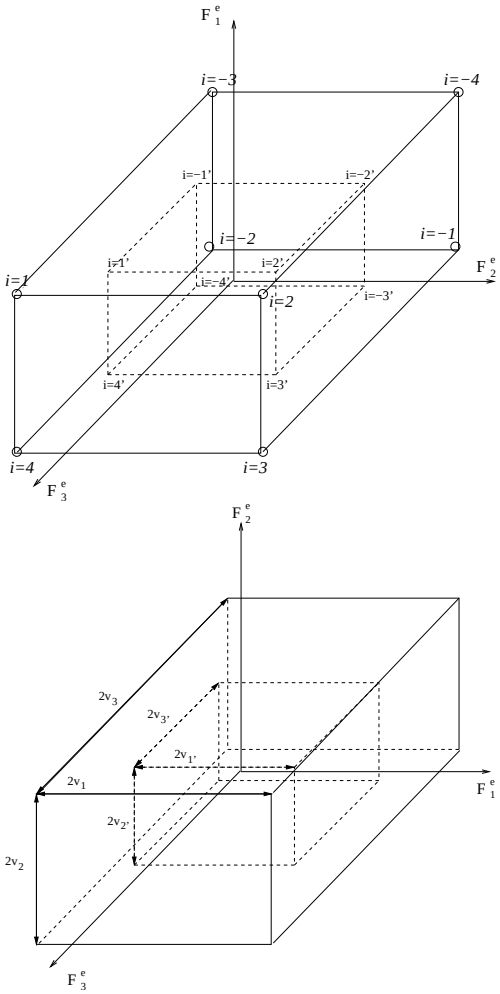

Figure 9.15: States of Markov chain EFL with peaks, in three dimensions.

We will consider that every time the process $\boldsymbol{F^e}$ is at one of the corners of the rectangles, $\boldsymbol{F^e}$ goes back to the state 0 with probability 1. Hence, we

can deduce the following transition matrix,

$$P = \begin{pmatrix} 0 & \cdots & 0 & 0 & \cdots & 0 & 1 & 0 & \cdots & 0 & 0 & \cdots & 0 \\ \vdots & & \vdots & \vdots & & \vdots & \vdots & \vdots & & \vdots & \vdots & & \vdots \\ 0 & \cdots & 0 & 0 & \cdots & 0 & 1 & 0 & \cdots & 0 & 0 & \cdots & 0 \\ p_{-\{2^n\}'} & \cdots & p_{-1'} & p_{-2^n} & \cdots & p_{-1} & 0 & p_1 & \cdots & p_{2^n} & p_{1'} & \cdots & p_{\{2^n\}'} \\ 0 & \cdots & 0 & 0 & \cdots & 0 & 1 & 0 & \cdots & 0 & 0 & \cdots & 0 \\ \vdots & & \vdots & \vdots & & \vdots & \vdots & \vdots & & \vdots & \vdots & & \vdots \\ 0 & \cdots & 0 & 0 & \cdots & 0 & 1 & 0 & \cdots & 0 & 0 & \cdots & 0 \end{pmatrix}.$$

The states $-1', \ldots, \{-2^n\}'$ and $1', \ldots, \{2^n\}'$ are contained in the subset of states S_p. The other states, $-1, \ldots, -2^n$ and $0, 1, \ldots, 2^n$ belong to S_{wp}. Moreover, we have assumed that the mean number of times the process $\boldsymbol{F}^e$ reaches a state in S_p is fixed to N_p, during the time period T_p. Hence,

$$\begin{aligned} \sum_{i=-2^n}^{2^n} p_i &= \frac{N_0 - N_p}{N_0}, \\ \sum_{j=-\{2^n\}'}^{\{2^n\}'} p_j &= \frac{N_p}{N_0}. \end{aligned} \tag{9.41}$$

Finally, as $\boldsymbol{F}^e$ is assumed to be symmetric around 0, then

$$\begin{aligned} p_i &= p_{-i}, \quad \text{for } i = 1, \ldots 2^n, \\ p_j &= p_{-j}, \quad \text{for } j = 1', \ldots \{2^n\}'. \end{aligned} \tag{9.42}$$

Then,

$$\begin{aligned} \sum_{i=1}^{2^n} p_i &= \frac{N_0 - N_p}{2N_0}, \\ \sum_{j=1'}^{\{2^n\}'} p_j &= \frac{N_p}{2N_0}. \end{aligned} \tag{9.43}$$

We therefore need to evaluate $2^{n+1} - 2$ different transition probabilities and $2n$ lengths of the rectangles. The unknown parameters belongs to the vector $\boldsymbol{\theta}_{mcp}$,

$$\boldsymbol{\theta}_{mcp} = (p_1, \ldots, p_{2^n-1}, p_{1'}, \ldots, p_{\{2^n-1\}'}, v_1, \ldots, v_n, v_{1'}, \ldots, v_{n'}). \tag{9.44}$$

The vector $\boldsymbol{\theta}_{mcp}$ belongs to the parameter space $\boldsymbol{\Theta}_{mcp}$,

$$\begin{aligned}\boldsymbol{\Theta}_{mcp} = (0 < p_1 < \frac{1}{2}, \ldots, 0 < p_{2^n-1} < \frac{1}{2},\\ 0 < p_{1'} < \frac{1}{2}, \ldots, 0 < p_{\{2^n-1\}'} < \frac{1}{2}, 0 < \sum_{i=1}^{2^n-1} p_i + \sum_{i=1}^{2^n} p'_i < \frac{1}{2}\\ v_{1'} > v_1 > 0, \ldots, v_{n'} > v_n > 0,).\end{aligned}$$

9.6.3 Equivalence of damage

The equivalence of damage is defined by Eq. (6.19) in the case of one-input EFL, or Eq. (6.22) for multi-input EFL. We aim to minimize the square distance between the damage induced by the EFL and the damage induced by the measurements, over different possible structures. We call $\boldsymbol{\theta}^p_{mcp}$ the vector containing parameters defining the peaks. The vector $\boldsymbol{\theta}^{wp}_{mcp}$ contains parameters defining the EFL without the peaks. Hence,

$$\boldsymbol{\theta}^{wp}_{mcp} = \boldsymbol{\theta}_{mcp} - \boldsymbol{\theta}^p_{mcp}.$$

One-input EFL

In the one input case, the vector $\boldsymbol{\theta}_{mcp}$ has been defined in Eq. (9.40). Hence,

$$\begin{aligned}\boldsymbol{\theta}^p_{mcp} &= (v'_1),\\ \boldsymbol{\theta}^{wp}_{mcp} &= (v_1).\end{aligned}$$

The entity $D^e(A_c, \boldsymbol{\theta}_{mcp})$ is the expected damage induced by the EFL. From Definition 6.3, the parameters of the one-input Markov chain EFL with peaks has to fulfill,

$$D^e(A_c, \boldsymbol{\theta}_{mcp}) = D(A_c, F). \tag{9.45}$$

The vector $\boldsymbol{\theta}_{mcp}$ is composed by two parameters. The equality of damage in Eq. (9.45) is therefore not enough for a unique solution.

Definition 9.4. ***Equivalence of damage for one-input Markov chain EFL with peaks.*** *The one-input Markov chain EFL with peaks is equivalent to measurements* $\boldsymbol{F}$ *if it satisfies,*

$$\begin{aligned}D_{wp}(A_c, F) &= D^e_{wp}(A_c, \boldsymbol{\theta}^{wp}_{mcp}),\\ D_p(A_c, F) &= D^e_p(A_c, \boldsymbol{\theta}^p_{mcp}).\end{aligned} \tag{9.46}$$

Multi-input EFL

In the Eq. (9.44), the vector $\boldsymbol{\theta}$ has been described,

$$\begin{aligned}\boldsymbol{\theta}^{p}_{mcp} &= (p_{1'}, \ldots, p_{\{2^n-1\}'}, v_{1'}, \ldots, v_{n'}),\\ \boldsymbol{\theta}^{wp}_{mcp} &= (p_1, \ldots, p_{\{2^n-1\}}, v_1, \ldots, v_n).\end{aligned}$$

We will consider that multi-input EFL with peaks are equivalent in terms of damage to measurements if Definition 9.5 is fulfilled.

Definition 9.5. ***Equivalence of damage for multi-input Markov chain EFL with peaks.*** *A multi-input Markov chain EFL with peaks, $\boldsymbol{F^e}$, is equivalent in terms of damage to measurements $\boldsymbol{F}$, if the vectors $\boldsymbol{\theta}^{p}_{mcp}$ and $\boldsymbol{\theta}^{wp}_{mcp}$ verify,*

$$\boldsymbol{\theta}^{wp}_{mcp} = arg \min_{\boldsymbol{\theta}^{wp}_{mcp} \in \boldsymbol{\Theta}^{wp}_{mcp}} \left(\int_{||\mathbf{a}||=1} \left(D_{wp}(A_c, \boldsymbol{F}) - D^{e}_{wp}(A_c, \boldsymbol{\theta}^{wp}_{mcp}) \right)^2 dS \right), \tag{9.47}$$

and,

$$\boldsymbol{\theta}^{p}_{mcp} = arg \min_{\boldsymbol{\theta}^{p}_{mcp} \in \boldsymbol{\Theta}^{p}_{mcp}} \left(\int_{||\mathbf{a}||=1} \left(D_{p}(A_c, \boldsymbol{F}) - D^{e}_{p}(A_c, \boldsymbol{\theta}^{p}_{mcp}) \right)^2 dS \right), \tag{9.48}$$

Using Morel's criterion and from Eq. (9.26), we can deduce that the damage $D^{e}_{p}(A_c, \boldsymbol{\theta}^{p}_{mcp})$ and $D^{e}_{wp}(A_c, \boldsymbol{\theta}^{wp}_{mcp})$,

$$\begin{aligned}D^{e}_{p}(A_c, \boldsymbol{\theta}^{p}_{mcp}) = \frac{T'_p}{qT(A_c)} \Bigg(& \sum_{i \in S_{wp}} \sum_{j \in S_p} f^{rfc}(i,j) \left(|v^*_i - v^*_j| - T(A_c) \right)_+ \\ & + \sum_{i \in S_p} \sum_{j \in S_p} f^{rfc}(i,j) \left(|v^*_i - v^*_j| - T(A_c) \right)_+ \\ & + \sum_{i \in S_{wp}} \sum_{j \in S_p} f^{rfc}(i,j) \left(|v^*_i - v^*_j| - T(A_c) \right)_+ \Bigg),\end{aligned}$$

with

$$T'_p = N_p \left(\sum_{i \in S_{wp}} \sum_{j \in S_p} f^{rfc}(i,j) + \sum_{i \in S_p} \sum_{i \in S_{wp}} f^{rfc}(i,j) + \sum_{i \in S_p} \sum_{i \in S_p} f^{rfc}(i,j) \right), \tag{9.49}$$

and

$$D^e_{wp}(A_c, \boldsymbol{\theta}^{wp}_{mcp}) = D^e(A_c, \boldsymbol{\theta}_{mcp}) - D^e_p(A_c, \boldsymbol{\theta}^p_{mcp}). \tag{9.50}$$

The damage $D^e(A_c, \boldsymbol{\theta}_{mcp})$ is defined in Eq. (9.26).

Using Basquin's criterion and Eq. (9.27), we deduce that,

$$\begin{aligned} D^e_p(A_c, \boldsymbol{\theta}^p_{mcp}) = T'_p\, C^B(A_c) \Bigg(& \sum_{i\in S_{wp}} \sum_{j\in S_p} f^{rfc}(i,j) \left(\frac{|v^*_i - v^*_j|}{2} \right)^\beta \\ & + \sum_{i\in S_p} \sum_{j\in S_p} f^{rfc}(i,j) \left(\frac{|v^*_i - v^*_j|}{2} \right)^\beta \\ & + \sum_{i\in S_p} \sum_{j\in S_{wp}} f^{rfc}(i,j) \left(\frac{|v^*_i - v^*_j|}{2} \right)^\beta \Bigg), \end{aligned}$$

where T_p is expressed in Eq. (9.49). The damage $D^e_{wp}(A_c, \boldsymbol{\theta}^{wp}_{mcp})$ can be deduced from Eq. (9.50). The damage $D^e(A_c, \boldsymbol{\theta}_{mcp})$ is computed from Eq. (9.27).

Example 9.6.9. An example of two-input Markov chain EFL with peaks is presented. The measurements are illustrated in Fig. 9.11. We evaluated the damage from Morel's criterion. We considered arbitrary values of $T(A_c) = 1$, for all critical points A_c. The number of cycles N_0 of the EFL is fixed at 1000 cycles. The number of peaks in the measurements is 10. In Fig. 9.16, a sample of $\boldsymbol{F}^e$ is given. The parameter vectors $\boldsymbol{\theta}^p_{mcp}$ and $\boldsymbol{\theta}^{wp}_{mcp}$ are,

$$\boldsymbol{\theta}^p_{mcp} = (0.1141, 0.53, 0.53),$$

$$\boldsymbol{\theta}^{wp}_{mcp} = (5.3\,10^{-4}, 2.1, 2.2).$$

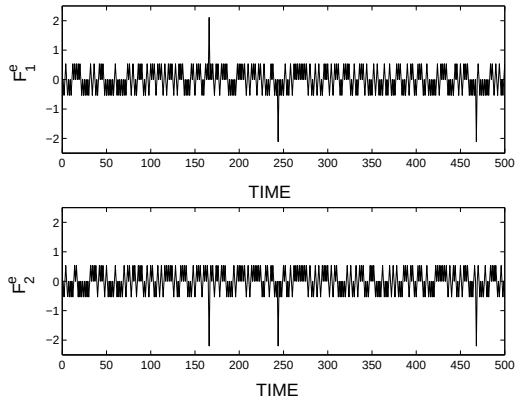

Figure 9.16: An example of two-input EFL with peaks.

□

9.7 Conclusion

We have constructed a first model of Markov chain EFL. It provides a simple multi-input load, equivalent to complicated measurements. A summarize can be found in [28]. The Markov chain can be easily extended and some levels added to the model, in order to get a better equivalence between the loads. The rare events called peaks have been modeled, as they usually contain a great amount of damage in a sequence of measurements. The Markov chain EFL with peaks are more faithful to the measurements and still simple. Moreover, we have considered that the mean value of the components of $\boldsymbol{F^e}$ are zero. In order for $\boldsymbol{F}$ and $\boldsymbol{F^e}$ to have the same mean value, the mean value of each components of $\boldsymbol{F}$ can be added to $\boldsymbol{F^e}$.

Chapter 10

Applications

In this chapter, some applications will be presented. First examples of three-input EFL will be described. The sinusoidal and the Markov chain EFL based on the same measurements and using Basquin's criterion, will be proposed. Moreover, we will compare the sinusoidal EFL, evaluated on the basis of Morel's and Basquin's criteria. Finally, a method for reducing multi-input variable amplitude data will be proposed, in order to reduce the forces to its damaging time points.

The determination of the EFL is based on the evaluation of the parameter vector $\boldsymbol{\theta} \in \boldsymbol{\Theta}$. It is governed by the equivalence of damage, from Definition 6.4. From Equations (6.23,6.24), the equivalence of damage depends on variables depending on the geometry and the material, such as the unit vector $\mathbf{a}(A_c)$. This unit vector is different from one geometry to another, loaded by multi-input forces $\boldsymbol{F}$. The equivalence of damage is valid for any structures, fulfilling the different assumptions presented in Chapter 6. In practice, the unit sphere, containing the unit vectors $\mathbf{a}(A_c)$ is discretized. The unit vectors are uniformly spread on the sphere. They are called $\mathbf{a}_k$, with $1 \leq k \leq K_a$. Each unit vector $\mathbf{a}_k$ corresponds to a structure, loaded by $\boldsymbol{F}$, and the location of the critical point A_c on it.

We aim to evaluate the parameter vector $\widehat{\boldsymbol{\theta}}$, so that,

$$\widehat{\boldsymbol{\theta}} = arg \min_{\widehat{\boldsymbol{\theta}} \in \boldsymbol{\Theta}} \left(\sum_{k=1}^{K_a} \left(D(\mathbf{a}_k, \boldsymbol{F}) - D^e(\mathbf{a}_k, \widehat{\boldsymbol{\theta}}) \right)^2 \right), \tag{10.1}$$

where $D(\mathbf{a}_k, \boldsymbol{F})$ is the damage induced by the measurements, for the unit vector $\mathbf{a}_k$, and $D^e(\mathbf{a}_k, \widehat{\boldsymbol{\theta}})$, the expected damage induced by the EFL. We evaluate the parameter vector from Eq. (6.24), using Basquin's criterion, and from Eq. (6.28), using Morel's criterion. From these two equations, we evaluate $\widehat{\boldsymbol{\theta}}$ using,

$$\widehat{\boldsymbol{\theta}} = arg \min_{\widehat{\boldsymbol{\theta}} \in \boldsymbol{\Theta}} \left(\sum_{k=1}^{K_a} \left(y_k - f(\mathbf{a}_k, \widehat{\boldsymbol{\theta}}) \right)^2 \right), \tag{10.2}$$

with,

$$\begin{aligned} y_k &= \textstyle\sum_i \left(F^*_{ri}(\mathbf{a}_k, \boldsymbol{F}) \right)^\beta, \\ f(\mathbf{a}_k, \widehat{\boldsymbol{\theta}}) &= \textstyle\sum_i \left[E\left(F^{e*}_{ri}(\mathbf{a}_k, \widehat{\boldsymbol{\theta}}) \right)^\beta \right], \end{aligned} \tag{10.3}$$

using Basquin's model. When using Morel's criterion,

$$\begin{aligned} y_k &= \textstyle\sum_i \left(F^*_{ri}(\mathbf{a}_k, \boldsymbol{F}) - T(A_c) \right)_+, \\ f(\mathbf{a}_k, \widehat{\boldsymbol{\theta}}) &= \textstyle\sum_i \left[E\left(F^{e*}_{ri}(\mathbf{a}_k, \widehat{\boldsymbol{\theta}}) - T(A_c) \right)_+ \right]. \end{aligned} \tag{10.4}$$

For each type of EFL, $f(\mathbf{a}_k, \widehat{\boldsymbol{\theta}})$ has a different expression depending on the parameter vector $\widehat{\boldsymbol{\theta}}$.

10.1 Three-input EFL

In the three-input equivalent fatigue approach, two different applications will be presented below. The first one concerns the sinusoidal EFL. An extension of them to the EFL defined with blocks of sinusoids is then explored. Finally, three-input Markov chain EFL will be described. Basquin's criterion is used in this section. The measurements have been stored during test tracks. They represent a sequence of measurements. Basquin's coefficient β has been fixed to 8. The number of cycles N_0 for Markov and sinusoidal forces has been fixed to 1000 cycles. The coordinates of $\mathbf{a}_k$, called a_{ki}, are given according to the following procedure. Let $X_{k1}, \ldots, X_{kn}$ be independent random variables from N(0,1),

$$a_{ki} = \frac{X_{ki}}{\sqrt{\sum_{i=1}^{n} X_{ki}^2}}.$$

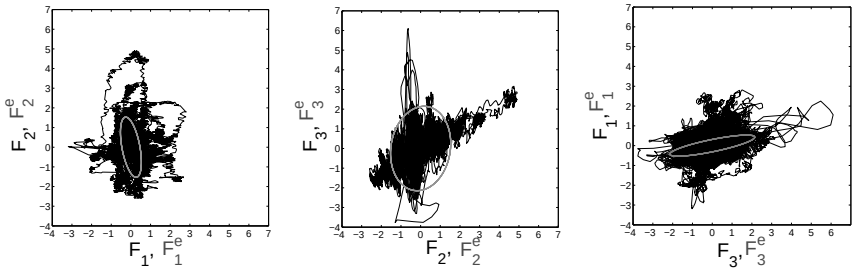

Figure 10.1: Three-dimensional sinusoidal EFL : the measurements are drawn in black and the ellipses representing the sinusoidal EFL, in grey. The number of cycles of the sinusoidal EFL is fixed to 1000 cycles.

10.1.1 Sinusoidal EFL

The parameter vector $\widehat{\boldsymbol{\theta}}_s$ contains the parameters defining the three-input sinusoidal EFL. The aim is to evaluate the vector $\widehat{\boldsymbol{\theta}}_s$ that fulfills Eq. (10.2). From Eq. (7.3),

$$\widehat{\boldsymbol{\theta}}_s = (A_1, A_2, A_3, \phi_2, \phi_3).$$

The parameters A_1, A_2, A_3 are the amplitudes of the components of $\boldsymbol{F^e}$. The phase shifts are denoted as ϕ_2, ϕ_3, assuming that $\phi_1 = 0$. From Basquin's model of damage, we evaluate y_k from Eq. (10.3). The variable $f(\mathbf{a}_k, \widehat{\boldsymbol{\theta}}_s)$ for the sinusoidal EFL is deduced from Eq. (7.8),

$$f(\mathbf{a}_k, \widehat{\boldsymbol{\theta}}_s) \quad = N_0 \left(A^*(\mathbf{a}_k, \widehat{\boldsymbol{\theta}}_s) \right)^{\beta},$$

where $A^*(\mathbf{a}_k, \widehat{\boldsymbol{\theta}}_s)$ is expressed in Eq. (7.5). In Fig. 10.1, the measurements and the sinusoidal loads have been drawn together. The fitting of y_k and $f(\mathbf{a}_k, \widehat{\boldsymbol{\theta}}_s)$ is drawn in Fig. 10.2. The k are ordered so that $f(\mathbf{a}_k, \widehat{\boldsymbol{\theta}}_s)$ increases. We can deduce a numerical evaluation of $\widehat{\boldsymbol{\theta}}_s$, such as,

$$\widehat{\boldsymbol{\theta}}_s = (0.53, 1.54, 2.15, 4.19, 5.65).$$

The parameters ϕ_2 and ϕ_3 are expressed in radians. In this example, we have considered $K_a = 200$.

An extension of the sinusoidal EFL will be described. The sequence of sinusoidal EFL is composed of two different blocks of sinusoids. The two

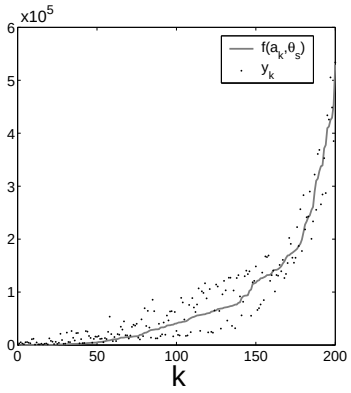

Figure 10.2: Equivalence of damage in the case of sinusoidal EFL with one block of sinusoids.

blocks have the same frequency. The number of cycles of each of them is fixed to 500 cycles. From Eq. (7.13), the parameter vector is,

$$\widehat{\boldsymbol{\theta}}_{sb} = (A_{11}, A_{21}, A_{12}, A_{22}, A_{13}, A_{23}, \phi_{12}, \phi_{22}, \phi_{13}, \phi_{23}).$$

The measurements and the EFL are shown in Fig. 10.3. The parameter vector $\widehat{\boldsymbol{\theta}}_{sb}$ fulfilling Eq. (10.1) is,

$$\widehat{\boldsymbol{\theta}}_{sb} = (0.95, 1.06, 0.64, 1.68, 2.64, 1.55, 5.36, 4.88, 0.65)\,.$$

We can conclude from Fig. 10.4 that the fitting is improved when the EFL are defined by two blocks of sinusoids. The same kind of improvement of the fitting can be done whatever the type of EFL.

10.1.2 Markov chain EFL

In the case of three-input Markov chain EFL, the expected damage evaluated from the multi-input EFL is expressed in Eq. (9.27),

$$f(\mathbf{a}_k, \widehat{\boldsymbol{\theta}}_{mc}) = \frac{N_0}{\sum_i \sum_j f^{rfc}(i,j)} \sum_i \sum_j \left(\frac{v_i^*(\widehat{\boldsymbol{\theta}}_{mc}, \mathbf{a}_k) - v_j^*(\widehat{\boldsymbol{\theta}}_{mc}, \mathbf{a}_k)}{2} \right)^{\beta} f^{rfc}(i,j).$$

The variable y_k is given in Eq. (10.3). The parameter vector $\widehat{\boldsymbol{\theta}}_{mc}$ fulfills Eq. (10.2). In this example, we still consider $K_a = 200$. The number of cycles N_0 is fixed to 1000 cycles.

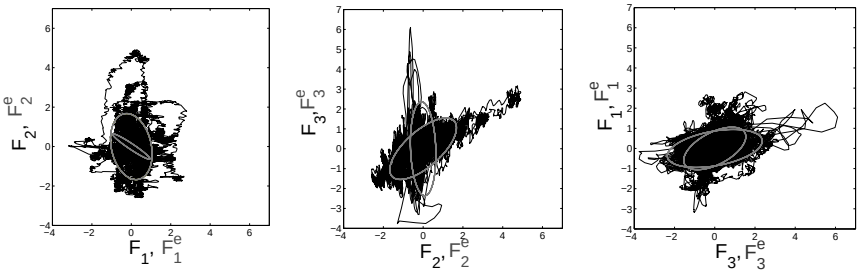

Figure 10.3: Three-dimensional sinusoidal EFL with two blocks. The measurements are drawn in black and the ellipses representing the sinusoidal EFL, in grey. Each block is a sequence of 500 cycles.

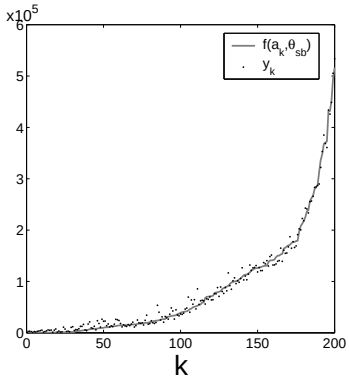

Figure 10.4: Equivalence of damage in the case of sinusoidal EFL with two blocks of sinusoids.

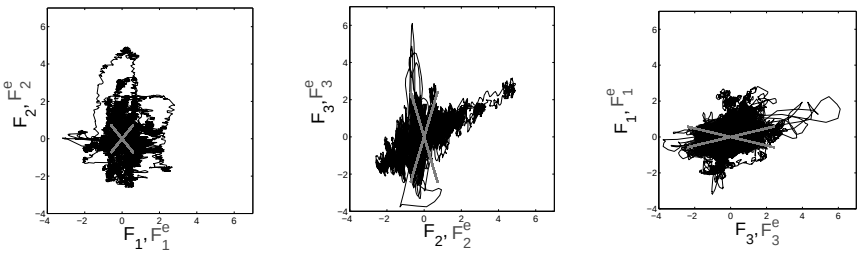

Figure 10.5: Three-dimensional Markov chain EFL. The measurements are drawn in black and the Markov chain EFL, in grey. The number of cycles of the Markov chain is 1000 cycles.

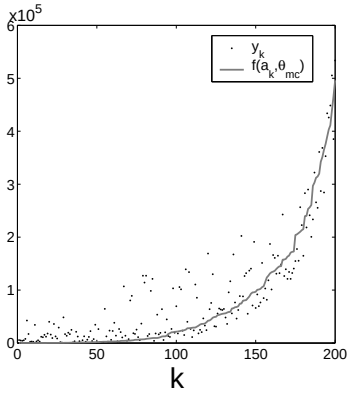

Figure 10.6: Equivalence of damage in the case of Markov chain EFL.

The function $f(\mathbf{a}_k, \widehat{\boldsymbol{\theta}}_{mc})$ and y_k are drawn in Fig. 10.6. The EFL and the measurements are drawn in Fig. 10.5. From Eq. (9.33), the vector $\widehat{\boldsymbol{\theta}}_{mc}$ for these measurements is,

$$\widehat{\boldsymbol{\theta}}_{mc} = (0.0577, 0.194, 0.0012, 0.58, 0.72, 2.42).$$

From these two models of multi-input EFL, we deduce that, in both cases, the amplitude of the component F_2^e is greater than the amplitude of the component F_1^e and smaller than F_3^e. Moreover, the amplitudes of the Markov chain and the sinusoidal EFL are of the same order of magnitude. From Fig. 10.2 and Fig. 10.6, the fitting for the sinusoidal EFL with one block seems to be better than the Markov chain EFL. This is not always the case.

10.2 Comparison between Basquin's and Morel's criteria

The aim of this study is to evaluate multi-input sinusoidal EFL, with Basquin and Morel's criteria, in order to compare the two multi-input EFL. The measurements are illustrated in Fig. 10.7. The comparison will be illustrated by a two-input sinusoidal EFL, with two blocks.

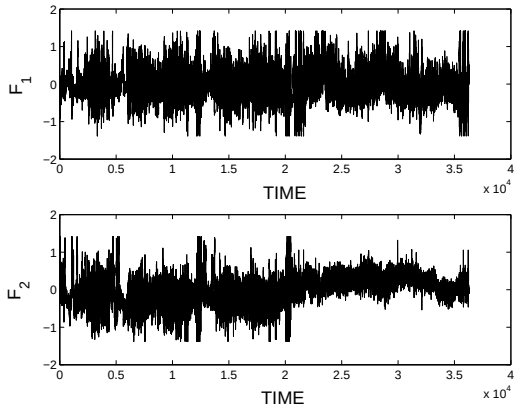

Figure 10.7: Measurements.

Here, we will emphasize the evaluation of the constants dependent on the material. For Morel's criterion, the material parameter is q, see Theorem 6.1. In the case of Basquin's criterion the material parameter is β, from Theorem 6.2. The evaluation of these constants is based on a Wöhler curve. We have chosen to use the data from [30]. In Morel's criterion, the material parameter q has been identified, $q = 23800$ cycles. The exponent related to Basquin's criterion is fixed to $\beta = 12.9$. The fitting of the Basquin's model and Morel's models are illustrated in Fig. 10.8.

From Morel's criterion, it is essential to have information about the threshold $T(A_c)$, a constant related to the geometry of the structures. Therefore, we need to characterize the optimal structures, made up of the material we have previously chosen. The loads F_{dl}, following Definition 6.7, are represented by 600 repetitions of the sequence of the measurements illustrated in Fig. 10.7.

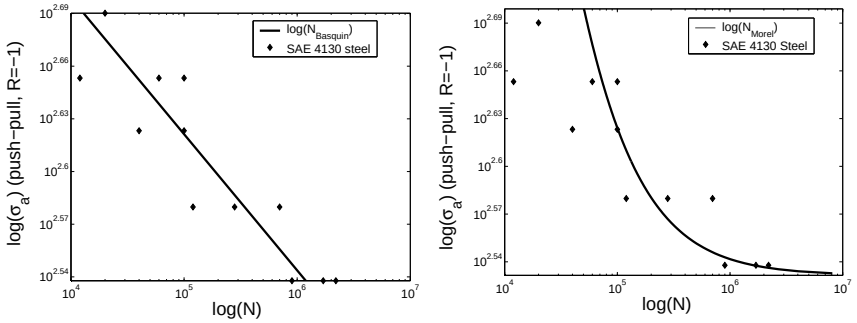

Figure 10.8: Fitting of Basquin's and Morel's models in order to find the constants related to the materials. In the case of Basquin's criterion, we get $\beta = 12.9$. In the case of Morel's criterion, we get q=23800 cycles.

We used Eq. (6.30) to evaluate $T(A_c)$. Here, we have chosen to express each unit vector $\mathbf{a}_k$ by an angle γ_k,

$$\mathbf{a}_k = (\cos(\gamma_k), \sin(\gamma_k)), \quad \text{with} \quad 0 < \gamma_k \leq \pi, \quad 1 \leq k \leq K_a. \tag{10.5}$$

In this application, we have considered $K_a = 36$, and,

$$\gamma_k = \frac{k\pi}{36}, \quad \text{with} \quad 1 \leq k \leq 36.$$

For each $\mathbf{a}_k$, i.e. each critical point on an optimal structure k, we evaluate the threshold $T(\gamma_k)$. The result is presented in Fig. 10.9.

Once the different constants linked to the geometry and the material are determined, we can evaluate the different y_k, from Eq. (10.3) and Eq. (10.4). The variable y_k is computed for one sequence of measurements, and is illustrated in Fig. 10.10. We observe that y_k is rather different from one criterion to another. For instance, in the directions from $\gamma_k = 0$ to $\gamma_k = \frac{\pi}{4}$, it decreases smoothly when Morel's criterion is used, due to the sensitivity to the big cycles. It decreases and increases rapidly when using Basquin's criterion.

We aim to model the bidimensional measurements with sinusoidal EFL with two blocks of sinusoids, with $N_0 = 10^6$ cycles ($5\,10^5$ cycles for each block). In the basis of Basquin's criterion, the damage induced by two-input sinusoidal EFL with two blocks can be found from Eq. (7.16),

$$f(\mathbf{a}_k, \widehat{\boldsymbol{\theta}}_{sb}) = \frac{N_0}{2} \sum_{k=1}^{2} \left(A_k^*(\mathbf{a}_k, \widehat{\boldsymbol{\theta}}_{sb}) \right)^{\beta}.$$

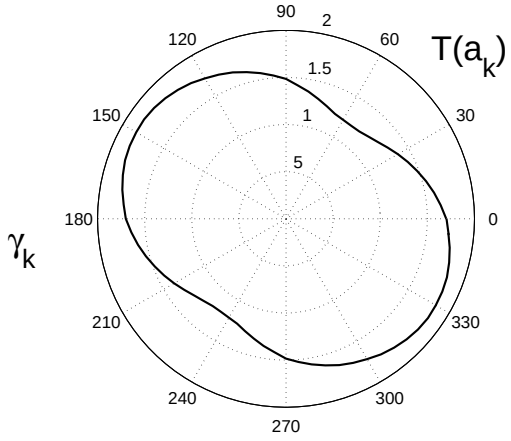

Figure 10.9: Evaluation of constants related to the geometries of the optimal structures, in Morel's criterion, $T(\gamma_k)$ and a_k. The angles γ_k are expressed in degrees.

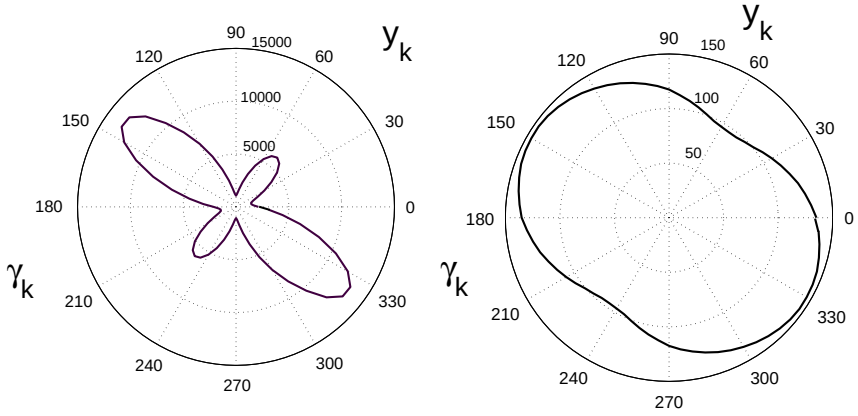

Figure 10.10: Evaluation of y_k when Basquin's criterion is used (left) and Morel's criterion is used (right).

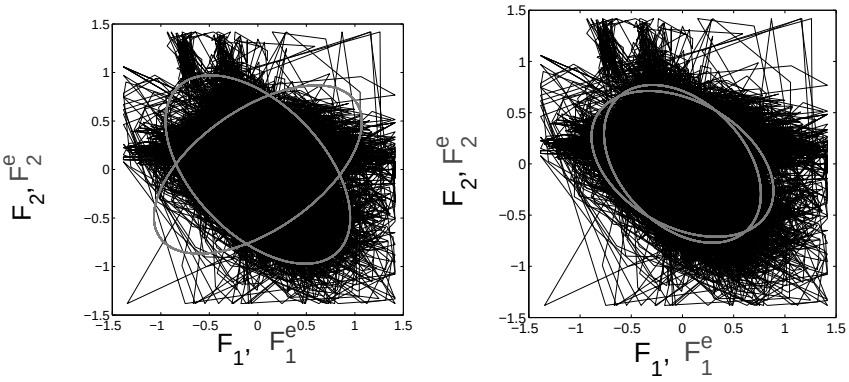

Figure 10.11: The measurements and the sinusoidal EFL computed with Basquin's (left) and Morel's (right) criteria.

The amplitude $A_k^*(\mathbf{a}_k, \widehat{\boldsymbol{\theta}}_{sb})$ is deduced from parameters of $\widehat{\boldsymbol{\theta}}_{sb}$, see Eq. (7.5).

Using Morel's criterion, the damage induced by the EFL can be deduced from Eq. (7.15),

$$f(\mathbf{a}_k, \widehat{\boldsymbol{\theta}}_{sb}) = \frac{N_0}{2} \sum_{k=1}^{2} \left(2A_k^*(\mathbf{a}_k, \widehat{\boldsymbol{\theta}}_{sb}) - T(\gamma_k) \right)_+ . \tag{10.6}$$

Using Basquin's or Morel's criterion, the parameter vector $\widehat{\boldsymbol{\theta}}_{sb}$ fulfills Eq. (10.2). The parameter vector related to the sinusoidal EFL with Basquin's criterion is,

$$\widehat{\boldsymbol{\theta}}_{sb} = (1.071, 0.868, 0.95, 0.97, -2.08, -0.92).$$

The parameter vector related to the sinusoidal EFL with Morel's criterion is,

$$\widehat{\boldsymbol{\theta}}_{sb} = (0.77, 0.89, 0.77, 0.712, -1.94, -1.97).$$

In Fig. 10.11, the measurements and the sinusoidal EFL are represented. The equivalence of damage is illustrated in Fig. 10.12. The EFL given by the two models are significantly different. This is mainly due to the differences in shape of the y_k, presented in Fig. 10.10. The EFL from Basquin's model are represented by two different ellipses. Their principal axes are shifted by $\pi/4$. This is mainly due to the increase of the y_k, at $\gamma_k = \pi/4$. In Fig. 10.13, the fitting of the equivalence of damage is represented, in the case of Basquin's criterion.

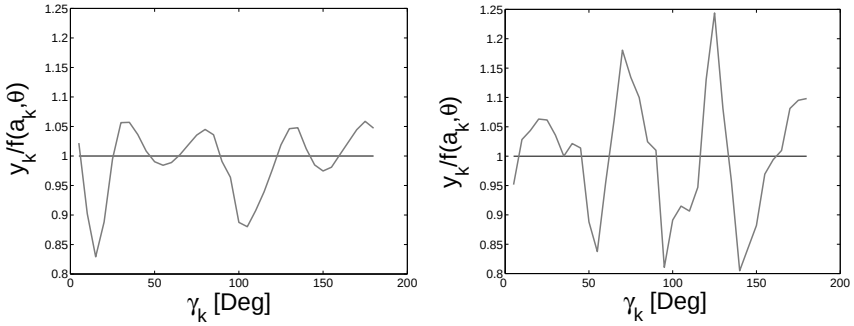

Figure 10.12: Equivalence of damage when Basquin's criterion used (left) and when Morel's criterion used (right).

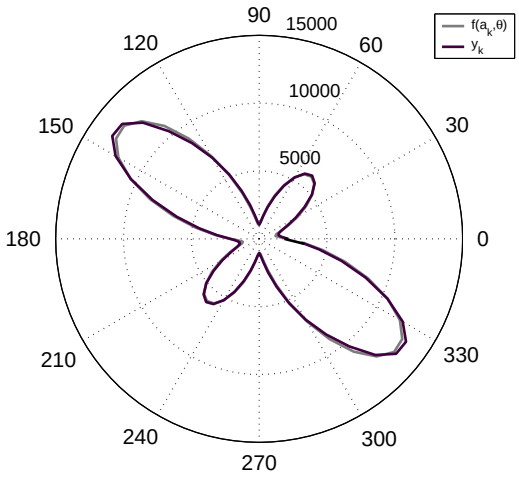

Figure 10.13: Representation of y_k and $f(\mathbf{a}_k, \widehat{\theta}_{sb})$ on the basis of Basquin's criterion.

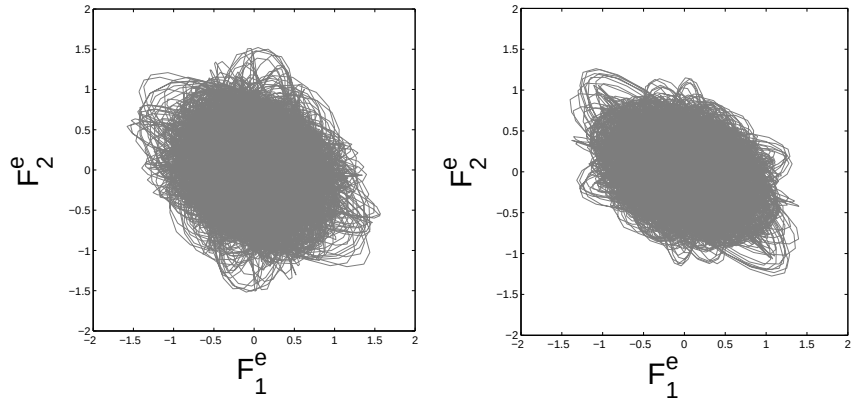

Figure 10.14: Gaussian EFL using Basquin's criterion (left) and Morel's criterion (right).

The evaluation of the Gaussian processes has been performed. They model the same measurements as represented in Fig. 10.7. The same constants linked to the geometry and the material of the optimal structures and previously described, have been used. In Fig. 10.14, the two Gaussian EFL, using Basquin's and Morel's models, are illustrated. The parameter vector $\boldsymbol{\theta}_g$ has been evaluated for each case, see Eq. (8.21). When Basquin's criterion is used,

$$\boldsymbol{\theta}_g = (0.373, 0.460, 2.23).$$

When Morel's criterion is used,

$$\boldsymbol{\theta}_g = (0.312, 0.460, 4.13).$$

The equivalence fatigue approach using Basquin's criterion provides Gaussian EFL with greater standard deviations. The amplitudes of the sinusoidal EFL, using Basquin's criterion was greater than the sinusoidal EFL obtained from Morel's criterion. However, in this study, we did not take into account the impact of the mean value of the rainflow cycles in the evaluation of the damage using Basquin's criterion.

10.3 Data reduction and turning points of multi-input forces

In order to facilitate their use in calculations or on test rigs, the time signals usually need to be reduced. Some time points, inducing almost no damage, are removed. When using methods of life prediction based on the rainflow content of the forces, the reduction of a one-input variable amplitude force is quite straightforward. The turning points are usually kept. The reduction of time signals is problematic in the case of multi-input forces, especially for non-proportional forces. In [17], a method of reduction of multi-input data has been proposed, which is based on the rainflow cycle counting method.

In this context, we will attempt to study a method of data reduction on multi-input forces, based on the damage criteria we have used. We will illustrate this with a two-input force.

Morel's and Basquin's criteria are both based on the rainflow content of the linear combinations of the forces, $F^*(A_c, \boldsymbol{F})$, characterized by $\mathbf{a}(A_c)$ and $\boldsymbol{F}$. The rainflow content of $F^*(A_c, \boldsymbol{F})$ is based on its turning points. Consequently, the turning points of the linear combinations are crucial to evaluate the damage. In order to reduce the signals of $\boldsymbol{F}$, we propose to keep the time points of $\boldsymbol{F}$ that are turning points in, at least, one linear combination $F^*(A_c, \boldsymbol{F})$, defined by the unit vector $\mathbf{a}(A_c)$.

In practice, we use a finite number of linear combinations $\mathbf{a}_k$, defined by the angle γ_k, as in Eq. (10.5). Let's consider $\boldsymbol{\gamma_d}$, a vector of different angles γ_k. The time points of $\boldsymbol{F}$ being turning points in, at least, one of the directions $\gamma_k \in \boldsymbol{\gamma_d}$, are kept. The time points of $\boldsymbol{F}$ that are not turning points in any of the linear combinations defined by $\gamma_k \in \boldsymbol{\gamma_d}$, are removed. How should we choose the vector $\boldsymbol{\gamma_d}$ in order to reduce the signals substantially and still keep the equivalence in damage, between the reduced signals and the original signals of forces ?

In the following example, the forces $\boldsymbol{F}$ are bidimensional, illustrated in Fig. 10.7. We attempt to reduce the bidimensional signals, for different vectors $\boldsymbol{\gamma_d}$.

Example 10.3.10. The reduced signal is called $\boldsymbol{F}_{red}$. Once the reduction of $\boldsymbol{F}$ to its damaging points is proceeded, we evaluate the damage from $\boldsymbol{F}_{red}$, called $D_{red}(\gamma_k, \boldsymbol{F}_{red})$, and compare it to the damage induced by $\boldsymbol{F}$, $D(\gamma_k, \boldsymbol{F})$.

In the example, we have chosen to evaluate the damage from Morel's criterion. The thresholds $T(\gamma_k)$ used for that are shown in Fig. 10.9. The evaluation of the damage can also be done with Basquin's criterion.

In the left column of Fig. 10.15, the different directions contained in $\boldsymbol{\gamma_d}$ are represented by arrows. We finally compare the damage induced by $\boldsymbol{F}_{red}$ and by $\boldsymbol{F}$, through the ratio $D_{red}(\gamma_k, \boldsymbol{F}_{red})/D(\gamma_k, \boldsymbol{F})$, over twenty angles γ_k, such that,

$$\gamma_k = \frac{k\pi}{20}, \quad \text{with,} \quad 1 \leq k \leq 20.$$

The results are illustrated in the right column.

For each case, we compare the length of $\boldsymbol{F}_{red}$ and $\boldsymbol{F}$. Let's consider L the data length of $\boldsymbol{F}$ and L_{red}, the data length of $\boldsymbol{F}_{red}$.

CASES	$\boldsymbol{\gamma_d}$ in rad.	$100\frac{L_{red}}{L}$
1	$\left(0, \frac{\pi}{2}\right)$	$\sim 63\%$
2	$\left(0, \frac{\pi}{4}, \frac{\pi}{2}, \frac{3\pi}{4}\right)$	$\sim 77\%$
3	$\left(0, \frac{\pi}{8}, \frac{\pi}{4}, \frac{3\pi}{8}, \frac{\pi}{2}, \frac{5\pi}{8}, \frac{3\pi}{4}, \frac{7\pi}{8}\right)$	$\sim 86\%$
4	$\left(0, \frac{\pi}{8}, \frac{\pi}{4}, \frac{3\pi}{8}\right)$	$\sim 67\%$

In the first case, we keep the turning points of $F^*(\gamma_k, \boldsymbol{F})$, where γ_k belongs to the vector $\boldsymbol{\gamma_d} = (0, \frac{\pi}{2})$. The damage induced by $\boldsymbol{F}_{red}$ and $\boldsymbol{F}$ are rather different. It means that we lose some damaging points of $\boldsymbol{F}$ in the data reduction. However, the reduction in terms of length is quite important. The length of $\boldsymbol{F}_{red}$ is two thirds of the length of $\boldsymbol{F}$.

In the cases 2 and 3, we increase the number of γ_k contained in $\boldsymbol{\gamma_d}$. They are uniformly spread from 0 to π. The damage of $\boldsymbol{F}_{red}$ is very close to the damage induced by $\boldsymbol{F}$. However, the reduction in length between $\boldsymbol{F}_{red}$ and $\boldsymbol{F}$ is not as effective as in the first case.

In the fourth case, the components of $\boldsymbol{\gamma_d}$ are not equally spaced, from 0 to π. We can conclude that we lose some time points in $\boldsymbol{F}$ that induces damage. In this case, it proves that the choice of the components of $\boldsymbol{\gamma_d}$ is very important. □

In this example, we have illustrated a proposition of data reduction, in accordance with the damage criteria used in the multi-input equivalent

fatigue approach. We deduce that the vector γ_d is important in the evaluation of $\boldsymbol{F}_{red}$. The components of γ_d are preferably uniformly spread in the 2D space. From Example 10.3.10, in order to have a good compromise between the length of F_{red} and the equality of damage between $\boldsymbol{F}_{red}$ and $\boldsymbol{F}$, case 2 is appropriate. This observation is in accordance with the method proposed in [17].

This method can be extended to more than two-input forces. The main problem is to find the unit vectors $\mathbf{a}_k$ that are equally spread in the nD space.

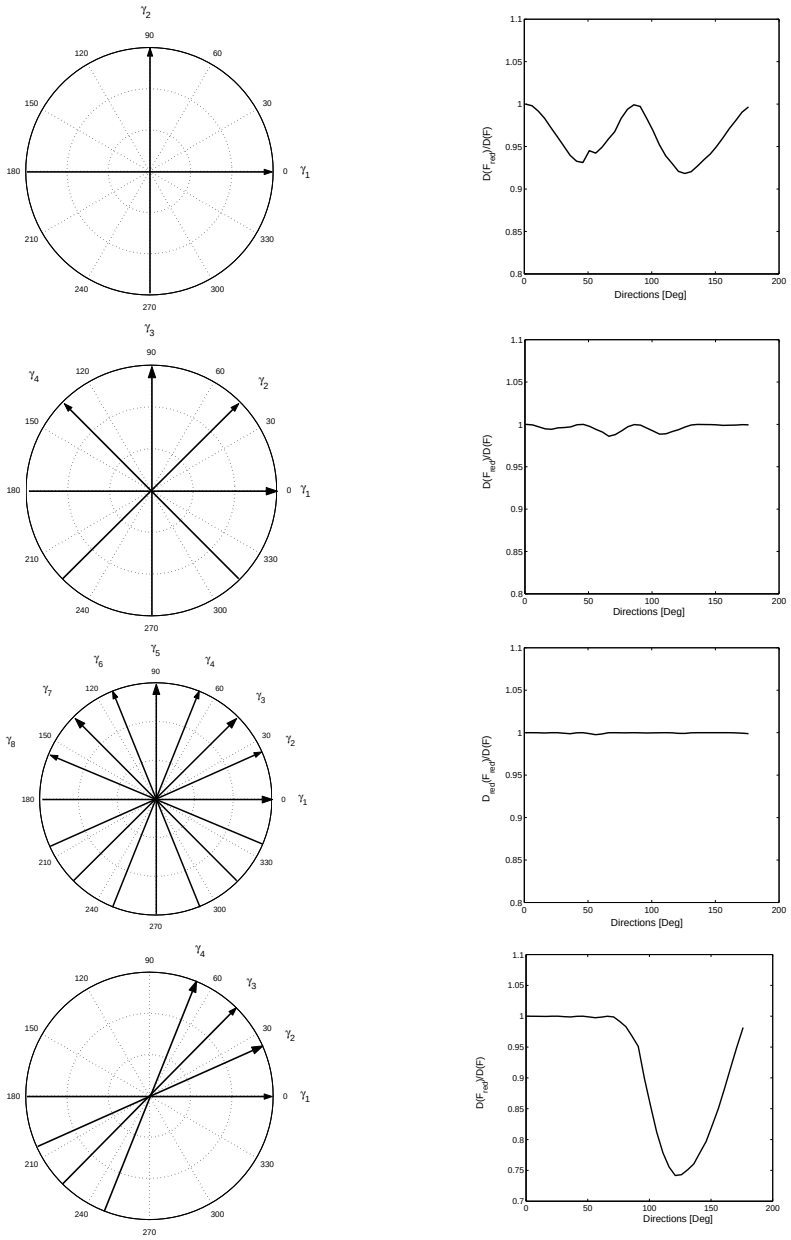

Figure 10.15: Data reductions. In the left column, each component $\gamma_k \in \boldsymbol{\gamma_d}$ is represented by arrows. In the right column, the ratio between $D_{red}(\gamma_k, \boldsymbol{F}_{red})$, the damage induced by $\boldsymbol{F}_{red}$ and $D(\gamma_k, \boldsymbol{F})$, the one induced by $\boldsymbol{F}$, are represented.

Chapter 11

Experiments

The industrial aim of the method of equivalent fatigue is, among other things, to define specifications for test benches. Therefore, it is essential to check if the equivalence of damage is fulfilled experimentally, between the measurements and the EFL. The aim of these experiments is to test the equivalence in damage between known measurements of forces, and the sinusoidal EFL, with two blocks. The tests will be performed in the case of two-input forces, on a suspension arm. The experimental set-up will be described. A brief presentation of the geometry, the material and the boundary conditions will be given.

After checking the validity of the different assumptions, i.e. Assumption 6.1 and Assumption 6.2, the evaluation of the EFL from predefined measurements will be done. The experimental life of the structure when the measurements or the EFL are applied, will be analyzed and compared.

11.1 The suspension arm

We have chosen to test the equivalence in damage between variable amplitude loads and the sinusoidal EFL on a suspension arm. The suspension arm is usually submitted to three different loads from the wheels, the transversal, the longitudinal and the vertical loads. In Fig. 11.1, a picture of a triangle as a part of the suspension system is presented. In our test,

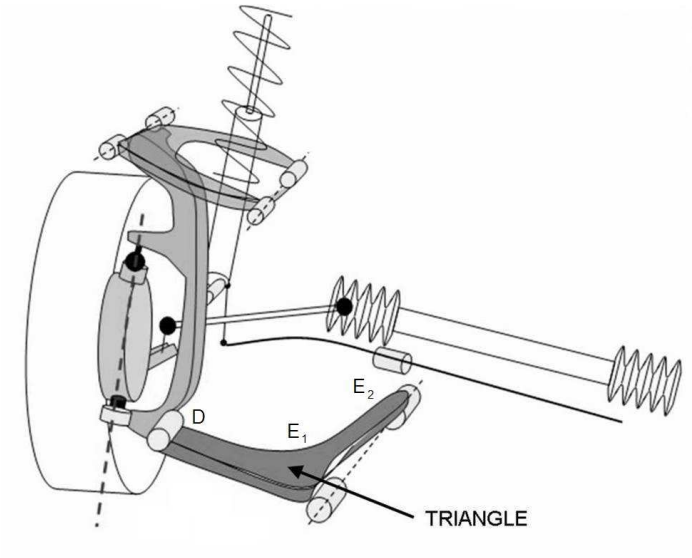

Figure 11.1: Location of the triangle in the suspension system.

the suspension triangle will be submitted to only two forces, applied in the plane of the triangle.

11.2 Experimental set-up

We associated three points in the triangle, the points E_1, E_2 and D. The triangle is linked to the wheel by a ball joint. The point D is the center of the fixture, where the forces are applied. The points E_1 and E_2 are illustrated in Fig. 11.2. They are located at the center of the holes. The origin of the axis system is E_1. The X-axis starts at the point E_1 and goes to E_2. The Y-axis is perpendicular to the X-axis. The Z-axis is perpendicular to the plane (X, Y).

In our test, the triangle will be submitted to two loads, in the plane of (X, Y). They are called,

$$\boldsymbol{F} = \begin{pmatrix} F_1 \\ F_2 \end{pmatrix}.$$

The two forces are applied at the point D, by hydraulic actuators. The ma-

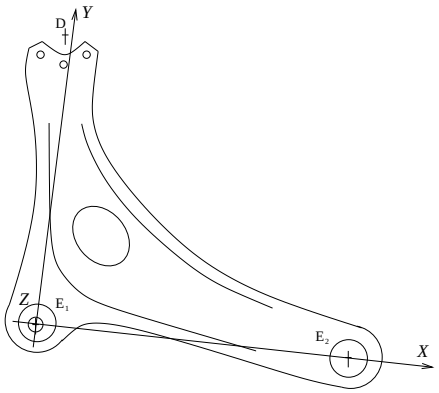

Figure 11.2: Axis system.

terial of the suspension is the HR55 steel[1]. From this data, we can deduce the different constants linked to the material, needed in the equivalent fatigue approach.

The boundary conditions of the experiments are exposed in Fig. 11.3. In E_1 and E_2, the translation displacements in the plane (X, Y) are blocked. This is performed by bearings linked with the frame. These two bearings are cylindrical roller bearings. The displacements of E_1 and E_2 in the Z-axis are not blocked. The actuators and the triangle are linked by a ball joint in D. This is illustrated in Fig. 11.3 by the link called $\{1\}$. A pivot links the ball joint to the frame. It is illustrated by the link called $\{2\}$.

11.3 Assumptions

In order to check the validity of the equivalence of damage between the measurements and the EFL, we need to check the validity of the assumptions in the critical area of the triangle. From Assumption 6.1, the structure has to be loaded under elastic and quasi-static conditions. In order to be elastic, the von Mises stress component has to be below a threshold σ_E. For the material HR55, σ_E is 460 MPa.

In order to fulfill Assumption 6.2, the stress tensor has to be proportional at the critical point of the triangle. In order to check if the assumptions

[1]The Wöhler curve has been found in internal database, ARCELOR ESOPE-HR55, 2002.

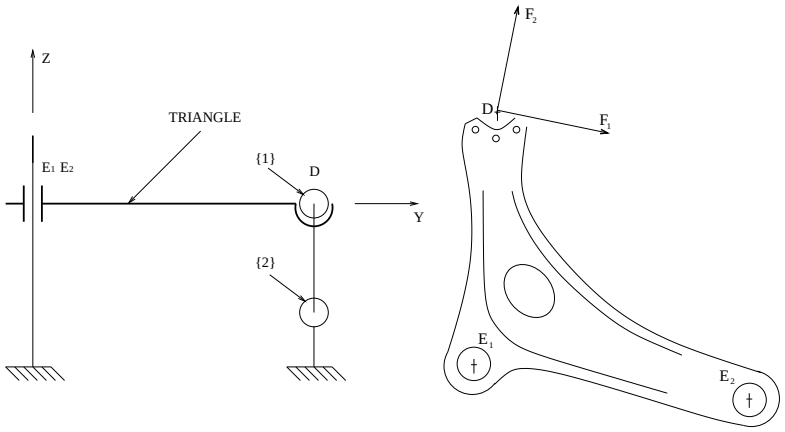

Figure 11.3: Boundary conditions and loads.

are fulfilled for the suspension arm, we will first locate the critical point. From the observation of the principal direction of the stress tensor at this point, we can deduce if the structure fulfills one of the two assumptions.

A finite element model of the triangle has been studied. The different elements are shells with a lower and an upper skin. In Fig. 11.4 and Fig. 11.5, two different cases of loads have been observed.

PICTURES of Fig. 11.4 and Fig. 11.5	Force F_1 in N	Force F_2 in N
CASE 1	1	0
CASE 2	0	1

The von Mises stresses have been plotted. The triangle has been plotted in the deformed configuration. The critical areas may be located where the von Mises stresses are greatest, represented by a dark grey zone. We could deduce that the critical area is located at the lower skin, in the gray box represented in Fig. 11.6.

From these two different cases, we can deduce the stress tensor of each point of the triangle, for any forces $\boldsymbol{F}$. The stress tensor has been considered as bidimensional. From Eq. (6.2), under the assumption of elastic

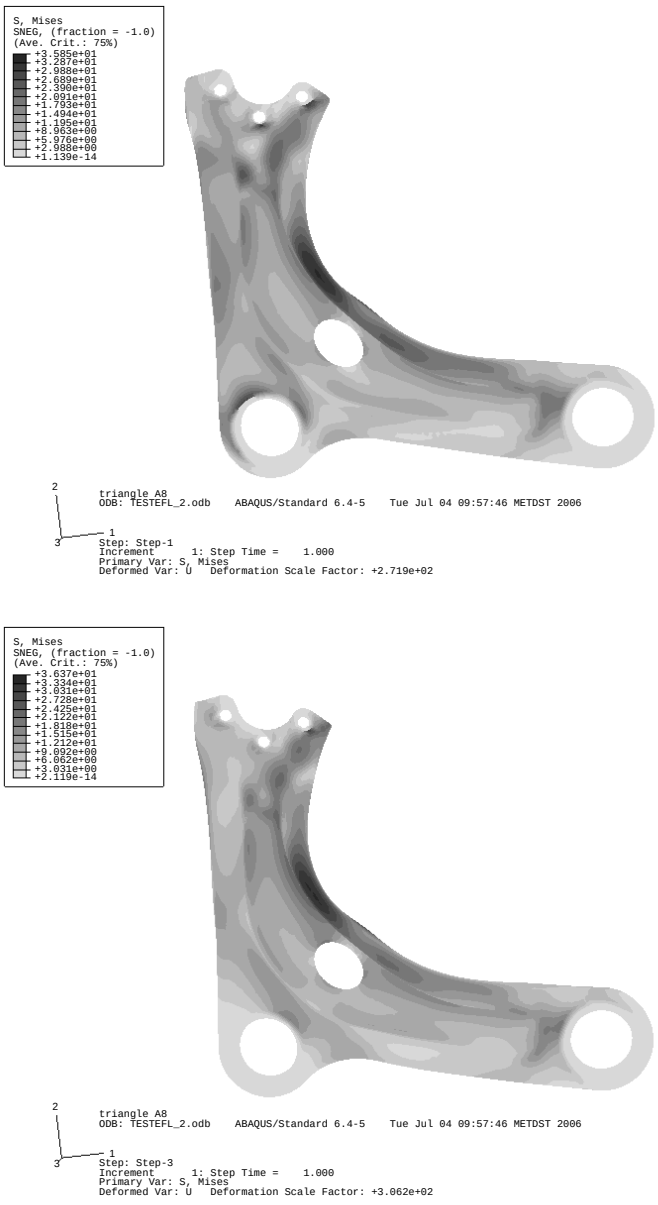

Figure 11.4: Localization of the critical zone on the lower skin, where the von Mises stresses are represented by a dark grey zone. For a better representation, we have plotted the case of $F_1 = 1000N$, and $F_2 = 0$ (top), and the case of $F_1 = 0$ and $F_2 = 1000$ (bottom).

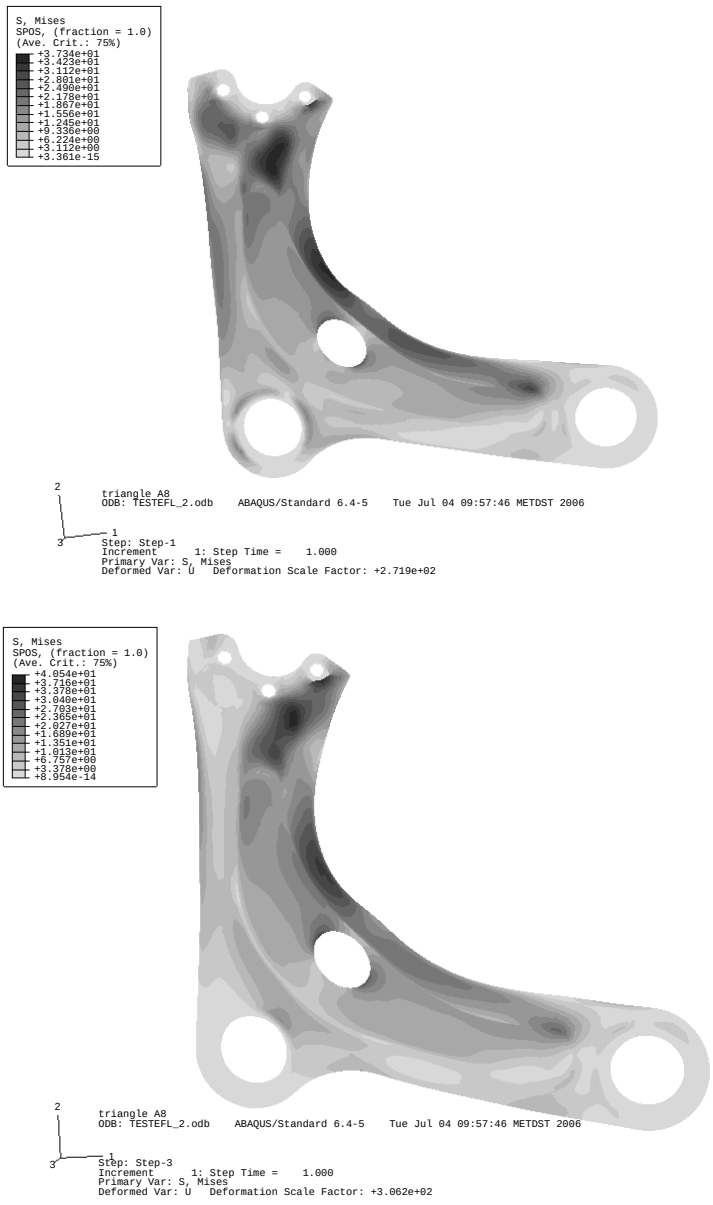

Figure 11.5: Localization of the critical zone on the upper skin, where the von Mises stresses are represented by a dark grey zone. For a better representation, we have plotted the case of $F_1 = 1000N$, and $F_2 = 0$ (top), and the case of $F_1 = 0$ and $F_2 = 1000$ (bottom).

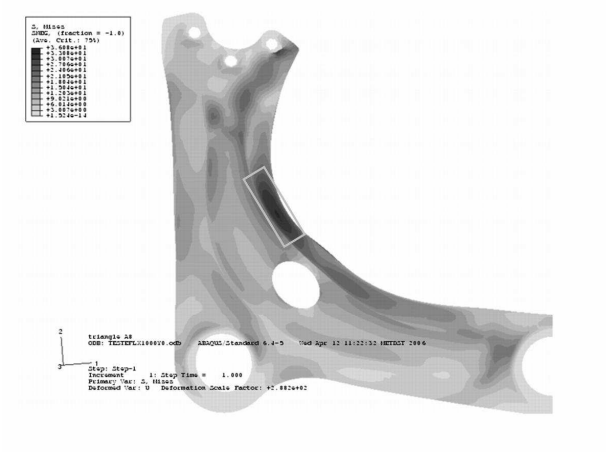

Figure 11.6: Location of the critical zone at the lower skin.

stresses, at any point A of the triangle, we deduce,

$$\begin{aligned} \boldsymbol{\Sigma}(A,t) &= \sum_{i=1}^{2} \boldsymbol{K_i}(A) F_i(t) && (11.1) \\ &= \sum_{i=1}^{2} \begin{pmatrix} K_{i,11}(A) & K_{i,12}(A) \\ K_{i,21}(A) & K_{i,22}(A) \end{pmatrix} F_i(t). && (11.2) \end{aligned}$$

Let's consider $\boldsymbol{\Sigma_1}(A)$ and $\boldsymbol{\Sigma_2}(A)$, the stress tensors at the point A of the structures, submitted to forces of the cases 1 and 2. Then,

$$\boldsymbol{\Sigma_1}(A) = \boldsymbol{K_1}(A),$$

and

$$\boldsymbol{\Sigma_2}(A) = \boldsymbol{K_2}(A).$$

Thus the stress tensor $\boldsymbol{\Sigma}(A,t)$ can be deduced from the stress tensors $\boldsymbol{\Sigma_1}(A)$ and $\boldsymbol{\Sigma_2}(A)$,

$$\boldsymbol{\Sigma}(A,t) = \boldsymbol{\Sigma_1}(A) F_1(t) + \boldsymbol{\Sigma_2}(A) F_2(t), \quad (11.3)$$

Let's assume that $\boldsymbol{\Sigma_1}(A)$ and $\boldsymbol{\Sigma_2}(A)$ are proportional. Their principal directions are similar, and they do not rotate. The tensors $\boldsymbol{\Sigma_{d,1}}$ and $\boldsymbol{\Sigma_{d,2}}$ are the diagonalized stress tensors. Thus,

$$\begin{aligned} \boldsymbol{\Sigma_{d,1}}(A) &= \boldsymbol{M}(A)^T \boldsymbol{\Sigma_1}(A) \boldsymbol{M}(A), \\ \boldsymbol{\Sigma_{d,2}}(A) &= \boldsymbol{M}(A)^T \boldsymbol{\Sigma_2}(A) \boldsymbol{M}(A). && (11.4) \end{aligned}$$

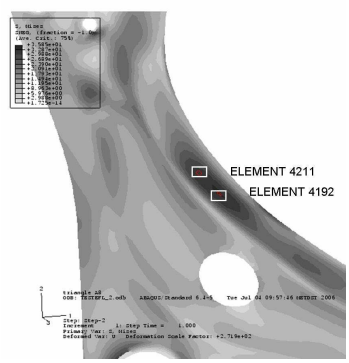

Figure 11.7: Location of elements ♯ 4211 and ♯ 4192.

From Eq. (11.3), we deduce that,

$$\begin{aligned} \boldsymbol{M}(A)^T \boldsymbol{\Sigma}(A,t) \boldsymbol{M} &= \boldsymbol{M}(A)^T \left(\boldsymbol{\Sigma_1}(A) F_1(t) + \boldsymbol{\Sigma_2}(A) F_2(t) \right) \boldsymbol{M}(A) \\ &= \boldsymbol{\Sigma_{d,1}}(A) F_1(t) + \boldsymbol{\Sigma_{d,2}}(A) F_2(t), \\ &= \boldsymbol{\Sigma_d}(A,t). \end{aligned} \tag{11.5}$$

If the stress tensors of the cases 1 and 2, at the point A, are proportional, with the same principal directions, we can deduce that the stress tensor is proportional at the point A. From Eq. (6.5), when the stress tensor is proportional at A, we deduce,

$$\begin{aligned} \boldsymbol{\Sigma_d}(A,t) &= \begin{pmatrix} \sigma_{d,1}(A,t) \\ \sigma_{d,2}(A,t) \end{pmatrix} \\ &= \sigma(A,t) \begin{pmatrix} 1 \\ \alpha(A) \end{pmatrix}. \end{aligned} \tag{11.6}$$

The components of the diagonalized stress tensor, $\sigma_{d,1}(A,t)$ and $\sigma_{d,2}(A,t)$, are proportional.

Two different points of the critical zone have been chosen, as shown in Fig. 11.7. The stress components $\sigma_{d,1}(A,t)$ and $\sigma_{d,2}(A,t)$ have been drawn in Fig. 11.8, when the triangle is submitted to variable amplitude and non proportional forces $\boldsymbol{F}$. We also observed that the principal directions are similar at these two points. Consequently, the stress tensors at the critical zone are proportional.

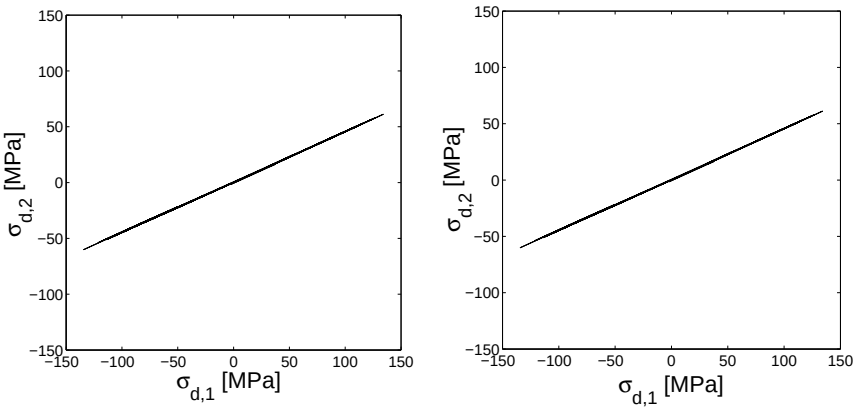

Figure 11.8: Stress tensors at the critical areas. The triangle was loaded by two-input variable amplitude forces $\boldsymbol{F}$. The stresses $\sigma_{d,1}$ and $\sigma_{d,2}$ are drawn for the element 4211 (left) and the element 4292 (right), at the lower skin.

11.4 Determination of the forces

In order to use Morel's criterion in the determination of the EFL, the two-input forces $\boldsymbol{F_{dl}}$ have to be known for the suspension arm. When the structure is submitted to these forces, the predicted damage at the critical point is one. The forces $\boldsymbol{F_{dl}}$ come from measurements from test tracks. We have chosen to scale these measurements and limited the maximum of the forces at 11000 N, in order to remain in the elastic domain of the structure. According to the criterion, the predicted damage reaches one at the critical point when the sequence presented in Fig. 11.9 is repeated 177 times. The forces $\boldsymbol{F_{dl}}$ we have chosen are the sequence presented in Fig. 11.9, repeated 177 times.

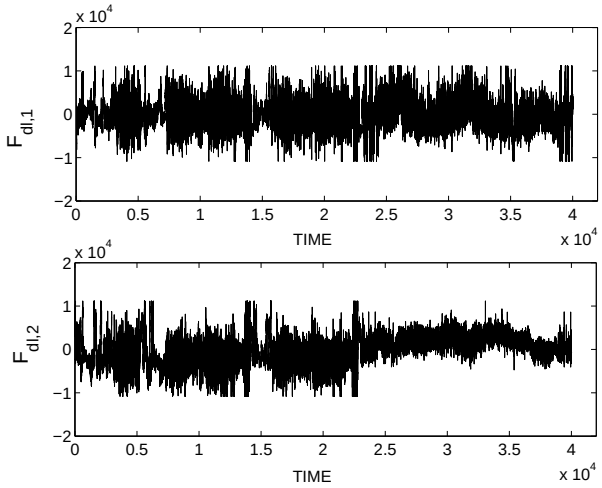

Figure 11.9: The forces $\boldsymbol{F_{dl}}$.

The evaluation of the geometrical characteristics of the optimal structures follows Definition 6.7. We will consider a finite number of unit vector $\mathbf{a}_k$, such as,

$$\mathbf{a}_k = (\cos(\gamma_k), \sin(\gamma_k)),$$

where,

$$\gamma_k = \frac{k\pi}{36}, \quad 1 \leq k \leq 36.$$

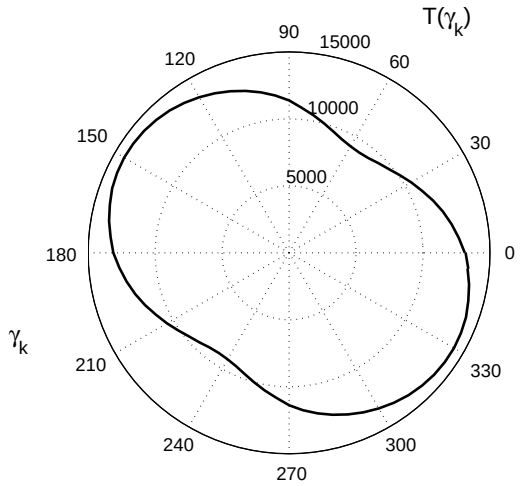

Figure 11.10: The thresholds $T(\gamma_k)$ of the optimal structures.

The thresholds $T(\widehat{A_c})$ are computed for each $\mathbf{a}_k$, or for each γ_k. The parameter q is needed to determine the thresholds of Morel's model. We deduce it from a push-pull Wöhler curve ($R = -1$),

$$q = 1.17\,10^4.$$

The thresholds are called $T(\gamma_k)$. They are illustrated in a polar plot, in Fig. 11.10. The EFL are sinusoidal forces. We have chosen sinusoidal EFL with two blocks, which is a good compromise between a good fitting and a small number of parameters. The variables $f(\mathbf{a}_k, \boldsymbol{\theta}_{sb})$ and y_k are defined in Eq. (10.4). For two-input sinusoidal EFL with two blocks, we deduce $f(\mathbf{a}_k, \boldsymbol{\theta}_{sb})$ from Eq. (10.6). From the fitting, we deduce the vector $\boldsymbol{\theta}_{sb}$, defined in Eq. (7.13),

$$\boldsymbol{\theta}_{sb} = (6690, 6110, 5421, 5785, -0.5297, 0.8509).$$

The forces $\boldsymbol{F_{dl}}$ and $\boldsymbol{F^e_{dl}}$ are represented in Fig. 11.12.

We do not know the vector $\mathbf{a}$ representative of the most critical point of the triangle. From Fig. 11.11, the damage induced by the forces $\boldsymbol{F_{dl}}$ and $\boldsymbol{F^e_{dl}}$ can be different, due to the fitting. This remark can be taken into account once the results are analyzed. Thus, it could be interesting to determine the linear combination $\mathbf{a}$ at the critical point of the structure, and to evaluate the predicted difference, from Fig. 11.11.

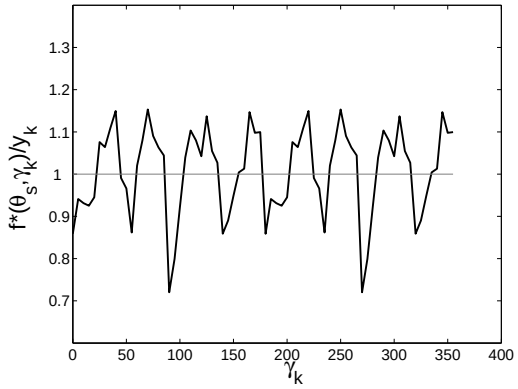

Figure 11.11: Fitting of the damage induced by the EFL.

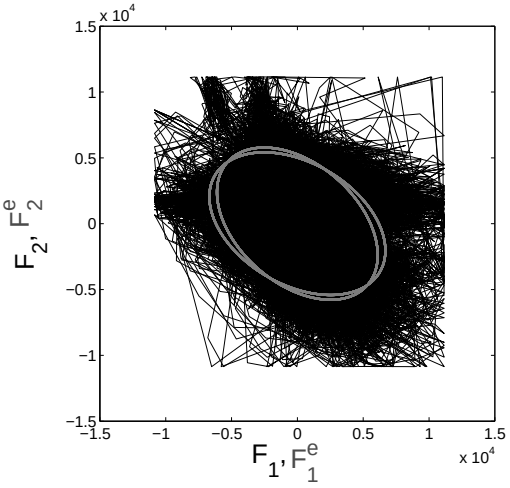

Figure 11.12: Measurements and two-input EFL with two blocks.

11.5 Analysis of the results

We choose to test ten specimens, five of them are submitted to the measurements $\boldsymbol{F_{dl}}$, and the others, to the EFL. The test should be carried out in the randomize order. Once the tests are done, we compare the number of cycles obtained in the two samples. Let's consider N^e, the life of the suspension arm submitted to the EFL, and N, the life of the structure submitted to $\boldsymbol{F_{dl}}$. We assume that both $\log^{10}(N)$ and $\log^{10}(N^e)$ are normally distributed with the same variance. In order to compare the mean of the two samples, we will use the Student's t-distribution to construct the confidence interval for the difference of the expected $\log^{10}$(life).

The mean of $\log(N_e)$ is called η_e and the mean of $\log(N)$ is η. The difference between η and η_e is called δ. Let's consider $\overline{m}$ and $\overline{m}_e$, the means of the sample of life of structures submitted to $\boldsymbol{F_{dl}}$, and the sample of life of structures submitted to the EFL, respectively. The number of observations of each sample are n and n_e (in our case $n = n_e = 5$). The standard deviation of the samples are s and s_e. We write the confidence interval for $\eta - \eta^e$ as I_δ, where,

$$I_\delta = \left[\overline{m} - \overline{m}_e \pm t\, S \sqrt{\frac{1}{n} + \frac{1}{n^e}} \right].$$

with

$$S = \frac{s + s_e}{\nu},$$

and $\nu = n + n_e$. The quantile t is a quantile in the t-distribution which determines the coefficient of confidence of the interval.

11.6 Conclusion

We have presented an approach to test the equivalence in damage in 2D. From the finite element model of the structure, we found the localization of the critical point, and checked the validity of the Assumption 6.1 and Assumption 6.2. In order to evaluate the EFL, we used Morel's criterion. The equivalent fatigue loads have been evaluated from the predefined loads $\boldsymbol{F_{dl}}$. Finally, an analysis of the results is proposed.

Chapter 12

Conclusion

The equivalent fatigue approach is a method for transforming complex multi-input loads into simple forces, equivalent in terms of damage, whatever the structures the forces are applied to. An approach to the multi-input equivalent fatigue loads has been described, in the framework of the uniaxial and multiaxial high cycle fatigue of metallic structures, in a quasi-static regime.

12.1 Models of life prediction and equivalence of damage

Structures in service often incur uniaxial fatigue at their critical point. However, the multiaxial fatigue phenomenon can also be observed. In order to design those structures, this phenomenon has to be taken into account. In this case, the stress tensor is frequently proportional at the critical point.

Basquin's criterion is used in the equivalent fatigue approach, for structures exposed to uniaxial fatigue. The damage is based on the rainflow cycle content of the stress component. The accumulation of the damage is chosen as linear. Morel's model provides life prediction from uniaxial and multiaxial, proportional and non-proportional stress tensors, in high cycle fatigue for finite life. It is based on the micro-macro approach. In

order to use Morel's criterion in the framework of the equivalent fatigue approach, we chose a simplified form, presented in Chapter 3. Thus we gain in simplicity and rapidity in the prediction of life. The accumulation of damage in this case is linear.

The structures to which the forces are applied are supposed to be elastic and quasi-static. When using Basquin's criterion in the equivalent fatigue approach, we have assumed that the stress tensor at the critical point is unidirectional. When using Morel's model, the stress tensor is supposed to be proportional. The principal directions do not move in time.

We provide an expression of the damage from the forces, using Basquin and Morel's models, under these different assumptions. The two expressions are based on the linear combinations of the components of the forces. The coefficients defining the linear combination are contained in a unit vector, dependent on the geometry of the structures. In both models, the damage is based on the rainflow content of the linear combinations.

In the expression of the equivalence in damage between two forces, using Basquin's criterion, only one constant linked to the material is needed, the exponent β. It has to be evaluated from a Wöhler curve of the material. Basquin's criterion is rather easy to use in the equivalent fatigue approach. However, it is restricted to structures exposed to uniaxial fatigue at their critical points.

In the case of Morel's model, the equivalence in damage between the measurements and the EFL is dependent on a threshold, under which a rainflow cycle of force does not induce damage. Under the different assumptions, this threshold depends on the material, the geometry and the mean value of the loads. Therefore, when Morel's model is used in the equivalent fatigue approach, we need extra assumptions on the structures. Thus the concept of optimal structures has been introduced. It is possible to evaluate the threshold for these structures. The damage reaches one at their critical points, when submitted to sequences of known loads, representative of their design life. These sequences of forces can be measurements stored during laps of tracks, and are predefined by the manufacturer. In order to evaluate the thresholds for the optimal structures, a Wöhler curve of the material is necessary. Thus, the determination of the threshold requires more accurate information about the structures.

In each criterion, the equivalence in damage between the EFL and the measurements is restricted to structures for which the constants appearing in the equivalence of damage and depending on the material and on the

geometry, are known. The number of geometries belonging to this family of structures is infinite. For models of EFL characterized by a finite number of parameters, the equality in damage between the measurements and the EFL over the different structures fulfilling the assumptions, observable in the one-input equivalent fatigue approach, is impossible in the case of multi-input equivalent fatigue approach. Thus, the two multi-input forces are equivalent if the distances between the damage induced by the measurements and the damage induced by the EFL are minimized, over the linear combinations characterizing the different structures. We rather use the least square method in order to evaluate the set of parameters defining the EFL. We deduce the set minimizing the distances between the damage induced by the EFL and the one induced by the measurements.

12.2 The equivalent fatigue loads

Different types of EFL have been treated. A deterministic model, such as the sinusoidal multi-input EFL, as well as probabilistic models, such as narrow band Gaussian processes and Markov chains, have been determined. These EFL have the common advantage that they are easily generated, and defined by a few number of parameters. From models like sinusoidal and Gaussian multi-input EFL, we evaluated the expected rainflow content of the linear combinations of the components of the EFL. For a Markov chain, the evaluation of the rainflow content of linear combinations of a multi-input Markov chain has been developed as well. We deduced the damage expressed from parameters characterizing the EFL. We used the condition of equivalence of damage to determine these parameters. In order to improve the fitting between the damage induced by the measurements and the damage induced by the EFL, different propositions have been explored. In the case of multi-input sinusoidal EFL, an extension to several blocks of sinusoids has been studied (the same method can be used for Gaussian EFL). For Markov chain EFL, the peaks observable in the multi-input measurements, have been modeled in the Markov chain EFL with peaks. In both cases, the number of parameters increases, which makes the fitting of the damage more accurate.

Sinusoidal EFL are convenient to implement in calculation for designing structures and easy to use on test benches. However, the rainflow content of the sinusoidal EFL is far from that of the measurements. Therefore the Gaussian EFL seem to be more appealing because they are variable amplitude loads. The Markov chain EFL is interesting to use because some

events, like damaging events, occurring in the measurements, can be modeled in the EFL. However, the computations of complicated Markov chain EFL can be time-consuming.

Different applications have been provided in order to illustrate the models of EFL we have chosen to study. These examples treat bidimensional and three-dimensional EFL. Moreover, the study focused on the evaluation of the damage. A method of data reduction has been applied. The aim is to remove the time points of the signals of forces that do not induce damage.

12.3 The requirements of the equivalent fatigue approach

Several different models of life prediction and EFL have been chosen to treat the equivalent fatigue approach. We can also study the possibility for a damage model and a multi-input process to be used in the equivalent fatigue approach.

Whatever the criterion we used in the equivalent fatigue approach, different constants linked to the geometry and the materials need to be identified. The use of a fatigue model of life prediction in the equivalent fatigue approach has to fulfill two points. In the industrial framework of equivalent fatigue approach, a complicated and time-consuming computation has to be avoided. Moreover, the constants depending on the geometry and on the materials have to be identified from the information available on the structures to which the equivalent fatigue approach is applied. Thus, the choice of the fatigue criterion depends on the information we have about the structures.

Several requirements concerning the multi-input process are needed, in order to be used in the equivalent fatigue approach. When using fatigue criteria based on the rainflow content of the loads, it is essential to be able to predict the rainflow content from parameters defining the EFL. Moreover, the number of parameters defining the EFL has to be lower than the number of equations, which allows us to evaluate them. The number of equations is infinite with the use of Basquin and Morel's criteria. Therefore, any EFL for which the rainflow content can be evaluated, defined with a finite number of parameters, can be used in the equivalent fatigue approach. However, the objective of the equivalent fatigue approach is to

transform complex loads with variable amplitudes to simple loads. Complex EFL do not fulfill the requirements imposed by the method. The complexity of the EFL depends on its use. Choosing an appropriate EFL is a compromise between accuracy in the equivalence in damage between the measurements and the EFL, and the simplicity of the EFL.

12.4 Perspectives

The stress-strength method allows us to take into account the scatter induced by the severity of the customers and the scatter linked to the strength of the structures induced by the manufacturing process. The severity is deduced from loads measured on test tracks. In the uniaxial equivalent fatigue approach, the severity is a scalar, the amplitude of the one-input sinusoidal EFL. Over a population of customers, we can determine the distribution of severity. The possibility to extend the stress strength method to the case of multi-input EFL could be interesting to explore. The difficulty lies in the choice of the variable representative of the severity, from multi-input EFL. The main advantage of a severity represented by a scalar is its simplicity in use. However, the completeness of the multi-input EFL may not be reproduced in a scalar.

As in the one-input EFL, Basquin's criterion can be associated with Gerber's parabola. It would be interesting to use Gerber's parabola in the multi-input case. The ratio between the maximal tensile strength and the endurance limit is necessary. The equivalence of damage between the two loads is valid on structures, incurring uniaxial fatigue, and made of material for which these mechanical characteristics are known. However, the computation of the damage and the characterization of the EFL may be more time-consuming with the use of Gerber's parabola.

We have assumed that the frequency does not impact the life prediction of the structures. Criteria of life prediction in high cycle fatigue taking into account the frequency content, have been developed. A frequency domain implementation of fatigue criteria, like Crossland's failure criterion, has been done. However, no criteria based on the microscopic phenomena of fatigue have been implemented in the frequency domain. Moreover, the equivalent fatigue approach is not specifically used for high cycle fatigue on metallic structures. It could be interesting to extend it to structures undergoing low cycle fatigue, or non linear structures. The requirements about the choice of criterion considering above are still valid.

We have evaluated the multi-input EFL under the hypothesis of proportional stress tensor. It would be interesting to study the evaluation of the EFL in the case of a non-proportional stress tensor. In this case, Morel's criterion can still be used. The critical plane and the critical direction on it change from one sequence of loads to another. Thus, the magnitudes, like the threshold, may not only depend on the geometry but also on the forces.

A proposition of experiments has been presented. The aim was to check if the equivalence between bidimensional variable amplitude loads and the sinusoidal EFL with two blocks, was verified. In the multi-input equivalent fatigue approach, two different criteria have been developed, and several different EFL have been studied. In order to verify the whole approach, the same experiment for each model and each criterion should be done. Moreover, the same loads should be tested on different structures, with different geometrical characteristics.

Appendix A

Evaluation of a threshold of non-damaging range of rainflow cycles in Morel's criterion

We will evaluate a theoretical expression of $T(A_c, \boldsymbol{F})$, in terms of the parameters depending on the stress tensors and on the loads, and prove Theorem 6.5. Moreover, a minimization of the threshold in terms of $\alpha(A_c)$ and $\beta(A_c)$ will be proposed.

Theorem A.1. ***Expression of the threshold*** $T(A_c, \boldsymbol{F})$**.** *The stress field fulfilling* Assumption 6.1 *and* Assumption 6.2 *can be written as,*

$$\boldsymbol{\Sigma}_d(A_c, \boldsymbol{F}, t) = C_s(A_c) \sum_{i=1}^{n} d_i(A_c)\, F_i(t) \begin{pmatrix} 1 \\ \alpha(A_c) \\ \beta(A_c) \end{pmatrix},$$

with

$$C_s(A_c) > 0, \quad -1 \leq \beta(A_c) \leq \alpha(A_c) \leq 1.$$

The threshold $T(A_c, \boldsymbol{F})$ *of any structure and point fulfilling* Assumption 6.1 *and* Assumption 6.2*, has an analytical expression,*

$$T(A_c, \boldsymbol{F}) = \frac{M_1}{M_2},$$

Appendix A. Evaluation of a threshold of non-damaging range of rainflow cycles in Morel's criterion

The variables M_1 and M_2 are defined by,

$$\begin{aligned} M_1 &= 2\left(\frac{\beta_d}{C_s(A_c)} - \frac{\alpha_d}{3}(1+\alpha(A_c)+\beta(A_c))\,F_m^*(A_c,\boldsymbol{F})\right) \\ M_2 &= \frac{\alpha_d}{3}|1+\alpha(A_c)+\beta(A_c)| + \frac{1-\beta(A_c)}{2}, \end{aligned} \tag{A.1}$$

where α_d and β_d are Dang Van's coefficients, dependent on the material. The variable $F_m^*(A_c,\boldsymbol{F})$ is the mean value of the $F^*(A_c,\boldsymbol{F})$.

Proof. The components $\alpha(A_c)$ and $\beta(A_c)$ depend on the geometry and on A_c. They are constant in time. Under the hypothesis of elastic and quasi-static structures, each component of $\boldsymbol{\Sigma}_d(A_c,\boldsymbol{F},t)$ is a linear combination of the forces. Thus,

$$\sigma(A_c,\boldsymbol{F},t) = C_s(A_c)\sum_{i=1}^{n} d_i(A_c)\,F_i(t) \quad \text{with} \quad \begin{cases} C_s(A_c) > 0 \\ \sum_{i=1}^{n}(d_i(A_c))^2 = 1. \end{cases}$$

Let's consider the unit vector $\boldsymbol{d}$,

$$\boldsymbol{d}(A_c) = (d_1(A_c), d_2(A_c), \ldots, d_n(A_c))\,.$$

When the geometry is known, parameters $C_s(A_c)$, $\boldsymbol{d}(A_c)$, $\alpha(A_c)$ and $\beta(A_c)$ are also known. These variables are independent as there exists an infinite number of structures and combinations of these parameters. Hydrostatic pressure and resolved shear stress are expressed from them.

Let's call the hydrostatic pressure $P(A_c,\boldsymbol{F})$ at a given point A_c of the structure:

$$P(A_c,\boldsymbol{F}) = \frac{1}{3}\,(1+\alpha(A_c)+\beta(A_c))\,\sigma(A_c,\boldsymbol{F}).$$

The standard deviation and the mean of P are called P_{rms} and P_m respectively,

$$\begin{aligned} P_{rms}(A_c,\boldsymbol{F}) &= \frac{1}{3}\,|1+\alpha(A_c)+\beta(A_c)|\,\sigma_{rms}(A_c,\boldsymbol{F}), \\ P_m(A_c,\boldsymbol{F}) &= \frac{1}{3}(1+\alpha(A_c)+\beta(A_c))\,\sigma_m(A_c,\boldsymbol{F}), \end{aligned} \tag{A.2}$$

where $\sigma_m(A_c,\boldsymbol{F})$ and $\sigma_{rms}(A_c,\boldsymbol{F})$ are the mean and the standard deviation of $\sigma(A_c,\boldsymbol{F})$.

From Mohr's circles, the resolved shear stress $\tau(A_c,\boldsymbol{F})$, is expressed by:

$$\tau(A_c,\boldsymbol{F}) = \frac{1}{2}(1-\beta(A_c))\,\sigma(A_c,\boldsymbol{F}).$$

Appendix A. Evaluation of a threshold of non-damaging range of rainflow cycles in Morel's criterion

From Eq. (6.8),

$$\tau(A_c, \boldsymbol{F}) = C(A_c)\, F^*(A_c, \boldsymbol{F}).$$

Thus, we deduce,

$$\begin{aligned} C(A_c) &= \frac{1-\beta(A_c)}{2}\, C_s(A_c), \\ \mathbf{a}(A_c) &= \boldsymbol{d}(A_c). \end{aligned} \tag{A.3}$$

As a consequence,

$$\tau(A_c, \boldsymbol{F}, t) = C_s(A_c)\frac{1-\beta(A_c)}{2} F^*(A_c, \boldsymbol{F}),$$

and

$$\tau_{rms}(A_c, \boldsymbol{F}) = C_s(A_c)\frac{1-\beta(A_c)}{2} F^*_{rms}(A_c, \boldsymbol{F}). \tag{A.4}$$

The stress $\sigma(A_c, \boldsymbol{F}, t)$ is proportional to $\tau(A_c, \boldsymbol{F}, t)$. They are both linked to the same combination of the forces $F^*(A_c, \boldsymbol{F}, t)$. Moreover, from Eq. (A.2), we get,

$$\begin{aligned} P_{rms}(A_c, \boldsymbol{F}) &= \frac{1}{3}\, |1 + \alpha(A_c) + \beta(A_c)|\; C_s(A_c) F^*_{rms}(A_c, \boldsymbol{F}), \\ P_m(A_c, \boldsymbol{F}) &= \frac{1}{3}(1 + \alpha(A_c) + \beta(A_c))\, C_s(A_c) F^*_m(A_c, \boldsymbol{F}). \end{aligned} \tag{A.5}$$

From Eq. (4.11) and Eq. (6.11), the parameter $T(A_c, \boldsymbol{F})$ is expressed from the hydrostatic pressure and the resolved shear stress:

$$T(A_c, \boldsymbol{F}) = \frac{M_1}{M_2}.$$

The magnitudes M_1 and M_2 are defined as,

$$\begin{aligned} M_1 &= 2\,(\beta_d - \alpha_d\, P_m(A_c, \boldsymbol{F}))\,, \\ M_2 &= C(A_c)\left(\frac{\alpha_d\, P_{rms}(A_c, \boldsymbol{F})}{\tau_{rms}(A_c, \boldsymbol{F})} + \frac{H}{\sqrt{\pi}}\right). \end{aligned}$$

The value of H for proportional stress tensors is known, see [39],

$$H = \sqrt{\pi}.$$

Consequently, we can deduce an analytical expression of the threshold $T(A_c, \boldsymbol{F})$, from Eq. (A.5,A.4),

$$M_1 = 2\left(\frac{\beta_d}{C_s(A_c)} - \frac{\alpha_d}{3}(1 + \alpha(A_c) + \beta(A_c))\, F_m^*(A_c, \boldsymbol{F})\right),$$
$$M_2 = \frac{\alpha_d}{3}|1 + \alpha(A_c) + \beta(A_c)| + \frac{1 - \beta(A_c)}{2}.$$

□

Thus, we can deduce that the threshold $T(A_c, \boldsymbol{F})$ depends on the mean value of the loads, and on the location of the critical point.

Bibliography

[1] AFNOR. Fatigue sous sollicitations d'amplitude variable. *Report A03-406*, 1993.

[2] A. ANDERSON, I. OLKIN, and I. G. UNDERHILL. Generation of random orthogonal matrices. *SIAM J. Sci. Stat. Comput.*, 8:625–629, 1987.

[3] J. A. BANNANTINE, J. J. COMER, and J. L. HANDROCK. *Fundamentales of Metal Fatigue Analysis*. Pretince Hall, 1989.

[4] A. BANVILLET, T. PALIN-LUC, and S. LASSERRE. A volumetric energy based hich cycle multiaxial fatigue criterion. *International Journal of Fatigue*, 25:755–769, 2003.

[5] O.H. BASQUIN. The exponential law of endurance tests. *ASTM*, 10:625–630, 1910.

[6] D. BENASCIUTTI and R. TOVO. Cycle distribution and fatigue damage assessment in broad-band non-Gaussian random processes. *Probabilistic Engineering Mechanics*, 20:115–127, 2005.

[7] A. BESTE, K. DRESSLER, H. KÖTZLE, W. KRÜGER, B. MAIER, and J. PETERSEN. Multiaxial rainflow, a consequence continuation of Professor Tatsuso Endo's work. *The Rainflow Method in Fatigue (in Y. Murakami, editor)*, 1992.

[8] A. BIGNONNET. Fatigue design in automotive industry. In *High-cycle Metal Fatigue in the Context of Mechanical Design*. Coordinated by K. Dang Van and I.V. Papadopoulos, September 8-12, 1997.

[9] A. BIGNONNET and J.-J THOMAS. Fatigue assessment and reliability in automotive design. *SAE Brasil-International Conference on Fatigue*, 2001.

[10] N. W. M. BISHOP and F. SHERRATT. A theoritical solution for the estimation of "rainflow" ranges from power spectral density. *Fatigue and Fracture Engineering in Materials and Structures*, 13:311–326, 1990.

[11] P.A. BRODTKORB, P. JOHANNESSON, G. LINDGREN, I. RYCHLIK, J. RYDÉN, and E. SJÖ. WAFO-A MATLAB toolbox for analysis of random waves and loads. In *10th International offshore and Polar Engng Conf., Seattle*, volume III, pages 343–350, 2000.

[12] K. DANG VAN. Sur la résistance à la fatigue des matériaux. *Sciences et Techniques de l'Armement, Mémorial de l'Artillerie française*, 1973.

[13] B.S. DHILLON. *Design Reliability, Fundamentals and Applications*. CRC Press LLC, 1999.

[14] N. E. DOWLING. Fatigue failure predictions for complicated stress-strain histories. *Journal of Materials, JMLSA*, 7(1):71–87, 1972.

[15] N. E. DOWLING. Estimation and correlation of fatigue lives for random loading. *Int. Journal of Fatigue*, 10(3):179–185, 1988.

[16] N. E. DOWLING. A review of fatigue life prediction methods. *SAE-Paper number 871966*, 1988.

[17] K. DRESSLER, R. CARMINE, and W. KRÜGER. The multiaxial rainflow method. *Low Cycle Fatigue and Elasto-Plastic behaviour of Materials, Elsevier Science Publications*, 1992.

[18] K. DRESSLER and V.B. KÖTTGEN. Tools for fatigue evaluation of non-proportional loading. *Fatigue Design '95*, 1995.

[19] F. ELLYIN. *Fatigue damage, crack growth and life prediction*. 1997.

[20] T. ENDO, K. MITSUNAGA, and H. NAKAGAWA. Fatigue of metals subjected to varying stress - prediction of fatigue lives. *Preliminary Proceedings of The Chukogu-Shikoku District Meeting, The Japan Society of Mechanical Engineering*, pages 41–44, Novembre 1967.

[21] T. ENDO, K. MITSUNAGA, H. NAKAGAWA, and K. IKEDA. Fatigue of metals subjected to varying stress - low cycle, middle cycles fatigue. *Preliminary Proceedings of The Chukogu-Shikoku District Meeting, The Japan Society of Mechanical Engineering*, pages 45–48, Novembre 1967.

[22] A. FATEMI and L. YANG. Cumulative fatigue damage and life prediction theories: a survey of the state of the art for homogeneous materials. *Int. J. Fatigue*, 20:9–34, 1998.

[23] M. FOGUE, B. KENMEUGNE, B. WEBER, and J.-L ROBERT. Compteur de cycles et calcul de durée de vie en fatigue multiaxial d'amplitude variable. *Mécanique industrielle et matériaux*, 51, 1998.

[24] M. FRENDAHL and I. RYCHLIK. Rainflow analysis: Markov method. *International Journal of Fatigue*, 15:265–272, 1993.

[25] Y. S. GARUD. Multiaxial fatigue : A survey of the state of the art. *Journal of Testing and Evaluation JTEVA*, 9:165–178, 1981.

[26] G. GENET, P. JOHANNESSON, D. GUALANDRIS, J. DE MARÉ, and NGUYEN-TAJAN M.L. An approach to multi-input equivalent fatigue loadings. In *ASME International Mechanical Engineering Congress and Exposition*, 5-11th November, Orlando, 2005.

[27] G. GENET, P. JOHANNESSON, and M.L. NGUYEN-TAJAN. Multi-input equivalent fatigue loadings. In *FATIGUE 2006 9th International Fatigue Congress*, 14-19th May, Atlanta, 2006.

[28] G. GENET, P. JOHANNESSON, M.L. NGUYEN-TAJAN, D. GUALANDRIS, and J. DE MARÉ. Multi-input Markov chain equivalent fatigue loadings. In *Journées de Printemps SF2M*, 30-31th May, 1st June, Paris, 2006.

[29] G. GRIMMET and D. STIRZAKER. *Probability and Random Processes*. Oxford University Press, Third edition 2002.

[30] H.J. GROVER, S.M. BISHOP, and L.R. JACKSON. Fatigue strength of aircraft materials. Axial load fatigue tests on unnotched sheet specimens of 24S-T3, 75S-T6 aluminium alloys and of SAE 4130 steel. *NACA TN 2324*, 1951.

[31] P. HEULER and T. SEEGER. A criterion for omission of variable amplitude loading histories. *Int. Journal of Fatigue*, 8(4):225–230, 1986.

[32] P. JOHANNESSON. *Rainflow Analysis of Switching Markov Loads*. PhD thesis, Lund institute of Technology, 1999.

[33] L. H. KOOPMAN. *The Spectral Analysis of Time Series*. Academic Press, 1995.

[34] T.E. LANGLAIS, J.H. VOGEL, and T.R CHASE. Multiaxial cycle counting for critical plane mathods. *International Journal of Fatigue*, 25:641–647, 2003.

[35] M. LEMAIRE, P. HORNET, and M. PENDOLA. *Fiabilité des structures mécaniques, couplage mécano-fiabiliste statique*. Institut pour la promotion des sciences de l'ingénieur, 2001.

[36] G. LINGREN and K.B. BROBERG. Cycle range distributions for Gaussian processes - exact and approximative results. *Extremes*, 7:69–89, 2004.

[37] E. MACHA. Generalization of fatigue criteria for multiaxial sinusoidal loadings in the range of random loadings. *In Biaxial and Multiaxial Fatigue, EGF3, (Edited by M.W.Brwon and K.J. Miller)*, pages 425–436, 1989.

[38] M. A. MINER. Cumulative damage in fatigue. *Journal of Applied Mechanics*, 12:A159–A164, 1945.

[39] F. MOREL. *Fatigue multiaxiale sous chargement d'amplitude variable*. PhD thesis, École Nationale Supérieure de Mécanique et d'Aérotechnique et Faculté des Sciences Fondamentales et Appliquées, 1996.

[40] F. MOREL. A fatigue life prediction method based on a mesoscopic approach in constant amplitude multiaxial loading. *Fatigue & Fracture of Engineering Materials & Structures*, 21:241–256, 1998.

[41] F. MOREL. A critical plane approach for life prediction of high cycle fatigue under multiaxial variable amplitude loading. *Int. Journal of Fatigue*, 22:101–119, 2000.

[42] F. MOREL. A critical plane fatigue model applied to out-of-phase bending and torsion load conditions. *Fatigue & Fracture of Engineering Materials & Structures*, 24:153–164, 2000.

[43] F. MOREL and G. HÉNAFF. *Fatigue des Structures. Endurance, critères de dimensionnement, propagation des fissures, rupture*. Ellipses édition, 2005.

[44] D. V. NELSON and H. O. FUCHS. Predictions of cumulative fatigue damage using condensed load histories. *SAE - Paper number 750045*, 1975.

[45] M. OLAGNON. Practical computation of statistical properties of rainflow counts. *International Journal of Fatigue*, 16:306–313, 1994.

[46] A. PALMGREN. Die lebensdauer von kugellagern. *Zeitschrift des Vereins Deutscher Ingenieure*, 68:339–341, 1924.

[47] I.V PAPADOPOULOS. *Fatigue polycyclique des métaux: une nouvelle approche, Ph.D thesis*. PhD thesis, École Nationale des Ponts et Chaussées, Paris, 1987.

[48] I.V. PAPADOPOULOS. A new criterion of fatigue strength for out-of-phase bending and torsion of hard metals. *Int. Journal of Fatigue*, 16:377–384, 1994.

[49] I.V. PAPADOPOULOS. Exploring the high-cycle fatigue behaviour of metals from the mesoscopic scale. *Journal of Mechanical Behaviour and Materials*, 6:93–118, 1996.

[50] I.V. PAPADOPOULOS, P. DAVOLI, C. GORLA, M. FILIPPINI, and A. BERNASCONI. A comparative study of multiaxial high-cycle fatigue criteria for metals. *International Journal of Fatigue*, 19:219–235, 1997.

[51] X. PITOISET, A. KERNILIS, A. PREUMONT, and V. PIÉFORT. Estimation du dommage en fatigue multiaxiale de structures métalliques soumises à des vibrations aléatoires. *Revue francaise de mécanique*, 1998-3:201–208, 1998.

[52] X. PITOISET and A. PREUMONT. Spectral methods for multiaxial random fatigue anlysis of metallic structures. *International journal of fatigue*, 22:541–550, 2000.

[53] S.-O RICE. The mathematical analysis of random noise, i and ii. *Bell Syst. Technical Journal*, 23, 1944-1945.

[54] I. RYCHLIK. *Course in Reliability Applications of Rice's Formula for the Intensity of Level Crossings*. Centre of Mathematical Sciences, Lund University.

[55] I. RYCHLIK. A new definition of the rainflow cycle counting method. *Int. J. Fatigue*, 9(2):119–121, 1987.

[56] I. RYCHLIK. Note of cycle counts in irregular loads. *Fatigue and Fracture of Engineering materials and structures*, 16:377–390, 1993.

[57] I. RYCHLIK. On the narrow banded approximation for expected fatigue. *Probabilistic Engineering Mechanics*, 1993.

[58] I. RYCHLIK and G. LINDGREN. Rainflow cycle distributions for fatigue life prediction under Gaussian load processes. *Fatigue for Engineering Materials*, 10:251–260, 1987.

[59] M. SCHEUTZOW. A law of large numbers for upcrossing measures. *Stoachastic Processes and their applications*, 53:285–305, 1994.

[60] J. SCHIJVE. *Fatigue of Structures and Materials*. Kluwer Academic Publisher, 2001.

[61] D.F. SOCIE and G.B. MARQUIS. *Multiaxial Fatigue*. Society of Automotive Engineers, Inc., 2000.

[62] C. M. SONSINO. Durabilité structurelle, comprendre, prédire, vérifier. 22^{eme} *Rendez-Vous de la Technologie*, 2000.

[63] R. I. STEPHENS, A. FATEMI, R. R. STEPHENS, and H. O. FUCHS. *Metal Fatigue in Engineering*. Wiley Interscience, 2001.

[64] P. THOFT-CHRISTENSEN and Y. MUROTSU. *Application of Structural Systems Reliability theory*. Springer-Verlag, 1986.

[65] J.-J. THOMAS, G. PERROUD, A. BIGNONNET, and D. MONNET. Fatigue design and reliability in automotive industry. *Fatigue Design and Reliability, ESIS Publication, Elsevier*, pages 1–12, 1999.

[66] R. TOVO. Cycle distribution and fatigue damage under broad-band random loading. *International Journal of Fatigue*, 24:1137–1147, 2002.

[67] H. WANG and Q. LIU. Forecast modelling for rotations of principal axes of multidimensional data sets. *Computational Statistics & Data Analysis*, 27:345–354, 1998.